THE UNIVERSITY
OF MICHIGAN

# REACTOR MATERIALS

*A Quarterly Technical Progress Review*

Prepared for DIVISION OF TECHNICAL INFORMATION, USAEC, by
R. W. DAYTON, E. M. SIMONS, and ASSOCIATES, BATTELLE MEMORIAL INSTITUTE

*Winter 1963-1964*

*FEATURE ARTICLE:*

**The Behavior of Fission Gases in Ceramic Reactor Materials**

● VOLUME 6

● NUMBER 4

# TECHNICAL PROGRESS REVIEWS

To meet the needs of industry for concise summaries of current atomic developments, the Atomic Energy Commission is publishing this series, Technical Progress Reviews. Issued quarterly, each of the reviews digests and evaluates the latest findings in a specific area of nuclear technology and science.

The five journals published in this series are:

*Isotopes and Radiation Technology*, P. S. Baker, A. F. Rupp, and associates, Oak Ridge National Laboratory

*Nuclear Safety*, Wm. B. Cottrell, W. H. Jordan, and associates, Oak Ridge National Laboratory

*Power Reactor Technology*, W. H. Zinn and J. R. Dietrich, General Nuclear Engineering Corporation

*Reactor Fuel Processing*, Stephen Lawroski and associates, Chemical Engineering Division, Argonne National Laboratory

*Reactor Materials*, R. W. Dayton, E. M. Simons, and associates, Battelle Memorial Institute

Each journal may be purchased ($2.00 per year for subscription and individual issues $0.55) from the Superintendent of Documents, U.S. Government Printing Office, Washington 25, D. C. See back cover for remittance instructions and foreign postage requirements.

The views expressed in this publication do not necessarily represent those of the United States Atomic Energy Commission, its divisions or offices, or of any Commission advisory committee or contractor.

## Availability of Reports Cited in This Review

*Unclassified AEC reports* are available for inspection at AEC depository libraries and are sold by the Office of Technical Services, Department of Commerce, Washington 25, D. C. Some of the reports cited are not available owing to their preliminary nature; however, the information contained in them will eventually be made available in formal progress or topical reports.

*Unclassified reports issued by other Government agencies or private organizations* should be requested from the originator.

*Unclassified British and Canadian reports* may be inspected at AEC depository libraries. British reports are sold by the British Information Service, 45 Rockefeller Plaza, New York, N. Y.; Canadian reports (AECL series) are sold by the Scientific Document Distribution Office, Atomic Energy of Canada, Ltd., Chalk River, Ontario, Canada.

*Classified U. S. and foreign reports* identified in this journal as Classified may be purchased by properly cleared Access Permit Holders from the Division of Technical Information Extension, U. S. Atomic Energy Commission, P. O. Box 1001, Oak Ridge, Tenn. Such reports may be inspected at classified AEC depository libraries.

# REACTOR MATERIALS

## A REVIEW OF RECENT DEVELOPMENTS

Prepared for DIVISION OF TECHNICAL INFORMATION, USAEC,
by R. W. DAYTON, E. M. SIMONS, and ASSOCIATES,
BATTELLE MEMORIAL INSTITUTE

WINTER 1963–1964

VOLUME 6

NUMBER 4

# Foreword

*Reactor Materials* is one of a series of quarterly technical progress reviews broadly covering the field of nuclear science and technology. Under the auspices of the USAEC Division of Technical Information, *Reactor Materials* is prepared by Battelle personnel from worldwide literature. It covers properties, behavior, and fabrication processes of materials applicable to nuclear reactor components and associated equipment.

The reader will recognize that the scope of this Review is too broad to permit detailed coverage of every topic. Rather, the authors and editors attempt to combine the highlights of significant new developments into an information summary of current research for both management and the technical specialist. As a rule, enough of the results are presented to define the research and summarize the findings. For readers desiring more information on any particular topic, a complete set of references is provided at the end of each section.

Each quarter, a number of bibliographies, monographs, and books appear on subjects within the scope of *Reactor Materials*. Although the main purpose of this Review is to call attention to findings that are new and significant, such publications are noted in the text because they often represent excellent compilations of available information on important materials topics.

R. W. DAYTON
E. M. SIMONS
R. W. ENDEBROCK
*Battelle Memorial Institute*

DEPOSITED BY THE
UNITED STATES OF AMERICA

FEATURE ARTICLE

## *The Behavior of Fission Gases in Ceramic Reactor Materials* . . . . . 1

*By David L. Morrison, Battelle Memorial Institute*

Foreword

I FUEL AND FERTILE MATERIALS . . . 11
Uranium Metal and Alloys . . . . . 11
Plutonium . . . . . 13
Thorium . . . . . 18
Metal-Ceramic Fuels . . . . . 18
Coated-Particle Fuel Materials . . . . . 21
Refractory Fuel and Fertile Materials . . . . . 29
Mechanism of Corrosion of Fuel Alloys . . . . . 31
Basic Studies of Irradiation Effects on Fuel Materials . . . . . 32
References . . . . . 33

II MODERATOR MATERIALS . . . . . 37
Graphite . . . . . 37
Beryllium Metal and Alloys . . . . . 40
Beryllium Oxide . . . . . 45
Solid Hydrides . . . . . 46
References . . . . . 49

III NUCLEAR POISONS . . . . . 51
Metallic Poison Materials . . . . . 51
Dispersion Control Materials . . . . . 51
References . . . . . 52

IV CLADDING AND STRUCTURAL MATERIALS . . . . . 54
Corrosion . . . . . 54
Radiation Effects in Nonfuel Materials . . . . . 59
Selected Mechanical Properties of Structural and Cladding Materials . . . 62
Selected Metallurgical Aspects of Cladding and Structural Materials . . . 63
Diffusion Studies . . . . . 65
Ceramic Technology . . . . . 66
References . . . . . 66

V SPECIAL FABRICATION TECHNIQUES . . . . . 70
Melting, Hot and Cold Working . . . . . 70
Cladding . . . . . 70
Welding and Brazing . . . . . 74
References . . . . . 77

INDEX, VOLUMES 4 to 6 . . . . . 81

Issued quarterly by the U. S. Atomic Energy Commission. Use of funds for printing this publication approved by the Director of the Bureau of the Budget on October 14, 1963.

FEATURE ARTICLE

# The Behavior of Fission Gases in Ceramic Reactor Materials

By David L. Morrison*

*(Editor's Note: The release of fission gases from nonmetallic fuel and cladding materials has a strong influence on fuel-element and reactor design. Consequently fission-gas release has been studied extensively since nonmetallic materials became dominantly important in reactor technology. From a practical point of view, this research has produced a large volume of useful data.*

*From a scientific point of view, the situation is less satisfactory because the detailed mechanism of release is not known. It is known that fission-gas release is not a simple diffusional process following well-known mathematical laws. Instead, it is governed by some more complicated process, in which gas is released in bursts on heating or cooling. The release pattern is affected by the amount of radiation the specimen has received, and the gases have an isotopic composition that cannot be rationalized. There has been a great deal of speculation about the causes for this unpredictable behavior, and several hypotheses have been proposed to explain the results. None of these hypotheses, however, has been subjected to a critical evaluation.*

*The following feature article discusses the situation briefly. In the space available, no attempt has been made to review the literature thoroughly, especially since several such reviews are already available in the literature. Rather, emphasis has been placed on the differences between the observed fission-gas release and that expected from a simple diffusional model of release. In this way, the peculiarities of the release of fission gas from nonmetallic materials are emphasized.)*

## Introduction

The release of fission products from nuclear materials is a matter of considerable importance which affects the design of fuel elements for fission-product containment and the amount of reactor-system contamination which comes from defects in fuel cladding. Owing to this importance, fission-product release has been studied extensively, particularly in the past two decades.

Although the release of all types of fission products from all kinds of materials is important, this review will be limited to a discussion of fission-gas behavior in ceramic materials. The experimental results for a number of different materials will be examined. Full details of the data will not be given; instead, data will be presented only in enough detail to illustrate the general trends of fission-gas behavior. It will become apparent that fission-gas release does not follow some simple pattern of behavior, and the data reported are selected to point up this fact. Attention will be given to mechanisms of fission-gas release which have been proposed to explain the experimental data.

## Diffusion Model

Fission-gas behavior in solids has conventionally been analyzed in terms of a simple dif-

*Senior Chemist, Chemical Physics Division, Battelle Memorial Institute.

fusion process, even though the data do not follow the predicted pattern of behavior. The diffusion model provides a convenient method for comparing data from various laboratories and for different materials. It will become apparent, however, that the predictions of a diffusion model are not confirmed experimentally. In order to point up this fact, let us first discuss the behavior predicted for simple diffusional release of fission gas from solids.

Fick's second law of diffusion can be modified to include terms describing the radioactive decay of fission gases and the creation of more fission gas in the material for the case of in-pile experiments. The resulting differential equation can then be solved to find the rate of release of fission gas as a function of time and of the radiation decay constant of the isotope being measured.

This treatment is quite straightforward and gives exact results for diffusion in specimens of simple geometric shape. However, many specimens of nonmetallic materials are porous, and diffusional release can occur from the surface of the pores, whose geometry is exceedingly complex. For such materials, a geometric shape must be assumed, and the solutions of the diffusion equations are only approximations for the physical situation.

A solution to Fick's equation for such materials is usually derived in terms of the equivalent sphere model suggested by Booth[1] and Lustman.[2] This approximation assumes that the fuel pellet or powder can be represented by uniform spheres of theoretical density with the same surface area-to-volume ratio as that of the pellet. The surfaces of these spheres are assumed to be interconnected by open porosity. The results of this model are conveniently expressed as apparent diffusion coefficients, $D' = D/a^2$, where $D$ is the diffusion coefficient in square centimeters per second and $a$ is the equivalent sphere radius in centimeters. It should be emphasized that this simplified model can no more than approximate the real situation in a porous material, whose geometry is very complex.

In such ways it is possible to predict, for diffusional release, the behavior to be expected either for postirradiation heating experiments or for in-pile experiments. The behavior expected is that the cumulative fractional release of fission gases during a postirradiation heating experiment should be proportional to the square root of the heating time for release up to about 20% of the contained amount. In-pile release rates of various isotopes under steady-state conditions should be directly proportional to the square root of the half-life of the isotope.

It will become apparent that these predictions are not realized. The departure of the observed release behavior from the diffusion-model predictions for a given material is important to understanding fission-gas behavior. In the following discussions of each of several materials studied, the departures from the diffusion model will be noted so that the limitations upon the use of this model will become apparent and the current thinking on the mechanisms of fission-gas behavior in reactor materials may be established.

## Uranium Dioxide

The behavior of fission gases has been studied more thoroughly in uranium dioxide than in any other material. As a result most of the current theories of the mechanisms of fission-gas behavior have evolved from studies of this material. In an article of this scope and size, it will not be possible to review all the data on the $UO_2$, and so note should be made of other review articles[3–9] limited to this material.

Because the simple diffusion model ignores such effects as grain boundaries, closed porosity, thermal gradients, stoichiometry, surface films, burnup, radiation damage, temperature changes, pore migration, and grain growth, it is not surprising that wide variances in $D$ or $D'$ values and activation energies have been found.[3,4] $D'$ values at a given temperature on powdered and low-density sintered materials[10] may vary by a factor of $10^4$, and activation energies between 30 and 80 kcal/mole have been reported for temperatures between 1000 and 1600°C.

For fused and sintered $UO_2$ having a density of 99% of theoretical and for single-crystal samples that should not be dependent upon some of these variables, the agreement between diffusion coefficients measured by different experimenters is generally better. In Fig. 1, diffusion coefficients for xenon release from high-density sintered[11] and single-crystal[12,13] samples are plotted. The activation energies of 90 to 120 kcal/mole reported in these experi-

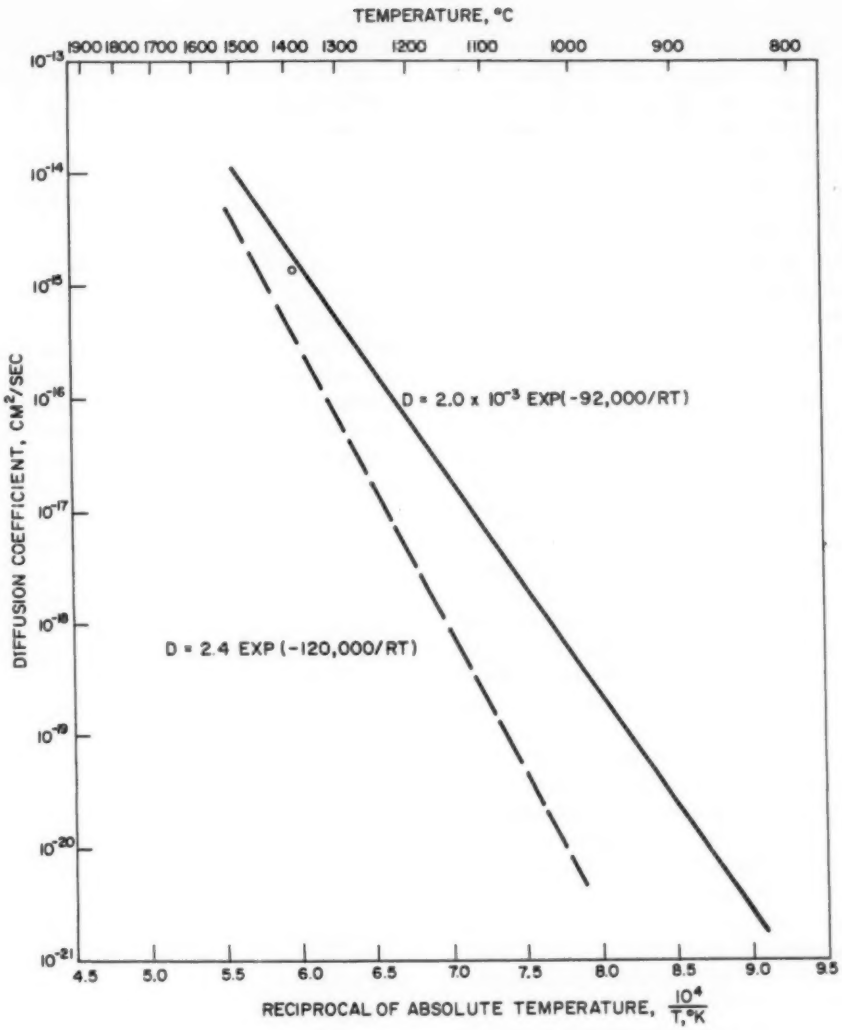
TEMPERATURE, °C
1900 1800 1700 1600 1500 1400 1300 1200 1100 1000 900 800
DIFFUSION COEFFICIENT, CM²/SEC
D = 2.0 x 10⁻³ EXP(-92,000/RT)
D = 2.4 EXP(-120,000/RT)
RECIPROCAL OF ABSOLUTE TEMPERATURE, 10⁴/T,°K

Fig. 1 $Xe^{133}$ diffusion coefficients in $UO_2$. ——, Melehan, 99% dense-sintered $UO_2$ (Ref. 11). — —, Stevens, single-crystal $UO_2$ (Ref. 12). ○, Berry, single-crystal $UO_2$ (Ref. 13).

ments are considerably higher than those for less dense materials and also higher than the 50 kcal/mole for a lower temperature range, 600 to 1000°C, reported by Carroll[14] for in-pile release of $Kr^{88}$ from single-crystal $UO_2$ plates.

This presentation of compilations of "diffusion coefficient" data should not be taken to imply that fission-gas release data are, in fact, in accord with the predictions of simple volume diffusion theory. This is not the case, for the release data show many points of divergence from the simple theory. Some of these departures are as follows.

One significant departure of fission-gas release from the simple-diffusion-model predictions is the appearance of a heating "burst." Such bursts occur in both in-pile and postirradiation heating experiments. In in-pile experiments it is frequently found that the rate of fission-gas release will rise markedly when the temperature is raised and then decrease to some new equilibrium value. The burst release

in this case is the temporary increase in the release rate of gas above its steady-state value. In postirradiation heating experiments, it is found that each time the temperature of the specimen is increased, the rate of release is initially rapid. After a period of a few minutes to a few hours, the rate of release decreases and thereafter is linear with the square root of time. In postirradiation experiments the initially rapid release of gas from the specimen is called the burst release. The burst release is important since 50 to 90% of all the gas released during the diffusion anneal is released during the initial burst.

Owing to these burst effects, and in the absence of any confirmed theory of their cause, one's ability to compute a diffusion coefficient is in considerable doubt; in order to compute a diffusion coefficient, the burst must be neglected and the diffusion coefficients calculated from the release following the burst. Such a procedure will be valid only if burst release occurs independently of the subsequent release and does not disturb the fission-gas distribution. Since this is an unproved assumption, diffusion coefficients calculated in the indicated way must be regarded with suspicion.

Owing to their frequent occurrence and their undoubted importance in affecting fission-gas release, a great deal of effort has been spent in attempting to arrive at a full understanding of burst phenomena. Some of the ideas as to the causes of bursts are as follows.

Part of the heating burst release in-pile can be attributed to the change in diffusion coefficients which occurs with the temperature change,[15] but the magnitude of the burst is, in general, larger than these changes indicate. The presence of excess oxygen may also be responsible for the burst release.[12] This appears to be a reasonable hypothesis since xenon release from $UO_x$ is observed to increase with increasing $x$.[16] Lewis[9] has suggested that rare-gas diffusion coefficients may be higher near the surface of the specimen, due either to a lowering of the activation energy for diffusion or to an increase in the available solid angle through which an atom may move to escape from the material. Kelly's work[17] on the release of "attached" atoms from solids may offer another explanation of the burst release. This release process is one where a single lattice jump is sufficient to free the atom from the surface. The release is controlled by a spectrum of activation energies. The kinetics of the release are first order with respect to gas concentration, and the fractional release calculated for these conditions, for short times, is given in the following equation:*

$$F = \frac{RT}{H_2 - H_1} \ln \gamma k_0 t - \frac{H_1}{H_2 - H_1}$$

where $\gamma = 1.781$, $k_0$ is the characteristic frequency factor from the Arrhenius equation, and $H_1$ and $H_2$ are the minimum and maximum values from a spectrum of equally weighted activation energies controlling the release process. Although all the suggested mechanisms can explain the burst release qualitatively, it is not yet possible to base quantitative predictions on any of them or even to know whether any of them is correct.

Another departure of the observed fission-gas release from a simple diffusion behavior, which assumes that all the gas in the specimen is available for diffusion, may be due to trapping or immobilization of the gas atoms. Irradiated $UO_2$ specimens heated for several days showed a release lower than that expected from the extrapolation of the square-root-of-heating-time release established during the earlier part of the diffusion anneal.[18] When sintered $UO_2$ pellets were ground to fine powder following heat-treatments,[9] much of the fission gas trapped in closed pores was released. Trapping of this type is to be expected, but the reduced concentration of gas atoms available for diffusion must be considered when the diffusion coefficients are calculated.

However, there are indications that trapping may also occur at lattice defects, or clusters of lattice defects, produced by irradiation. Frigerio[19] has reported that $D'$ measured in postirradiation experiments decreases by factors of up to $10^3$ for xenon release from sintered $UO_2$ pellets when the exposure is increased from $2 \times 10^{17}$ to $5 \times 10^{18}$ fissions/cm$^3$. Carroll[14] has observed a decrease in the rate of fission-gas release from single-crystal $UO_2$ during an in-pile experiment. The rate of release stabilized after a burnup of $1.4 \times 10^{18}$ fissions/cm$^3$. Until these measurements were reported, the release of fission gas was pre-

*It should be noted that this equation breaks down for $t = 0$.

sumed[8] to be independent of burnup up to $9 \times 10^{20}$ fissions/cm$^3$. It has been suggested that the decrease in the release of fission gas with irradiation exposure at low burnup may be due to a reduction in the surface area of the specimen by radiation-induced smoothing of microscopic imperfections[14] or to immobilization of the gas atoms at irradiation-induced point defects[19,20] which saturate at about $10^{19}$ fissions/cm$^3$. More experimental work will be necessary to evaluate either of these hypotheses.

Hurst[21] has recently reported the results of calculations of the fractional release from spheres, assuming that both trapping and release from trapping sites can occur during the anneal. Unpublished calculations at Chalk River, assuming trapping only, predicted releases lower than the observed values at long heating times. With the assumption that fission gases are released from traps and returned to the lattice where diffusion takes place, a better agreement with experimental data was found. Valuable information on the trapping of fission gases may be obtained by pursuing this approach further.

The appearance of cooling bursts in some postirradiation[19,22,23] and in-pile experiments is also a departure from the predictions of a simple diffusion model. The amount of fission gas released during the cooling burst depends upon the temperature of the specimen (the higher the temperature, the larger the burst)[19,23,24] and upon the rate of cooling (the faster the rate, the larger the burst).[22] Mechanisms suggested to explain the occurrence of a cooling burst are either a disproportionation into $UO_2$ and uranium metal[22] of a substoichiometric oxide formed at the high temperatures or thermal-stress cracking of the material.

The release rates of fission gases from $UO_2$ during postirradiation experiments at high temperatures (>1600°C) are much greater than those predicted from lower temperature diffusion release.[10,22,25] At these temperatures the behavior of fission gas is strongly influenced by grain growth, sintering, void migration, and vaporization (Refs. 8, 9, 10, and 25), which cannot be treated by diffusion model.

The release of fission gas from $UO_2$ during in-pile experiments is characterized by two temperature regions. For temperatures below 600°C, the release rate is nearly independent of temperature; above 600°C, the release rate is temperature dependent and the release is assumed to be controlled by a diffusion process. In the temperature-independent region, if the release of fission gases were due to recoil alone, the release rate would be independent of $\lambda$, the decay constant of the isotope. Both Melehan[11] and Carroll[14] have observed a release rate dependent upon $\lambda$ in low-temperature in-pile experiments. The isotopic composition of the gas released is between that expected for a recoil release and that expected for a diffusion process. These results have been explained by the release of gas that has migrated or been transported to a trapping region just below the surface of the crystal. The composition of the fission gas in the trapped region will be some function of the decay constant, and the release occurs when a recoiling fission fragment passes through the region.

## Uranium Carbides

The uranium carbides are the only other ceramic fuel materials in which a considerable number of fission-gas release measurements have been made. This fuel is sensitive to contaminants in the heating atmosphere[26] and is reactive with a number of metals commonly used for heating boats;[27] so meaningful diffusion coefficients are difficult to obtain. The reported diffusion coefficients, assuming a simple diffusion mechanism for fission-gas release from the uranium carbides, are plotted in Fig. 2. Heating bursts are not always observed,[32] but, when they are, the diffusion coefficients are calculated from the slope of the portion of the release curve which is linear with the square root of the heating time. Shaked[29,30] reports an apparent diffusional release during a heating time of 5 to 6 hr, whereas Zumwalt[31] and Auskern[32] observe a linear behavior with the square root of the heating time only during longer anneals. Since the lowest apparent diffusion coefficients are calculated from the longest heating times, a trapping process may be influencing fission-gas behavior. Lindner[28] found the diffusion coefficients to be independent of particle size, but Shaked reports a lowering of the diffusion coefficient with increasing grain size. The diffusion coefficients and activation energies for release from uranium carbides are relatively independent of the specimen composition. The magnitude of the diffusion coefficient reported by Zumwalt for $UC_2$ is within an order of mag-

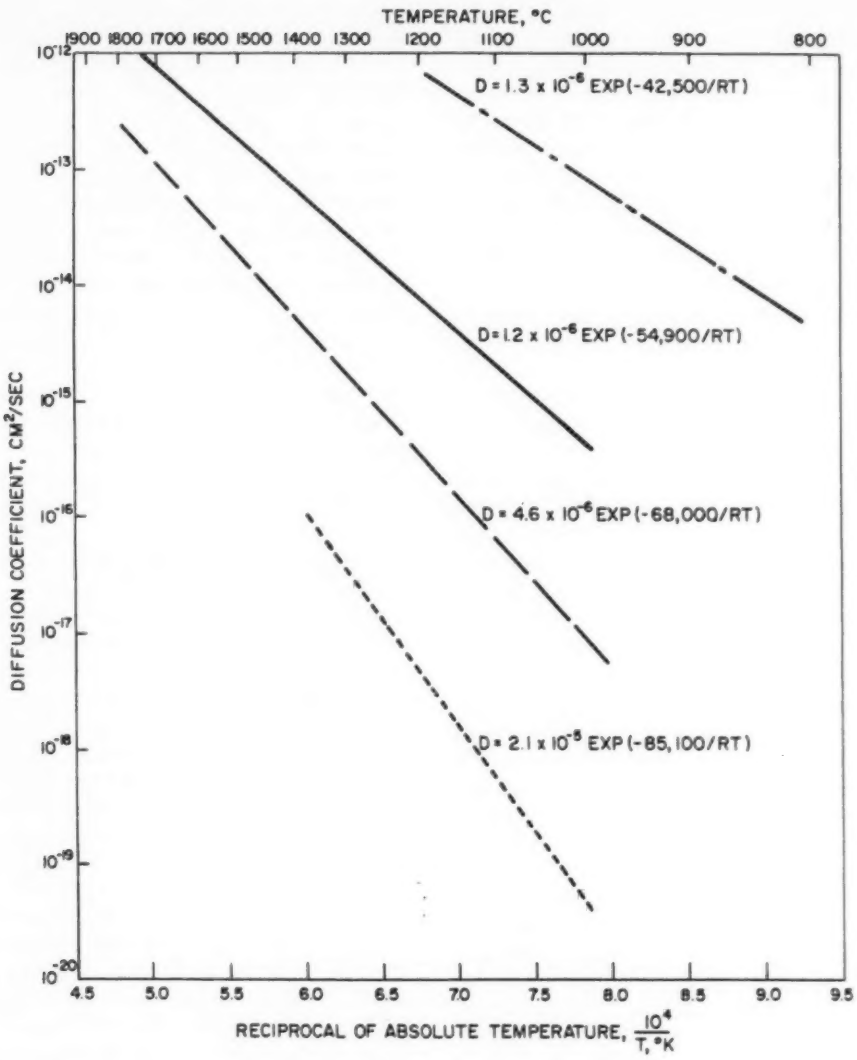


Fig. 2 $Xe^{133}$ diffusion coefficients in uranium carbides. ———, Lindner, UC (Ref. 28). ——, Shaked, UC (Refs. 29 and 30). — —, Zumwalt, $UC_2$ (Ref. 31). ----, Auskern, UC (Ref. 32).

nitude of that observed by Shaked for UC. The reported activation energies for $UC_2$ (Ref. 31) and UC (Refs. 30 and 33) are not greatly different. Some unpublished Battelle results[34] show no substantial difference between the release from UC and $U_2C_3$. Zumwalt reports the same activation energy for xenon release in in-pile and postirradiation experiments. There are insufficient data on the uranium carbides to determine whether cooling bursts and burnup effects are present.

## Ceramic Oxides and Other Ionic Crystals

Fission-gas release from nonfuel materials has been studied for two purposes: (1) to provide data on fission-gas release from potential coating materials for fuel particles[35–38] and (2) to investigate the fundamental behavior of inert gases in ionic solids.[39–42] For the first type of study,[35–38] fission gases have been re-

coiled into ceramic oxides by irradiation of single-crystal samples of these oxides in contact with $UO_2$. Following irradiation, the $UO_2$ is removed, and the release rate of xenon is determined during postirradiation heating experiments. Heating bursts that persist for a short time are observed, whereas the release for heating times between 1 and 6 hr is linear with the square root of time. However, in some longer time heating experiments on $\alpha$-$Al_2O_3$, the cumulative fractional release decreased with time. Heating bursts are insensitive to the

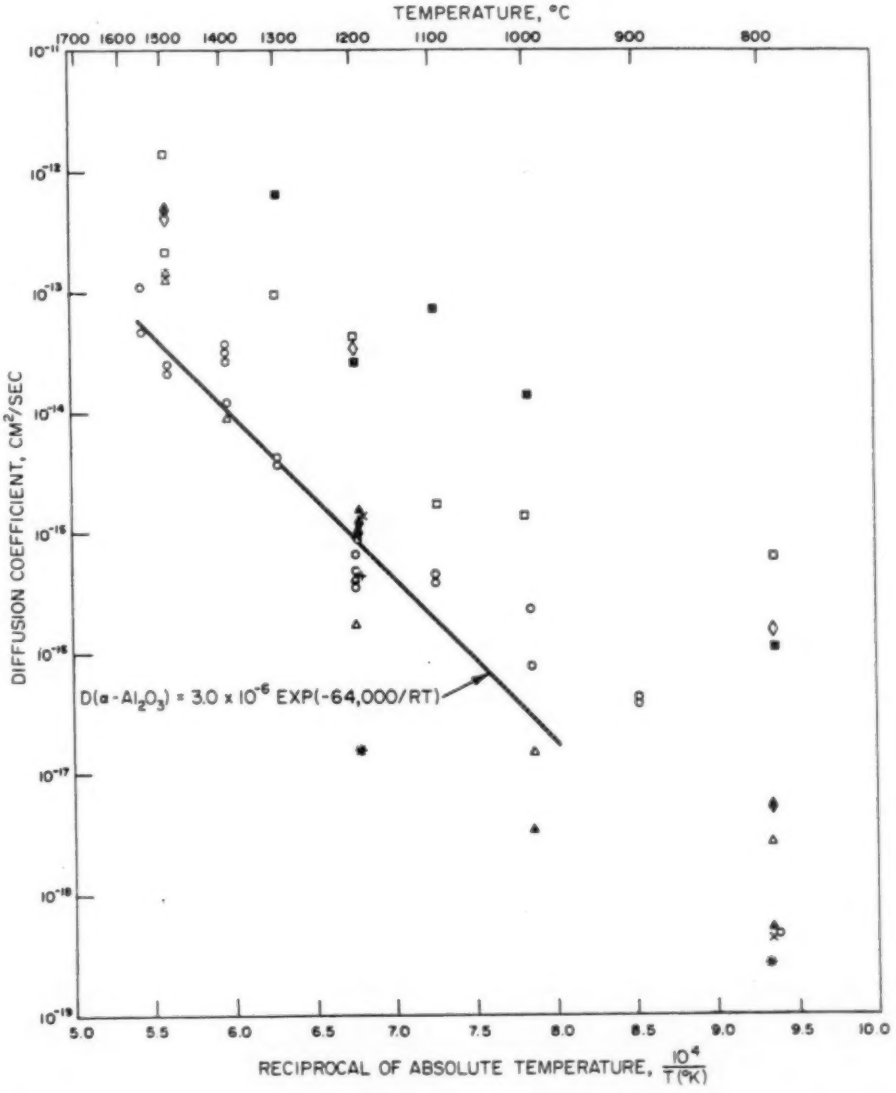
TEMPERATURE, °C
1700 1600 1500 1400 1300 1200 1100 1000 900 800
DIFFUSION COEFFICIENT, CM²/SEC
D(α-Al2O3) = 3.0 x 10⁻⁶ EXP(-64,000/RT)
RECIPROCAL OF ABSOLUTE TEMPERATURE, 10⁴/T(°K)

Fig. 3 $Xe^{133}$ diffusion coefficients for ceramic oxides.[35–38] ○, single-crystal alpha alumina. △, single-crystal beryllia. ▲, single-crystal magnesia, undoped. ×, single-crystal magnesia, iron doped. +, single-crystal magnesia, zirconia doped. *, single-crystal magnesia, nickel doped. □, fused zirconia, undoped. ■, fused zirconia, calcia doped. ◊, single-crystal zirconia, undoped. ♦, single-crystal zirconia, yttria doped.

amount of oxygen present in the atmosphere over the specimens during the postirradiation heating, so that a change in stoichiometry cannot be the cause of the burst for these oxides. Increased release due to radiation damage of the specimen surface may be a possible mechanism.[17] Diffusion coefficients calculated from the slopes of the release curves, assuming a simple diffusion model for release after the burst, are given in Fig. 3 for the ceramic oxides studied.[35–38] The diffusion coefficients are insensitive to the nature of the oxide, and, for $\alpha$-$Al_2O_3$, a correspondence between xenon and oxygen diffusion coefficients has been shown.[35]

In the fundamental investigations, the inert gases are introduced into the crystal lattices by processes that give rise to lower energy recoils, such as $K^{41}(n,p)Ar^{41}$ and $Ca^{44}(n,\alpha)Ar^{41}$ reactions,[39,40,43] alpha decay of thorium to give radon,[42] and gas discharge.[41] For the release of argon from single-crystal samples of $CaF_2$ (Ref. 43), KF, and KCl (Ref. 39) during diffusion anneals, a pure volume-diffusion release with no heating bursts was observed. In pressed-powder pellets of KF, heating bursts were observed.[39] Heating bursts have also been reported in the release of radon and xenon from polycrystalline samples of alkali-metal chlorides.[41] The burst release in alkali halides is thought to occur during the recovery of radiation damage to the surface. The fundamental rare-gas studies[39] have suggested also that grain-size distribution, recrystallization, closed pores, damage to the crystal in the nuclear recoil range, general lattice damage caused by radiation, and temperature gradients may influence inert-gas behavior in ionic solids.

## Graphite

The release of fission gas from graphite has been studied by a number of workers.[44–50] The fission gas is introduced into the graphite during irradiation by recoil from a fuel material in contact with the graphite. The release process is complex, but a number of significant features have been noted. As in the case of fission-gas release from $UO_2$ and the uranium carbides, a heating burst persists for a short period of time, followed by an apparent diffusional release for up to 5 or 6 hr of heating.[46] For longer heating times, the rate of release decreases, but, between 16 and 250 hr, the cumulative release is again linear with the square root of the heating time.[49] This suggests that trapping of gas atoms may be occurring during the diffusion anneal. A difference exists between the observed release patterns from laminar and columnar type pyrolytic carbon, and this difference too has been associated with trapping of fission gas.[50]

From their experiments with graphites of various particle sizes, Findlay and Laing[49] concluded that release from the individual crystallites in graphite is not the sole rate-controlling process. They observed two activation energies for diffusion of xenon in graphite: 17 kcal/mole below 1000°C and 53 kcal/mole from 1000 to 1400°C. Yajima et al.[48] have observed peaks in the release curves in differential-heating experiments. As the fission-product concentration increased from $10^{11}$ to $10^{18}$ fission-product atoms per cubic centimeter, the observed peak in the differential release curve near 1000°C shifted to higher temperatures. The peak shift is postulated to be due to trapping of fission-gas atoms in sites requiring higher activation energy for removal as the fission-product concentration is increased. The existence of trapping sites of various energies may in part explain the two activation energies found by Findlay and Laing.

## Conclusions

The complex behavior of fission gases in reactor materials is still most conveniently described as a diffusion process. However, it is now realized that availability of gas atoms for diffusion may be modified by surface or subsurface processes which give rise to variations in the rate of release from that expected from a strictly diffusional process. One of the more likely causes of these variations in rate of release may be the existence of trapping sites for gas atoms, which may be closed pores or other defects initially present in the material or which may be radiation-induced defects. The trapping process tends to retard the later stages of release. If trapping sites do exist, release may be complicated since it may be dependent upon a spectrum of activation energies rather than on the single activation energy expected for a diffusion process. Finally, nondiffusional processes with respect to the gas atoms, such as grain growth and vaporization, may influence the fission-gas behavior under some conditions.

## References


1. A. H. Booth and G. T. Rymer, Determination of the Diffusion Constant of Fission Xenon in $UO_2$ Crystals and Sintered Compacts, Canadian Report CRDC-720, August 1958.
2. B. Lustman, Release of Fission Gases from $UO_2$, USAEC Report WAPD-173, Westinghouse Electric Corp., Bettis Atomic Power Laboratory, March 1957.
3. J. Belle, *Uranium Dioxide: Properties and Nuclear Applications*, U. S. Government Printing Office, Washington, 1961.
4. W. B. Cottrell, H. N. Culver, J. L. Scott, and M. M. Yarosh, Fission-Product Release from $UO_2$, USAEC Report ORNL-2935, Oak Ridge National Laboratory, Sept. 13, 1960.
5. Fission-Product Release from $UO_2$, *Nucl. Safety*, 1(2): 14-15 (December 1959).
6. Fission-Gas Release from Reactor Fuels, *Nucl. Safety*, 2(2): 20-22 (December 1960).
7. Fission-Product Release from $UO_2$, *Nucl. Safety*, 3(2): 15-20 (December 1961).
8. Fission-Product Release from $UO_2$, *Nucl. Safety*, 4(1): 35-42 (September 1962).
9. W. B. Lewis, Behaviour of Fission Gases in $UO_2$ Fuel, Canadian Report DL-45, November 1961.
10. D. F. Toner and J. L. Scott, Study of Factors Controlling the Release of Xenon-133 from Bulk $UO_2$, in *Proceedings of the Symposium on Radiation Effects in Refractory Fuel Compounds*, June 27-28, 1961, American Society for Testing and Materials.
11. J. B. Melehan, R. H. Barnes, J. E. Gates, and F. A. Rough, Release of Fission Gases from $UO_2$ During and After Irradiation, USAEC Report BMI-1623, Battelle Memorial Institute, Mar. 26, 1963.
12. W. H. Stevens, J. R. MacEwan, and A. M. Ross, The Diffusion Behavior of Fission Xenon in Uranium Dioxide, in Nuclear Reactor Chemistry. First Conference, Gatlinburg, Tennessee, October 12–14, 1960, USAEC Report TID-7610 (pp. 7-22), October 1960.
13. J. L. Berry, R. Darras, H. Chevilliard, and T. Gerevini, Contribution á l'Étude de l'Echappement des Gaz de Fission Hor de l'Oxyde d'Uranium Fritte Irradie, *J. Nucl. Mater.*, 8(1): 102-115 (1963).
14. R. M. Carroll, Fission-Gas Release from Single-Crystal $UO_2$ During Irradiation, *Trans. Am. Nucl. Soc.*, 6(1): 121 (June 1963).
15. F. J. Stubbs and G. N. Walton, Fission Gas Emission During Temperature Changes in a Reactor, British Report AERE-R-3093, October 1959.
16. R. Lindner and H. J. Matzke, Diffusion of $Xe^{133}$ in Uranium Oxide of Different Oxygen Contents, *Z. Naturforsch.*, 14a: 582-584 (1959).
17. R. Kelly, The Diffusion of "Attached" Inert-Gas Activity, *Can. J. Chem.*, 39: 2411-2422 (1961).
18. W. A. Bostrom, as reported in Ref. 3, p. 509.
19. G. Frigerio, contribution to VIII Congresso Nuclear organizzato dal CNEN, presented at Symposium on Ceramic Type Fuel Elements for Power Reactors, Rome, June 19-20, 1963.
20. J. A. L. Robertson, High Temperature Properties of Ceramic Fuels: Their Significance and Measurement, Canadian Report AECL-1529, June 1962.
21. D. G. Hurst, Diffusion of Fission Gas: Calculated Diffusion from a Sphere Taking into Account Trapping and Return from Traps, Canadian Report AECL-1550, Nov. 15, 1962.
22. E. Rothwell, The Release of $Kr^{85}$ from Irradiated Uranium Dioxide on Postirradiation Annealing, *J. Nucl. Mater.*, 5: 241-249 (1962).
23. G. W. Parker, G. E. Creek, and W. J. Martin, Fission Product Release from $UO_2$ by High Temperature Diffusion and Melting in Helium and Air, USAEC Report CF-60-12-14, Oak Ridge National Laboratory, Feb. 14, 1961.
24. R. M. Carroll, The Continuous Release of Fission Gas from $UO_2$ During Irradiation, in *Proceedings of the Symposium on Radiation Effects in Refractory Fuel Compounds*, June 27-28, 1961, American Society for Testing and Materials.
25. G. Long, D. Davies, and J. R. Findlay, Diffusion of Fission Products in Uranium Dioxide and Uranium Monocarbide, in Nuclear Reactor Chemistry. First Conference, Gatlinburg, Tennessee, October 12–14, 1960, USAEC Report TID-7610, pp. 1 and 2, October 1960.
26. R. W. Endebrock (Ed.), Properties of Fuels for High-Temperature Reactor Concepts, USAEC Report BMI-1598, Battelle Memorial Institute, Nov. 1, 1962.
27. G. W. Cunningham, J. J. Ward, and C. A. Alexander, Thermodynamics for Compatibility Studies of Metal-Clad Uranium Carbide, USAEC Report BMI-1601, Battelle Memorial Institute, Oct. 30, 1962.
28. R. Lindner and H. Matzke, Diffusion Radioaktiven Edelgase in Uranoxyden und Uranmonokarbid, *Z. Naturforsch.*, 14a: 1074 (1959).
29. H. Shaked, Diffusion of Xenon in Uranium Monocarbide (Thesis), USAEC Report UCRL-10462, University of California, Nov. 7, 1962.
30. H. Shaked, D. R. Olander, and T. H. Pigford, Diffusion of $Xe^{133}$ in Uranium Monocarbide, *Trans. Am. Nucl. Soc.*, 6(1): 131 (June 1963).
31. L. R. Zumwalt, P. E. Gethard, and E. E. Anderson, Fission-Product Release from "Single Crystal" $UC_2$ Particles, *Trans. Am. Nucl. Soc.*, 6(1): 132 (June 1963).
32. A. Auskern and Y. Osawa, Xenon Diffusion in Uranium Carbide Powder, *J. Nucl. Mater.*, 6: 334 (1962).
33. P. Schmeling, Preliminary Results on the Release of Xenon-133 from Uranium Monocarbide Powder, Technical Report No. 5, November 11, 1961, to March 12, 1962, USAEC Report EURAEC-361, Hahn-Meitner-Institut für Kernforschung, 1962.

34. D. L. Morrison, Battelle Memorial Institute, unpublished data.
35. D. L. Morrison, R. H. Barnes, T. S. Elleman, and D. N. Sunderman, Postirradiation Release of Xenon-133 from Single-Crystal Alpha Alumina, USAEC Report BMI-1592, Battelle Memorial Institute, Aug. 23, 1962.
36. Battelle Memorial Institute, Progress Relating to Civilian Applications During May 1962, USAEC Report BMI-1581(Del.), June 1, 1962.
37. Battelle Memorial Institute, Progress Relating to Civilian Applications During June 1962, USAEC Report BMI-1583(Del.), July 1, 1962.
38. Battelle Memorial Institute, Progress Relating to Civilian Applications During December 1962, USAEC Report BMI-1607(Del.), Jan. 1, 1963.
39. Diffusion of Rare Gases in Solids, Final Report, September 1961 to August 1962, USAEC Report EURAEC-526, Hahn-Meitner-Institut für Kernforschung, December 1962.
40. Rare Gas Diffusion in Solids, Final Report No. 1, July 1, 1960, to August 31, 1961, USAEC Report EURAEC-312, Hahn-Meitner-Institut für Kernforschung, Apr. 17, 1962.
41. C. Jech, Release of Inert Gas Label from Ionic Crystals During Thermal Treatment, *Phys. Stat. Solids*, 2: 1299 (1962).
42. J. S. Anderson, D. J. M. Bevan, and J. P. Burden, The Behavior of Recoil Atoms in Ionic Solids, *Proc. Roy. Soc. (London), Ser. A*, 272: 15 (February 1963).
43. T. Lagerwall, Diffusion of Argon-41 in Calcium Fluoride, *Nukleonik*, 4: 158 (1962).
44. D. Cubicciotti, The Diffusion of Xenon from Uranium Carbide Impregnated Graphite at High Temperatures, USAEC Report NAA-SR-194, North American Aviation, Inc., Oct. 13, 1952.
45. G. N. Walton, The Migration of Fission Products in Graphite, *Nucl. Eng.*, 7: 97 (March 1962).
46. T. Nakai, S. Yajima, K. Shiba, J. Osugi, and D. Shinodu, The Behavior of Fission Products Captured in Graphite by Nuclear Recoil. II. The Diffusion of Xenon-135 in Graphite at a High Temperature, *Bull. Chem. Soc. Japan*, 33: 497 (1960).
47. S. Yajima, S. Ichiba, Y. Kamemoto, K. Shiba, and M. Kosi, The Behavior of Fission Products Captured in Graphite Powder by Nuclear Recoil. IV. Further Studies on the Diffusion of Xenon-133 in Graphite, *Bull. Chem. Soc. Japan*, 34: 697 (1961).
48. S. Yajima, S. Ichiba, K. Imamoto, and K. Shiba, The Behavior of Fission Products Captured in Graphite Powder by Nuclear Recoil. V. Effect of Fission Fragment Damage on the Diffusion of Fission Product Xenon, *Bull. Chem. Soc. Japan*, 35: 1263 (1962).
49. J. R. Findlay and T. F. Laing, The Diffusion of Fission Products from Graphite, *J. Nucl. Mater.*, 7: 182 (1962).
50. D. L. Morrison, T. S. Elleman, R. H. Barnes, and D. N. Sunderman, Postirradiation Release of $Xe^{133}$ from Pyrolytic Carbon, USAEC Report BMI-1634, Battelle Memorial Institute, June 3, 1963.

Section

I

Reactor Materials

# Fuel and Fertile Materials

## Uranium Metal and Alloys

### Unalloyed Uranium

The phase transformations of uranium at high pressures were studied by Livermore.[1] The alpha-beta-, beta-gamma-, and alpha-gamma-phase transformations in uranium were studied up to 45 kilobars at cooling and heating rates of 3 to 5°C/sec. The overheating and undercooling intervals for the alpha-beta and beta-gamma transformations at high pressures are about the same as the hystereses expected at zero pressure and do not vary appreciably with increasing contamination. Progressive contamination and resultant lowering of the transformation temperatures of the uranium samples were evident for all containers used but were least for tantalum containers. The equilibrium alpha-beta-gamma triple point occurs at less than 31.5 kilobars and at greater than 803°C. The gamma phase is definitely more compressible than the beta phase, and the beta phase is probably more compressible than alpha. There is only a small hysteresis in the alpha-gamma transformation.

The British[2] have performed experiments to study the effects of temperature cycling on alpha-uranium polycrystals undergoing steady-state creep. The results of these experiments are discussed in terms of the internal stresses generated by anisotropic expansion of individual crystals in the aggregate; a theory that was developed earlier is extended to cover the case of large temperature cycles when the physical properties of uranium polycrystals vary during the cycle. An analogy between this theory and Parkes' theory of thermally induced stresses in engineering structures is pointed out, and it is shown that deformations caused by thermal transients may comprehensively be understood in terms of elastic cycling, shakedown, and incremental collapse.

The British[3] have shown that a pseudo-creep effect arises when small stresses act on uranium fuel bars that have a central beta core that varies in size. The pseudo-creep process is analyzed in detail and its magnitude is estimated. The effect is most severe when the beta core fluctuates about a critical radius, and it can predominate over creep effects arising from thermal cycling of the alpha phase.

Hanford[4] irradiated Zircaloy-2-clad uranium rods in NaK-filled capsules. It was shown that the rods exhibit significant increases in volume at uranium volume average temperatures of 400°C and above. Also, at uranium irradiation temperatures of 450°C and above, uranium cracking becomes significant. The swelling results are shown in Fig. I-1.

Circumferential cladding strains as large as 6% were measured on a high-temperature rod without indications of cladding failure, whereas a brittle cladding failure occurred on a lower-temperature rod at less than 2% cladding strain. Irradiation damage to the lower-temperature cladding may be in part responsible for the low-strain failure; however, the possibility exists that NaK interaction with the Zircaloy-2 may play a role in this failure.

Livermore[5] describes the use of ultrasonics for uranium grain-size measurements, and the British[6] report an improved method of visual presentation of ultrasonic measurements on coarse-grained uranium.

Battelle[7] investigators determined the coefficient of friction between uranium and steel at high alpha-uranium temperatures to be approximately 0.25 to 0.33.

The results of a study on inclusions in uranium have been published by Columbia University.[8] (M. S. Farkas)

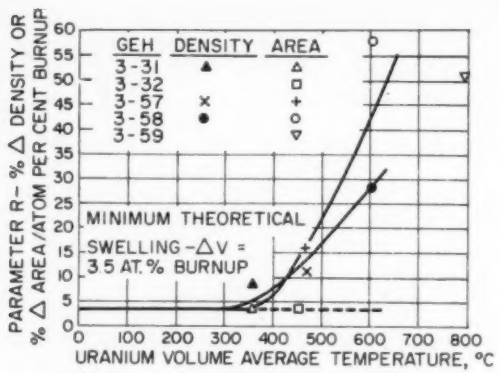
PARAMETER R – % Δ DENSITY OR % Δ AREA/ATOM PER CENT BURNUP
URANIUM VOLUME AVERAGE TEMPERATURE, °C
GEH DENSITY AREA
3-31
3-32
3-57
3-58
3-59
MINIMUM THEORETICAL SWELLING – ΔV = 3.5 AT.% BURNUP
0 5 10 15 20 25 30 35 40 45 50 55 60
0 100 200 300 400 500 600 700 800

Fig. I-1 Density and cross-sectional area change of Zircaloy-2-clad unalloyed uranium as a function of temperature.[4]

## Alpha-Uranium Alloys

The British[9] have reported on the transformations that occur when uranium-molybdenum alloys in the 0.9 to 4.17 at.% composition range are cooled at various rates from the gamma-phase field. The sequence of phases observed at various cooling rates has been elucidated. It has been shown that there is direct transformation from gamma to alpha or alpha plus gamma for alloys containing 2.5 at.% or more of molybdenum and that the gamma-grain size has an effect on the decomposition product.

Investigations of the transformation characteristics of uranium–2.5 and 5 at.% niobium alloys have been reported by the French.[10,11] In another report[12] the time-temperature-transformation curves for uranium-chromium alloys containing 0.37, 0.6, 2, and 4 at.% chromium are given.

The Israel Atomic Energy Commission[13] has reported on dilute uranium-chromium alloys. The grain refinement of alloys containing 0.3, 0.45, and 0.6 at.% chromium was studied. Samples were isothermally transformed from beta to alpha in the temperature range 600 to 300°C. The transformation temperature that produced the finest grain size decreased with increasing chromium content. The range of isothermal transformation temperatures and of chromium contents yielding maximum grain refinement was determined. In another study[14] the grain growth occurring when heat-treated uranium–0.45 at.% chromium alloy samples are annealed for long periods at high temperatures in the alpha range was investigated. Maximum growth (by a factor of 2) was found in a sample isothermally transformed at 525°C and annealed for 100 hr at 625°C. This low rate of grain growth at elevated temperatures is a point in favor for the use of this alloy as a nuclear fuel.

The ternary system uranium-aluminum-iron has been completed by German investigators.[15] The phase relations were determined in the uranium-rich portion up to the quasi-binary section, $UFe_2$-$UAl_2$. Typical for the system in the solid state are the extended three-phase equilibria. Uranium solid solutions show a limited ternary solubility, but not the intermetallic compounds $UAl_2$, $U(Fe,Al)_2$, $UFe_2$, and $U_6Fe$.

The behavior of neutron-irradiated, metastable beta-phase uranium-base alloys has been investigated by Nuclear Metals.[16] Materials irradiated were unalloyed uranium, uranium–0.3 wt.% chromium, and uranium–0.3 wt.% chromium–0.3 wt.% molybdenum with various metallurgical histories.

The irradiation experiments were designed to yield maximum central metal temperatures of 450°C and burnups of 0.01 and 0.3 at.% in thermal-neutron fluxes of $10^{13}$ nv; actual conditions produced temperatures of 340 to 430°C and burnups of about 0.006 and 0.3 at.% in a flux of $0.5 \times 10^{13}$ nv.

The data indicate that irradiation behavior of the beta-phase uranium alloys is related to grain size, composition, and texture. In all cases the beta phase transformed to alpha in varying amounts depending on the above metallurgical parameters. The most promising of these materials are the beta-quenched binary and ternary alloys, which exhibited a 1% increase in density compared to the 1% decrease of the alpha specimens. (M. S. Farkas)

## Gamma-Phase Uranium Alloys

Time-temperature-transformation diagrams for a series of uranium-molybdenum base alloys, including uranium–10 wt.% molybdenum, uranium–8 wt.% molybdenum, and uranium–8 wt.% molybdenum–½ and 1 wt.% titanium have been developed by Case Institute researchers.[17] Metallographic techniques developed for phase-identification purposes are described.

Epitaxial relations between oxide formed on gamma-phase uranium–7 wt.% molybdenum and

uranium–10 wt.% niobium alloys have been studied at Los Alamos.[18] Highly oriented oxide films formed on cold-rolled specimens of these alloys with the dodecahedral planes of the oxide parallel to the specimen surface. The oxide film on the niobium alloy was more highly oriented than that on the molybdenum alloy. It is speculated that the large oxide-metal mismatch could strain the alloy inhomogeneously and lead to fracture.

The uranium–14 wt.% molybdenum alloy was successfully rolled at 950°C to a total 30% reduction at Argonne.[19] However, although the alloy can be rolled to a ½-in.-diameter bar (about 80% reduction) at 1000°C, it cracks on rolling at 950°C. Attempts to coextrude the alloy with a Zircaloy cladding at 1000°C were unsatisfactory, probably because of the large differences in strength of the two materials.

(A. A. Bauer)

# Plutonium

## Plutonium Alloys

Hanford investigators have shown that plastic deformation decreases the beta-to-alpha transformation rate in plutonium.[20] This supports the contention that the beta-to-alpha transformation is a nucleation and shear reaction. Further support was obtained when bands of columnar alpha grains increased in number rather than size when transformation was allowed to proceed under a compressive stress.

Los Alamos is continuing studies of plutonium–rare-earth alloy systems.[21] Plutonium and europium form immiscible liquids, and there apparently is little or no solubility of plutonium in europium or of europium in plutonium.

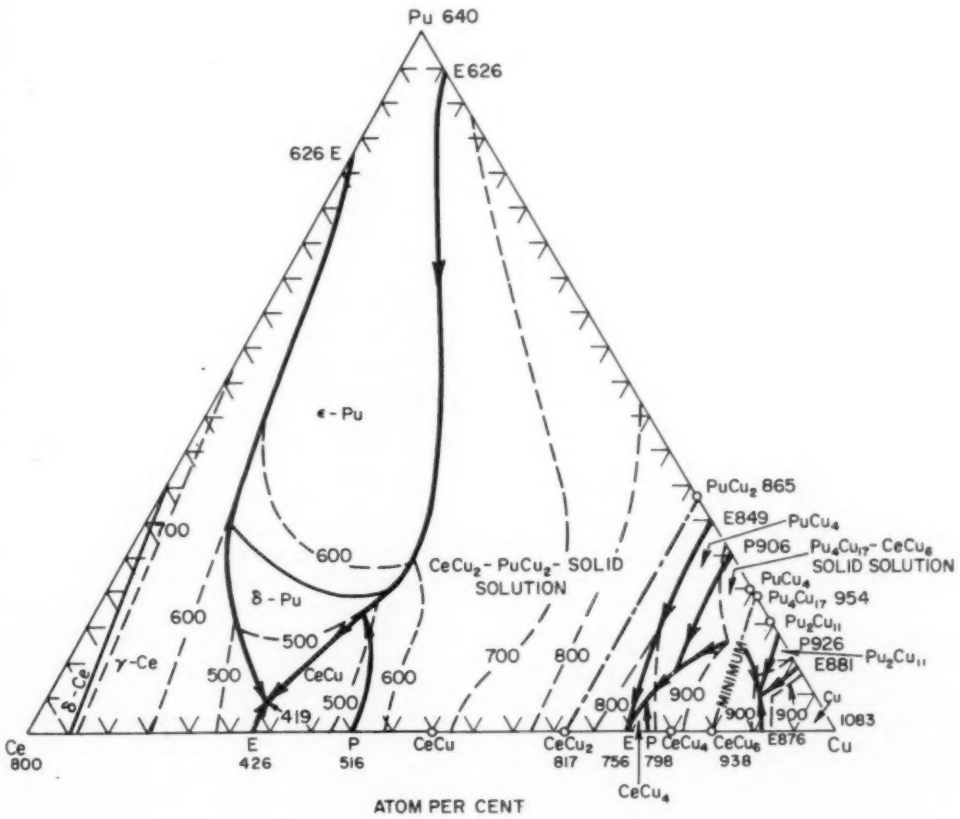


Fig. I-2 Plutonium-cerium-copper phase diagram.[22]

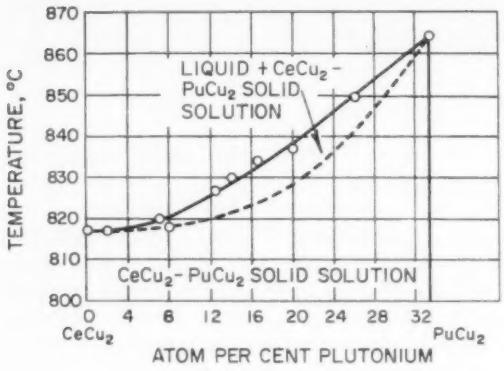


Fig. I-3 $CeCu_2$-$PuCu_2$ quasi-binary system.[22]

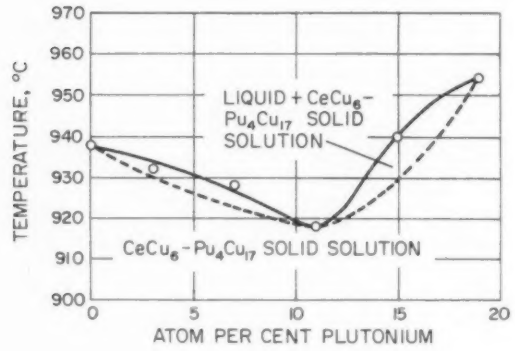


Fig. I-4 $CeCu_6$-$Pu_4Cu_{17}$ solid solution quasi-binary system.[22]

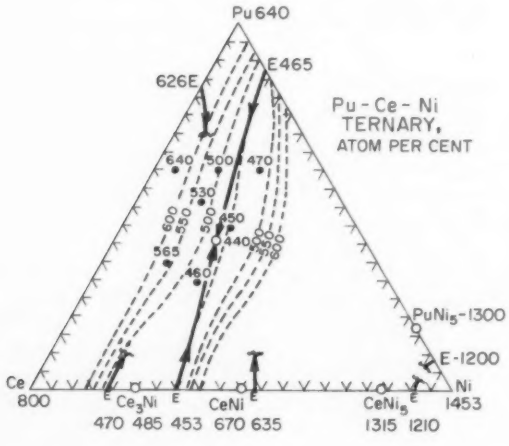


Fig. I-5 Plutonium-cerium-nickel ternary diagram.[22]

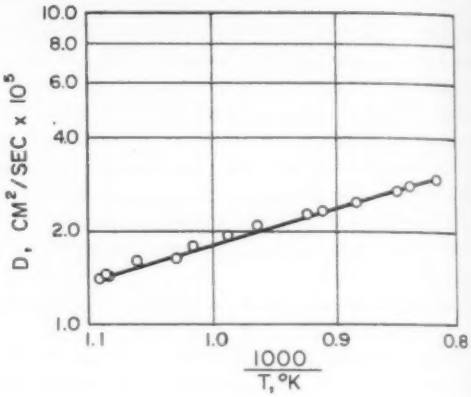


Fig. I-6 Self-diffusion of molten plutonium as a function of reciprocal absolute temperature.[23]

Table I-1 $Pu^{238}$-SEA-WATER REACTION AND SOLUBILITY STUDIES[24]

| Sample | Weight, g | Sea-water, ml | Reacted sample, g | Reaction time | $Pu^{238}$ solubility, mg/ml |
|---|---|---|---|---|---|
| 1 | 0.366 | 250 | 0.209 | 90 min | 0.0016 |
| 2 | 0.711 | 300 | 0.368 | 70 min | 0.0007 |
| 3 | 0.504 | 250 | Total | ~60 hr | Not available |
| 4 | 0.675 | 250 | Total | >4 hr | Not available |
| 5 | 0.363 | 250 | Total | ~12 hr | Not available |
| 6 | 0.086 | 250 | 0.046 | 95 min | Not available |

Solubility of plutonium in praseodymium increases with temperature and reaches a maximum of 30 at.% at about 800°C. At 450°C the maximum solubility is 16 ± 1 at.% plutonium. Alpha praseodymium forms peritectically with the peritectic horizontal extending from about 25 to 90 at.% praseodymium. The temperature of the eutectic reaction, liquid ⇌ epsilon plutonium plus alpha praseodymium, is 626 ± 2°C and that of the peritectoid reaction, epsilon plutonium plus alpha praseodymium ⇌ delta plutonium, is 484 ± 1°C.

Maximum solubility of plutonium in scandium is about 20 at.%. Epsilon plutonium and beta scandium appear to form a continuous series of solid solutions at least up to 25 at.% scandium. A peritectoid reaction, epsilon plutonium – beta scandium solid solution plus alpha scandium ⇌ delta plutonium, was found at 663°C and about 25 at.% scandium. The lattice parameter of a delta plutonium – 15 at.% scandium alloy was found to be 4.532 ± 0.0001 A. Calculated density

for the alloy is 13.84 g/cm$^3$ as compared with a measured density of 13.85 g/cm$^3$.

Maximum solubility of yttrium in delta plutonium appears to be low. Maximum solubility of plutonium in yttrium is about 20 at.%.

Investigations of Los Alamos Molten-Plutonium Reactor Experiment (LAMPRE) type fuels are continuing. Preliminary experiments at 800°C show that carbon additions to plutonium-cobalt-cerium alloys containing 5 g of plutonium per cubic centimeter decrease the thickness of the $Ta_6Co_7$ reaction layer.

Plutonium additions to a uranium-manganese alloy were found to have a beneficial effect on the corrosion resistance of yttrium capsules. After 500 hr at 900°C, a uranium–5 at.% plutonium–22 at.% manganese alloy had penetrated less than 1 mil of yttrium. Under similar conditions a uranium–22 at.% manganese alloy penetrated 2.5 mils of yttrium.

Mound Laboratory[22] is continuing the investigation of phase equilibria in plutonium-alloy systems. The plutonium-cerium-copper ternary system is shown in Fig. I-2, and the quasi-binary systems $CeCu_2$-$PuCu_2$ and $CeCu_6$-$Pu_4Cu_{17}$ are shown in Figs. I-3 and I-4. The lowest melting ternary eutectic found in the system is at plutonium–68 at.% cerium–28 at.% copper which melts at 417°C. A preliminary survey of the plutonium-cerium-nickel system by differential thermal analysis has resulted in the temperature contours shown in the phase diagram in Fig. I-5.

Self-diffusion of liquid plutonium as estimated by viscosity measurements[23] is shown in Fig. I-6.

Table I-2 EFFECT OF COMPOSITION AND HEAT-TREATMENT ON AMBIENT-TEMPERATURE STRENGTH OF INJECTION-CAST URANIUM-PLUTONIUM ALLOYS[19]

| Composition (balance U), wt.% | Heat-treatment | Fracture force, lb | Maximum stress at fracture, psi | Average stress at fracture, psi |
|---|---|---|---|---|
| 10 Pu | As-cast | 1,062 | 119,800 | 60,960 |
| 10 Pu–10 Fz | As-cast | 920 | 103,800 | 59,600 |
| 20 Pu–10 Fz | As-cast | 575 | 64,900 | 33,000 |
| 10 Pu | 48 hr at 900°C, 2 hr at 450°C, furnace cool | 1,152 | 129,900 | 66,120 |
| 10 Pu–10 Fz | 24 hr at 750°C, 144 hr at 800°C, 48 hr at 650°C, oil quench | 1,720 | 194,000 | 111,400 |
| 20 Pu–10 Fz | 192 hr at 780°C, oil quench | 1,319 | 148,800 | 85,400 |
| 10 Pu–10 Fz | 24 hr at 750°C, 144 hr at 800°C, 168 hr at 450°C, furnace cool | 1,050 | 118,400 | 60,300 |

Table I-3 STRESS DEPENDENCE OF MINIMUM STRAIN RATE FOR URANIUM–10 WT.% PLUTONIUM AND URANIUM–10 WT.% PLUTONIUM–10 WT.% FIZZIUM[19]

| Composition (balance U), wt.% | Temp., °C | Strain rate ($\dot{\epsilon}$), in./(in.)(min), in terms of stress ($\sigma$), psi | Testing conditions: Stress ($\sigma$), psi | Testing conditions: Strain rate ($\dot{\epsilon}$), in./(in.)(min) | Fracture strain ($\bar{\epsilon}_f$), in./in. |
|---|---|---|---|---|---|
| 10 Pu | 300 | $\sigma\ 3.63 \times 10^{-26}\ \sigma^{5.64}$ | 9,000–14,000 | $4 \times 10^{-6}$–$3 \times 10^{-5}$ | Specimen failed prematurely at macroscopic defect |
| 10 Pu | 550 | $7.89 \times 10^{-18}\ \sigma^{3.68} \pm 15\%$ | 3,500–7,500 | $1 \times 10^{-6}$–$2 \times 10^{-6}$ | 0.015 |
| 10 Pu–10 Fz | 409 | $9.99 \times 10^{-7} \exp(3.51 \times 10^{-4})\sigma \pm 15\%$ | 12,000–25,000 | $1 \times 10^{-6}$–$5 \times 10^{-6}$ | 0.0288 |
| 10 Pu–10 Fz | 551 | $2.20 \times 10^{-7} \exp(8.45 \times 10^{-4})\sigma \pm 8\%$ | 3,500–7,500 | $4 \times 10^{-6}$–$2 \times 10^{-4}$ | 0.0185 |

Table I-4 TIME FOR 1% CREEP AT A SURFACE TEMPERATURE OF 550°C WITH AND WITHOUT STRESS RELAXATION IN A URANIUM–10 WT.% PLUTONIUM–10 WT.% FIZZIUM 0.144-IN.-DIAMETER FUEL PIN[19]

| Power, watts/cm³ | ΔT, °C | Effective surface stress, psi | Time for 1% creep under effective stress, hr | Time for 1% creep with stress relaxation, hr |
|---|---|---|---|---|
| 1,735 | 50 | 6,300 | 3.5 | Stress relaxed before 1% creep |
| 4,000 | 115 | 14,600 | $2.9 \times 10^{-3}$ | 3,350 |
| 5,205 | 150 | 18,600 | $9.3 \times 10^{-5}$ | 106 |

Table I-5 WIDTH OF DIFFUSION BANDS[19]

(All Compositions in Weight Percent and Versus Niobium)

| Temp., °C | Width, mils | | | | | |
|---|---|---|---|---|---|---|
| | 7-day anneal | | 17-day anneal | | 42-day anneal | |
| | U–10 Pu–10 Fz | U–20 Pu–10 Fz | U–10 Pu–10 Fz | U–20 Pu–10 Fz | U–10 Pu–10 Fz | U–20 Pu–10 Fz |
| 550 | 0.12 | 0.25 | 0.19 | 0.34 | 0.22 | 0.50 |
| 600 | 0.28 | 0.47 | 0.41 | 0.78 | 0.63 | 1.44 |
| 650 | 0.59 | 1.00 | 1.16 | 2.94 | 3.16 | 6.70 |

The reaction and solubility of $Pu^{238}$ in seawater has been studied. Results are listed[24] in Table I-1.

Argonne has reported some of the mechanical properties of uranium-plutonium and uranium-plutonium-fizzium alloys.[19] Mechanical strength data are tabulated in Table I-2. Creep data are shown in Tables I-3 and I-4. A technique has been devised for rolling the uranium–20 wt.% plutonium–10 wt.% fizzium alloy to foil. Previously, the alloy was considered too brittle to permit rolling. The alloy casting was jacketed in a cold-rolled steel pack and rolled in the temperature range 590 to 620°C. Alumina and Aquadag were used to prevent reaction between the alloy and steel. Results of compatibility studies of uranium-plutonium-fizzium alloys and niobium are shown in Table I-5. Interdiffusion bands appeared to form almost completely in the niobium. (V. W. Storhok)

## Plutonium Compounds

Studies on the spheroidization of $PuO_2$ mixed with other oxides have been reported by Mound.[25] Lattice parameters for $PuO_2$–10 wt.% $UO_2$ and $PuO_2$–20 wt.% $UO_2$ were measured as 5.4023 ± 0.0005 A and 5.4008 ± 0.0005 A, respectively. These values are slightly lower than predicted from Vegard's law, and this anomaly is postulated to be due to inhomogeneity or incomplete solution of $UO_2$ in $PuO_2$. Mound has also attempted the preparation of solid solutions[23] between $PuO_2$ and $ZrO_2$. $ZrO_2$–5 wt.% $PuO_2$ mixtures resulted in a monoclinic $ZrO_2$ structure, whereas a $ZrO_2$–45 wt.% $PuO_2$ composition was determined by X-ray diffraction to consist entirely of stabilized cubic $ZrO_2$.

Investigations at Nuclear Materials[26] have demonstrated that no visual evidence of corrosion product was noted after 100 hr in 680°F water for the composition range 0.5 to 100 wt.% $PuO_2$–$UO_2$ solid solutions. The same report presents evidence that there is no reaction between either type 304 or 316 austenitic stainless steels and any $PuO_2$-$UO_2$ composition at 1000°C. Hanford workers[27] have extensively investigated reduction of $PuO_2$ by carbon. Results of sintering various mixtures at 1300 to 1400°C for 6 hr in flowing helium are summarized in Table I-6. The data suggest that the formation of PuC by carbon reduction of $PuO_2$ may proceed by the following route:

$$PuO_2 \xrightarrow{+C} \alpha\ Pu_2O_3 \xrightarrow{+C} \beta\ Pu_2O_3$$

$$\xrightarrow{+C} Pu_2C_3 \xrightarrow{+\beta\ Pu_2O_3} PuC$$

A recent European report[28] essentially substantiates these data as well as previously reported

Hanford data concerning a eutectic between β $Pu_2O_3$ and PuO at approximately 1780°C.

In regard to the preparation of $PuO_2$, Mound has obtained indications that it is feasible to convert metallic plutonium to the dioxide without utilizing the hydroxide precipitation step.[23] Belgian workers[29] report that peroxide precipitates are less sinterable than oxalate precipitated material and consist of more perfect crystalline structure than the latter.

$PuO_2$-MgO mixtures have been shown to be immiscible in all proportions, with no stable compound formation.[27] MgO–13.52 wt.% $PuO_2$ irradiated to an exposure of $0.5 \times 10^{20}$ fissions/$cm^3$ at a maximum calculated core temperature of 1700°C showed no crystallographic change, as determined by X-ray techniques.[30] Data for irradiated $UO_2$-$PuO_2$ mixtures[27] are presented in Table I-7. In irradiation studies by Argonne,[19] PuC (6.22 wt.% carbon) was irradiated to 5.3% metal atom burnup at a surface temperature of 570°C, which resulted in the rupture of the specimen for undetermined reasons. UC–20 wt.% PuC specimens irradiated to 2.2% metal atom burnup are still in the reactor operating satisfactorily at a surface temperature of 380 to 625°C.

Plutonium compounds exhibit spontaneous lattice expansion as a function of time. The most probable mechanism for lattice damage is the creation of Frenkel defects and residual helium atoms by alpha decay in the plutonium. Values of lattice parameters as a function of time[27] for various carbides are presented in Fig. I-7.

For $PuO_2$, a rate of lattice-parameter change of $0.35 \times 10^{-3}\ \Delta a/a$/100 days has been reported.[20]

Table I-6 $PuO_2$-CARBON REACTION PRODUCTS[27]

| Sample | Initial carbon, wt.% | Desired product | Carbon in reaction product, wt.% |
|---|---|---|---|
| 1 | 1.91 | $PuO_{1.86}$ | 1.1 |
| 2 | 1.66 | $PuO_{1.82}$ | 1.0 |
| 3 | 1.31 | $PuO_{1.76}$ | 0.60 |
| 4 | 1.22 | $PuO_{1.72}$ | 0.80 |
| 5 | 11.20 | PuC (46 at.% C) | 6.0 |
| 6 | 13.40 | $Pu_2C_3$ | 8.6 |
| 7 | 15.10 | $PuC_2$ | 10.2 |

Table I-7 MICROHARDNESS AND DENSITY DATA[27] FOR IRRADIATED $UO_2$-$PuO_2$

| Capsule (GEH-14-) | $UO_2$-$PuO_2$, mole % $PuO_2$ | Average exposure,* $10^{18}$ fissions/$cm^3$ | Approximate hardness,† KHN (500 g) | | Density, % of theoretical | | |
|---|---|---|---|---|---|---|---|
| | | | | | Measured | Estimated from hardness | |
| | | | Center | Average | Preirradiation | Preirradiation | Postirradiation |
| 20 | 0.0259 | 84 | 477 | 437 | 90 | | 89–92 |
| 91 | 0.0259 | 104 | 595 | 536 | 90 | | 92–96 |
| 82 | 1.02 | 160 | 627 | 570 | 93 | | 96–98 |
| 88 | 5.67 | 16 | 618 | 638 | 91 | 93–94 | 94–97 |
| 22 | 0.0259 | 72 | | 681 | 65 | | 98–100 |
| 66 | 0.187 | 79 | | 723 | 65 | | 98–100 |
| 68 | 1.46 | 110 | | 503 | 65 | | 91–93 |
| 69 | 3.47 | 116 | | 443 | 64 | | 88–90 |
| 71 | 5.46 | 104 | | 420 | 63 | | 87–89 |
| 73 | 7.45 | 113 | | 500 | 63 | | 91–93 |
| 66 (sphere) | | | | 543 | | | |
| 66 (core-to-cap interface) | | | | 198 | | | |
| 66 (Zircaloy-2 cap) | | | | 225 | | | |

*From flux-monitoring wire data.
†Center, average of three values; average, average of 13 to 19 values.

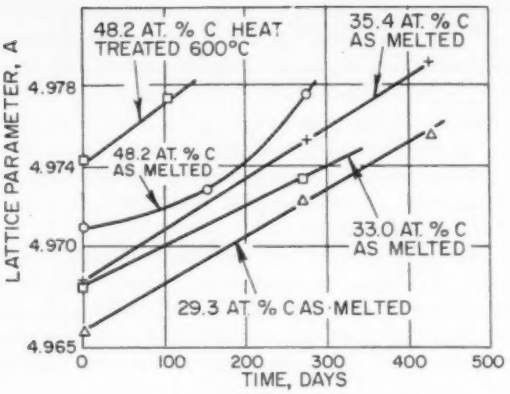


Fig. I-7 Lattice parameter change in PuC as a function of time.[27]

Rates per 100 days for β $Pu_2O_3$ are: $\Delta a/a = 0.7 \times 10^{-3}$, $\Delta c/c = 1.16 \times 10^{-3}$, $\Delta(c/a)/(c/a) = 0.43 \times 10^{-3}$.

It is reported[30] that PuN pellets slumped and flowed together after heating in flowing hydrogen for 12 hr at 1700°C, presumably due to the formation of metallic plutonium. Battelle[31] reports that PuN exists over a composition range, with lattice parameters decreasing with increased nitrogen content. The same source indicates that no visual attack was observed in PuN exposed to unpurified sodium for 6 hr at 600°C. Complete dissolution of PuN within 3 min in HCl or $H_3PO_4$ has been observed.[27]

PuC sintered 2 hr at 1400°C in vacuum showed no change in carbon content.[32] Such data are contradicted to some extent by another report[33] which indicates high volatility for PuC and PuN. This report also claims that 58% of the original plutonium content of a PuN pellet is lost after 30 min at 1700°C. Hanford[20] is also investigating this volatility, or decomposition, phenomenon and is preparing PuN–50 vol.% tungsten cermets by impaction techniques to eliminate the volatilization.[34] It is reported that approximately 60% of the mass of a PuN–50 vol.% AlN pellet volatilized in flowing helium during 12 hr at 1700°C (Ref. 34).

The sesquisulfide, $Pu_2S_3$, melts congruently at 1725 ± 10°C in a vacuum of $5 \times 10^{-3}$ mm Hg, as demonstrated by subsequent X-ray studies.[35] In argon, however, $Pu_2S_3$ was stable to 2300°C. No attack by boiling demineralized water was observed.[27]

An attempt by Hanford to prepare PuS by reacting plutonium chips with sulfur at 300°C for 20 hr produced PuS, some unreacted plutonium metal, and traces of $Pu_2O_2S$. The latter apparently stemmed from oxygen impurities in either the plutonium or the chamber atmosphere.[27]

Additional interesting data on the properties of mixed plutonium and uranium carbides have been obtained by British workers. An electrical resistivity value of 222 μohm-cm at 500°C has been reported for PuC containing 37.2 at.% carbon.[34] (W. M. Pardue)

# Thorium

Two thorium specimens have been irradiated to 0.18 and 0.92 at.% burnup by Hanford.[20] Hardness and density values for the specimens are shown below:

| Source of metal | Burnup, at.% | Hardness, $R_B$ | Density, g/cm³ | Volume increase, % |
|---|---|---|---|---|
| Battelle | 0.18 | 78 ± 1 | 11.67 ± 0.01 | 0 |
| Hanford | 0.92 | 65 ± 2 (center)<br>73 ± 2 (edge) | 11.50 ± 0.01 | 1.5 |

Battelle[36] investigators have reported results of an extensive survey of the properties of thorium-base alloys. Results of hot-hardness measurements, tensile tests, and creep tests are presented in Tables I-8 and I-9 and Figs. I-8 and I-9. Also, the effects of cold work and annealing on the hardness of the alloys are shown in Table I-10. (V. W. Storhok)

# Metal-Ceramic Fuels

## Dispersion Fuels

Plate type fuel elements containing a 37 wt.% fully enriched $UO_2$ loading in a matrix of 80 wt.% nickel–20 wt.% chromium clad with an 80 wt.% nickel–20 wt.% chromium alloy have been irradiated by workers at General Electric.[37] The first test was made for check-out purposes with a specimen temperature of 870°C for 100 hr. A burnup level of 1% of the $U^{235}$ atoms was determined, and postirradiation examination revealed no unusual surface defects besides the normal surface oxidation. The sec-

Table I-8 HOT HARDNESS OF AS-CAST THORIUM-BASE ALLOYS[36]

| Composition (balance Th), wt.% | Melting method | Thorium | Vickers hardness number, kg/mm² | | | | | | |
|---|---|---|---|---|---|---|---|---|---|
| | | | 25°C | 200°C | 400°C | 500°C | 600°C | 800°C | 900°C |
| 5 U* | Arc | Ames | 139 | 102 | 81.6 | 62.8 | 45.4 | 24.0 | 14.1 |
| | Arc | Iodide | 100 | 76.5 | 58.6 | 51.2 | 41 | | |
| | Induction | Ames | 134 | 100 | 73.9 | 65.4 | 45.1 | 9.0 | |
| 10 U* | Arc | Ames | 137 | 96.6 | 76.4 | 65.5 | 45.4 | 22.1 | 11.2 |
| | Arc | Iodide | 111 | | 71.5 | 59.5 | 44.0 | 17.1 | 10.6 |
| | Induction | Ames | 141 | 102 | 76.2 | 62.2 | 47.3 | 24.6 | |
| | Induction | Iodide | 104 | 80.5 | 66.3 | 55.4 | 38.8 | 18.8 | 11.8 |
| 15 U* | Arc | Ames | 145 | | 82.3 | 65.8 | 39.2 | 10.6 | 4.2 |
| | Arc | Iodide | 115 | 90.1 | 67.9 | 56.2 | 34.4 | 13.6 | |
| 20 U* | Arc | Ames | 148 | 120 | 90.0 | 68.6 | 46.2 | 14.0 | |
| | Arc | Iodide | 119 | 92.2 | 73.2 | 57.0 | 43.3 | | |
| | Induction | Ames | 148 | 101 | 78.5 | 66.0 | 41.8 | 15.3 | 10.2 |
| | Induction | Iodide | 118 | 102 | 82.5 | 59.3 | 37.5 | 12.5 | 9.2 |
| 10 U–1.5 Mo | Arc | Iodide | 72.9 | 59.4 | 54.4 | 48.4 | 41.1 | 22.4 | |
| | Induction | Ames | 121 | 99.6 | 82.0 | 77.3 | 73.3 | 43.3 | 30.4 |
| 10 U–2 Nb | Arc | Iodide | 89.4 | 71.3 | 60.7 | 57.2 | 42.7 | 20.3 | |
| | Induction | Ames | 112 | 88.0 | 78.0 | 74.3 | 58.7 | 30.1 | 23.4 |
| | Induction | Iodide | 84.7 | 65.2 | 59.4 | 57.6 | 54.1 | 33.1 | 20.4 |
| 10 U–10 Zr | Arc | Iodide | 161 | 152 | 128 | 116 | 54.5 | 22.2 | |
| | Induction | Ames | 173 | 152 | 141 | 120 | 68.7 | 23.2 | 14.5 |
| | Induction | Iodide | 172 | 142 | 133 | 125 | 69.7 | 23.9 | 13.4 |
| 10 U–10 Zr–2 Nb | Arc | Iodide | 138 | 119 | 110 | 96.4 | 73.2 | 17.2 | 8.5 |
| | Induction | Ames | 149 | 125 | 117 | 106 | 78.6 | 27.9 | 18.0 |
| 10 U–20 Zr | Arc | Iodide | 153 | | 140 | 109 | 42.4 | 10.7 | 7.1 |
| | Induction | Ames | 159 | 157 | 146 | 126 | 46.6 | 19.0 | 9.7 |
| 10 U–25 Zr | Arc | Ames | 153 | 191 | 191 | 129 | 38.0 | 6.9 | 3.4 |
| | Arc | Iodide | 160 | | 165 | 113 | 39.2 | 11.8 | 7.5 |
| | Induction | Ames | 161 | 171 | 186 | 130 | 40.7 | 14.7 | 8.1 |
| | Induction | Iodide | 171 | 157 | 131 | 129 | 46.7 | 17.3 | 9.0 |
| 10 U–0.1 Be | Arc | Ames | 110 | 91.0 | 76.0 | 73.8 | 69.1 | 27.3 | 17.6 |
| 10 U–0.2 Be | Arc | Ames | 110 | | 91.2 | 71.8 | 62.3 | 29.6 | 17.0 |
| 10 U–0.2 C | Arc | Ames | 24.7 | 137 | 114 | 101 | 67.3 | 22.5 | 14.0 |
| 10 U–0.5 Al | Arc | Ames | 128 | 125 | 106 | 94.1 | 75.7 | 26.9 | 18.3 |
| 10 U–2 Mo | Arc | Ames | 91.2 | 74.2 | 58.3 | 55.7 | 49.3 | 17.0 | 11.4 |
| 10 U–4 Nb | Arc | Ames | 96.3 | 82.1 | 68.7 | 62.9 | 56.6 | 21.3 | 14.6 |
| 10 U–2 Nb–0.2 C | Arc | Ames | 149 | | 88.4 | 74.0 | 58.0 | 19.8 | 17.3 |
| 10 U–1.5 Mo–0.2 C | Arc | Ames | 239 | 139 | 103 | 89.9 | 64.7 | 24.3 | 14.5 |
| 10 U–10 Y | Arc | Ames | 90 | 91.2 | 78.4 | 69.6 | 66.1 | 22.4 | 13.8 |

*Tested in the hot-rolled condition.

ond test was conducted at a peak specimen temperature of 815°C and was terminated after 876.5 hr. Following examination, it was evident that the specimen sustained 9.74% burnup of the $U^{235}$ atoms without failure. In addition, a test currently in progress has successfully reached burnup levels of approximately 25% of the $U^{235}$ atoms for 15,000 hr at 815°C without failure. This burnup is equivalent to 15,000 hr of full-power operation.

Oak Ridge[38] reports fabrication development on two fuels containing 25 vol.% $UO_2$ and 20 vol.% UC dispersed in a matrix of gamma-uranium alloy (10 to 15 wt.% molybdenum). Compacts of these compositions have been cold pressed at 50 tsi, sintered at 1100°C, and cold coined at 50 tsi to about 80% of theoretical density. The study revealed that the fabrication results varied with the type of matrix powder, the occluded gas content of the matrix powders,

Table I-9 TENSILE PROPERTIES OF THORIUM-BASE ALLOYS[36]

| Composition (balance Th), wt.% | Test temp., °C | Yield strength (0.2% offset), psi | Tensile strength, psi | Elongation in 1 in., % |
|---|---|---|---|---|
| Ames thorium | Room | 34,900 | 37,700 | 13 |
| 5 U | Room | 27,900 | 39,300 | 23 |
| 10 U | Room | 26,900 | 37,700 | 13.5 |
| 20 U | Room | 32,100 | 42,000 | 30 |
| 10 U–1.5 Mo | Room | 26,400 | 41,000 | 15 |
| 10 U–2 Nb | Room | 22,900 | 35,400 | 22 |
| 10 U–10 Zr | Room | 35,200 | 53,200 | 12 |
| 10 U–10 Zr–2 Nb | Room | 39,200 | 60,400 | 14 |
| Ames thorium | 600 | 13,800 | 15,700 | 26 |
| 5 U | 600 | 11,600 | 15,950 | 44 |
| 10 U | 600 | 13,800 | 17,970 | 41 |
| 20 U | 600 | 11,200 | 15,160 | 50 |
| 10 U–1.5 Mo | 600 | 11,220 | 17,700 | 43 |
| 10 U–2 Nb | 600 | 12,550 | 18,000 | 37 |
| 10 U–10 Zr | 600 | 19,600 | 28,400 | 44 |
| 10 U–10 Zr–2 Nb | 600 | 19,200 | 25,640 | 48 |
| Ames thorium | 700 | 4,280 | 8,090 | 58 |
| 5 U | 700 | 6,590 | 11,700 | 51 |
| 10 U | 700 | 8,800 | 10,300 | 44 |
| 20 U | 700 | 6,700 | 8,170 | 58 |
| 10 U–2 Nb | 700 | 8,400 | 10,800 | 66 |
| 10 U–10 Zr | 700 | 15,400 | 20,000 | 39 |
| 10 U–10 Zr–2 Nb | 700 | 12,100 | 13,910 | 77 |
| 10 U–0.1 Be | 700 | 8,610 | 11,200 | 47 |

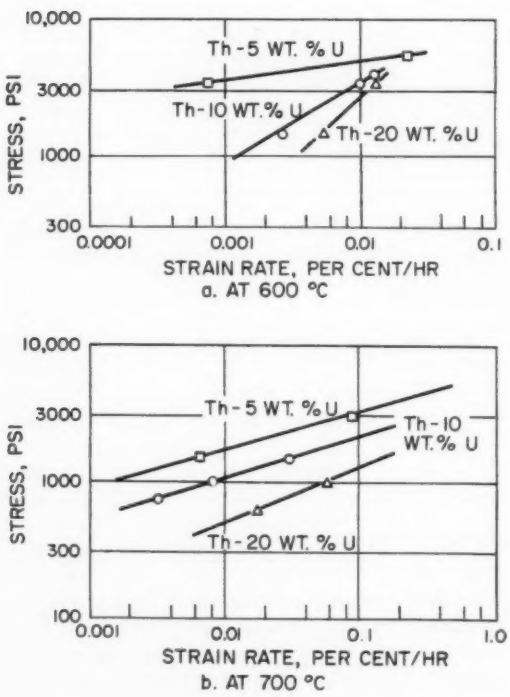


Fig. I-8 Creep strength of thorium-uranium alloys.[36]

pour density, and surface cleanliness. The most suitable pressing and sintering results were obtained when the prealloyed uranium-molybdenum powders or elemental molybdenum and calcium-reduced uranium powders were used. The densified 25 vol.% $UO_2$–75 vol.% gamma-uranium alloy (10 to 15 wt.% molybdenum) cores were assembled into rolling billets with molybdenum (type 304 stainless-steel sheathing), Fansteel 82 (type 304 stainless-steel cladding), or zirconium–3 wt.% aluminum (Ti-Namel or type 347 stainless-steel sheathing) used as cladding material. These assemblies were rolled at 1150°C, and metallographic examinations revealed that the molybdenum-clad cores exhibited a good metallurgical bond between the claddings and core.

Phillips Petroleum[39] reports dimensional change of two sample fuel plates which have undergone 40% burnup in the Materials Testing Reactor (MTR). The cores of these samples contained 50 wt.% $UAl_3$, fully enriched uranium, and 0.19 wt.% $B_4C$ dispersed in a matrix of 6061 or X8001 aluminum powder. Table I-11 summarizes the effects of irradiation on the two samples. It was noted in the two irradiation plates that the fission gas and helium buildup caused the formation or enlargement of voids

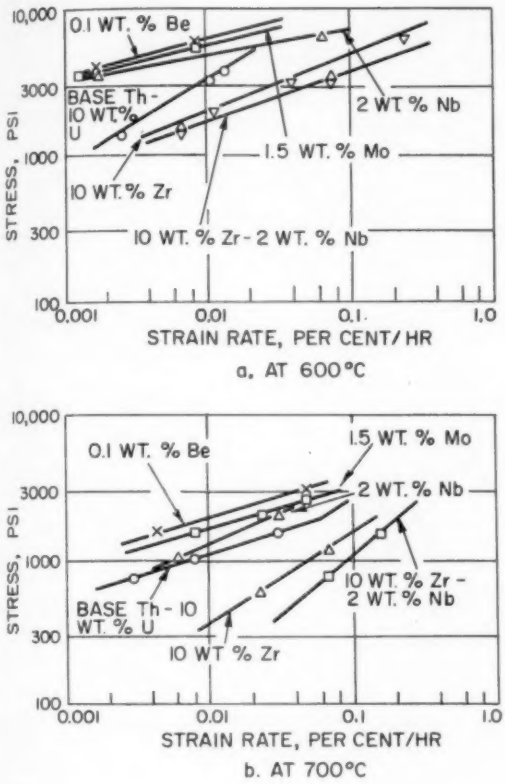


Fig. I-9 Creep strength of thorium–10 wt.% uranium alloys containing indicated additions.[36]

in the cores. Microstructures of the cores are shown in Fig. I-10 and indicate the increase in voids near the fuel particles. Possibly, an improvement in the density prior to irradiation will decrease the amount of swelling.

(D. L. Stoltz)

### Cermet Fuels

Battelle[31] reports that thermal-conductivity data were obtained at temperatures to 1000°C for the 50 and 70 vol.% $UO_2$–tungsten and 60 vol.% $UO_2$–molybdenum cermets. Figure I-11 shows reported interpolated values which, at 1000°C, were 9 to 16 times greater than values reported for dense $UO_2$. Values for electrical resistivity measured concurrently are shown in Fig. I-12. (D. E. Kizer)

## Coated-Particle Fuel Materials

### Preparation and Fabrication

A recent publication includes a historical summary of the development of coated-particle technology.[40] Most of the developments now being reported in the field of coated-particle technology involve refinement of coating processes so that the properties of the coating can be tailored to meet specific applications.

Table I-10 EFFECT OF COLD WORK AND ANNEALING ON THE HARDNESS OF HOT-ROLLED THORIUM-URANIUM ALLOYS[36]

| Composition (balance Th), at.% | Type of thorium | Melting method | Hardness, VHN (10-kg load) | | | | | |
|---|---|---|---|---|---|---|---|---|
| | | | Percentage cold reduction | | | | Annealed 15 min at indicated temp. | |
| | | | 0 | 60 | 80 | 90 | 700°C* | 725°C† |
| 5 U | Iodide | Arc | 107 | 123 | 123 | 134 | 95 | |
| 10 U | Iodide | Arc | 103 | 130 | 135 | 143 | 114 | 84 |
| 10 U | Ames | Arc | 122 | 151 | 159 | 177 | | |
| 15 U | Iodide | Arc | 98 | 138 | 138 | 157 | 116 | |
| 10 U | Iodide | Arc | 105 | 141 | 150 | 157 | 116 | |
| 10 U | Ames | Induction | 123 | 153 | 159 | 175 | 125 | 92 |
| 10 U | Iodide | Induction | 94 | 121 | 128 | 138 | 113 | 89 |
| 10 U–1.5 Mo | Ames | Induction | 137 | 157 | 171 | 187 | 147 | 148 |
| 10 U–2 Nb | Ames | Induction | 129 | 139 | 145 | 157 | 128 | 122 |
| 10 U–2 Nb | Iodide | Induction | 110 | 130 | 144 | 148 | | |
| 10 U–10 Zr | Ames | Induction | 144 | 171 | 192 | 198 | 144 | 142 |
| 10 U–10 Zr | Iodide | Induction | 153 | 187 | 199 | 218 | | |
| 10 U–10 Zr–2 Nb | Ames | Induction | 149 | 169 | 182 | 203 | 143 | 146 |

*After 80% cold reduction.
†After 90% cold reduction.

Table I-11 EFFECTS OF IRRADIATION ON DIMENSIONS OF SAMPLE FUEL PLATES USING POWDERED $UAl_3$ CORES[39]

| Sample fuel-plate composition | | Dimension | Before irradiation | After irradiation to 40% burnup | Change, % |
|---|---|---|---|---|---|
| Core | Cladding | | | | |
| 50 wt.% $UAl_3$ (U fully enriched) + 0.19 wt.% $B_4C$ + 6061 Al powder | 6061-T6 Al | Thickness, in. | 0.050 | 0.053 | +6.0 |
| | | Length, in. | 2.875 | 2.872 | −0.2 |
| | | Width, in. | 2.308 | 2.308 | 0 |
| | | Volume, cu in. | 0.330 | 0.350 | +6.1 |
| 50 wt.% $UAl_3$ (U fully enriched) + 0.18 wt.% $B_4C$ + X8001 Al powder | X8001 Al with 20% cold work | Thickness, in. | 0.050 | 0.053 | +6.0 |
| | | Length, in. | 2.876 | 2.872 | −0.1 |
| | | Width, in. | 2.310 | 2.311 | 0 |
| | | Volume, cu in. | 0.332 | 0.350 | +5.4 |

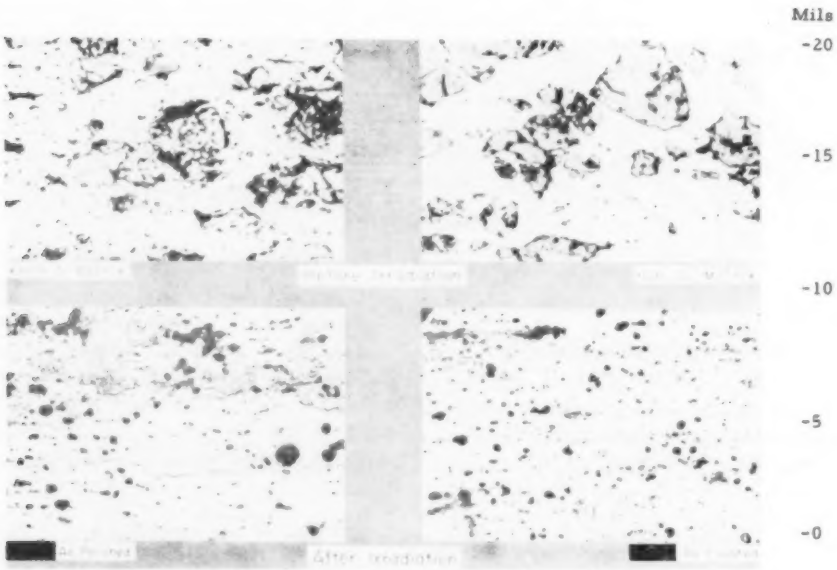


Fig. I-10 Microstructure of fuel-plate cores containing 50 wt.% $UAl_3$ + 0.19 wt.% $B_4C$ in two aluminum-alloy matrix materials.[39]

Martin[41] has described fabrication of a dispersion type fuel element in which 20- to 50-$\mu$-thick stainless-steel-coated $UO_2$ particles were consolidated without the addition of filler material so that the coating formed the entire matrix of the element. It was concluded that fabrication may be the limiting factor in dispersion quality. Criteria are given for the fabrication of a fully dense tubular element in which the wall of the element contains the fuel particles in a fracture- and stringer-free condition. Densification by isostatic pressing produced nearly ideal cermets (Fig. I-13), whereas cermets produced by roll-bonding techniques were inferior (Fig. I-14). The stainless-steel coatings were applied to $UO_2$ by an oxide-reduction coating process. Photomicrographs of the stainless-steel-coated particles, Fig. I-15, show some variation in coating thickness. However, for the intended application, the variation in coating thickness is probably not a significant factor. It is interesting to note that, in this case, the fabrication procedure was tailored to fit the properties of the coated particles. Often this direction cannot be pursued either because alternative fabrication schemes are economically prohibitive or because they are nonexistent and, consequently, the properties

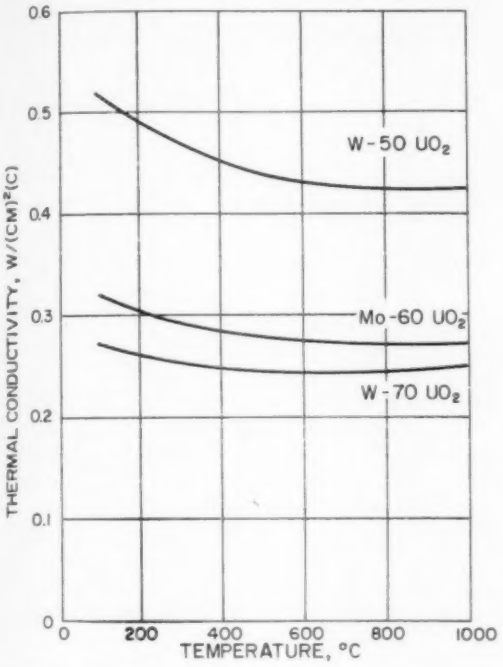


Fig. I-11 Interpolated thermal-conductivity data for molybdenum–60 vol.% $UO_2$ and tungsten–50 and 70 vol.% $UO_2$ cermets.[31]

of the coatings and the particles must be improved to withstand a specific fabrication scheme.

With nonductile metal oxide and pyrolytic carbon-coated fuel particles, coating conditions and techniques are being sought which will (1) improve the coating strength and thereby alleviate some restrictions on the consolidation procedures and (2) improve the resistance of the coating to the intended reactor environment. Evaluation of $Al_2O_3$-coated particles intended for a specific application has been reported by Oak Ridge.[42] $Al_2O_3$ coatings on $UO_2$ particles were found to be incompatible with molten LiF-NaF eutectic (m.p. 652°C). Coatings either dissolved or severely corroded, and cracking was frequently observed. This information suggests a possible stripping method for recovery of the fuel. Studies were also undertaken at Oak Ridge to determine the rate of reaction of pyrolytic carbon coatings on uranium carbide particles with water vapor at temperatures near 1000°C. Steam-helium mixtures at a total pressure of 1 atm were passed down through a bed of coated particles at temperatures ranging from 700 to 1100°C. Weight loss and resistance of steam-helium treated particles to 8*M* $HNO_3$ were measured on three lots of coated material. Wide variations in resistance to steam among batches of comparable thickness and microstructure were noted. However, processing conditions were proprietary, and, as a result, coating conditions and resistance to the steam-helium treatment could not be checked for possible correlation. Particle-to-particle variations within lots of coated material were noted. Localized attack or pitting was observed on some particles, whereas others were generally attacked. It was concluded that prolonged exposure at or below 800°C to steam-helium atmospheres appears to be permissible.

Additional information has been reported[43] on coating conditions that affect the microstructure of the coated product. Some control of the grain structure of vapor-deposited BeO coating has been achieved at coating temperatures of 1500°C in oxide-coating studies at Battelle. At a preparation temperature of 1500°C, a smooth coating is obtained which consists of large equiaxed grains of BeO which provide adequate protection of the substrate in the standard acid leach test. A rough columnar-grained BeO coating is

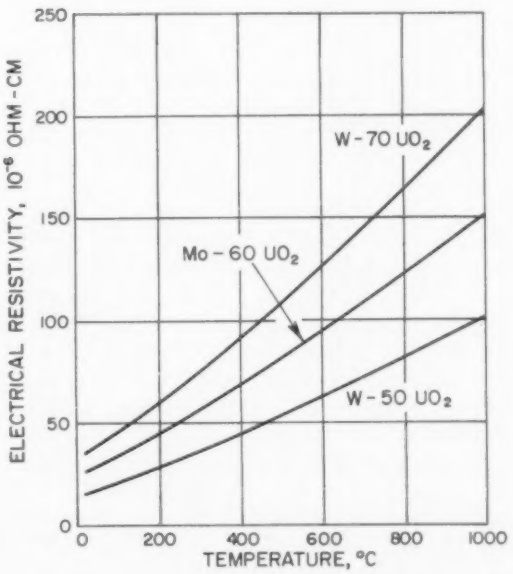


Fig. I-12 Interpolated electrical-resistivity data for molybdenum–60 vol.% $UO_2$ and tungsten–50 and 70 vol.% $UO_2$ cermets.[31]

obtained at 1400°C. Deposition of an equiaxed grain structure at 1500°C was not expected. Identification of the mechanism that causes the change in grain structure at the higher deposition temperature is being sought. BeO coatings deposited at a lower temperature (1100°C), where a finer grain structure might be expected, showed no significant improvement in surface roughness and exhibited poor resistance to acid leaching tests.

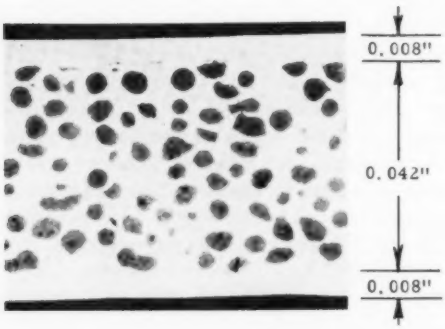


Fig. I-13 Nearly ideal cermet[41] tube wall results from extruding a slurry mixture of stainless-steel-coated spherical 105- to 149-$\mu$-diameter $UO_2$ particles to form the 40 wt.% $UO_2$ cermet and then isostatically pressing to densify it (longitudinal section).

Oak Ridge[44] has reported their findings on the effect of coating conditions on the structure of pyrolytic carbon coatings applied to $UC_2$. At deposition temperatures of 1400°C, the microstructure was controlled by regulating the $CH_4$ partial pressure and flow rates which, in effect, controlled the deposition rates. A columnar structure formed at deposition rates below 12 $\mu$/hr, and a laminar structure resulted at rates of 25 $\mu$/hr. Pyrolytic carbon coatings deposited at 1800°C were of uniform but poorly developed columnar structure under the conditions used.

(N. D. Veigel)

## Irradiation and Evaluation of Coated-Particle Fuels

*Oxide-Base Fuel.* Recent fission-gas-release data obtained by Oak Ridge[44,45] and Battelle[31,43–46] for coated-particle fuels are summarized in Table I-12.

A graphite-matrix specimen of $Al_2O_3$-coated $UO_2$ particles was irradiated at 1100°C to an estimated burnup of 10 at.% at Battelle.[43] This is the highest burnup that has been attained with $Al_2O_3$ coatings. The $R/B$ values of $10^{-9}$ to $10^{-8}$ indicate that no coating failure occurred. In an earlier irradiation of another specimen of the same material at a lower temperature (815°C), approximately 1% failure occurred after 6.4 at.% burnup. This is consistent with previous data at lower burnups and confirms that the performance of $Al_2O_3$ coatings improves with increasing temperature.

Studies of the low-temperature failure of $Al_2O_3$ coatings have continued at Battelle, and recent data indicate that the cracking of the alumina can be prevented by increasing the coating thickness and decreasing the density of the $UO_2$ fuel particles. A 63-$\mu$ $Al_2O_3$ coating on 80% dense, 127-$\mu$ $UO_2$ survived irradiation to 3.5 at.% burnup at 100°C. Some failure occurred at very low burnups, however, with specimens having comparable coating thicknesses but more dense $UO_2$ fuel cores. Radiation-induced expansion of the $UO_2$ appears to be the most likely explanation for this behavior.

Composite coatings on $UO_2$ particles are also being evaluated at Battelle. Three specimens were irradiated to about 1 at.% burnup at 100°C without failure. The coatings consisted of BeO overcoated with $Al_2O_3$, $Al_2O_3$ overcoated with laminar pyrolytic carbon, and $Al_2O_3$ overcoated with columnar pyrolytic carbon. It is not yet clear whether the good performance of these coatings is due mainly to the porosity of the $UO_2$ employed, the thickness of the coatings, or the

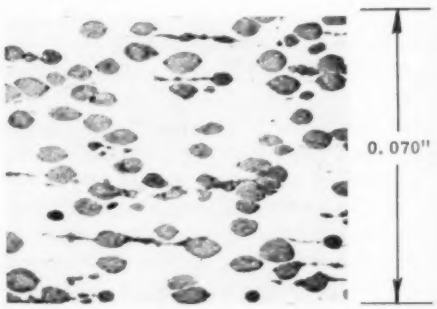


Fig. I-14 Cermet produced by full-bonding technique. Longitudinal section shown here is 0.070-in.-thick portion of 0.102-in.-thick cermet portion of 34 wt.% stainless steel; cladding plates are 0.005 in. each.

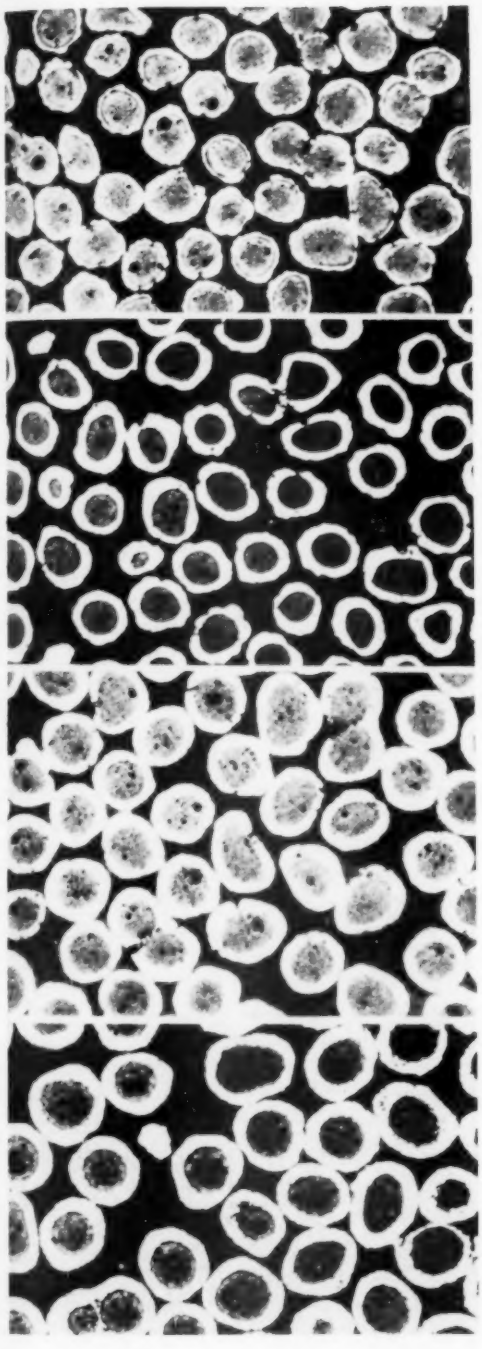

Fig. I-15 Stainless-steel coatings 20 to 50 $\mu$ thick on 105- to 120-$\mu$-diameter spherical $UO_2$ particles.[41] From top to bottom, the samples contain 65, 55, 45, and 35 wt.% $UO_2$.

use of layers of different materials. It is likely that each of these factors contributes to some degree. One of these materials is currently being irradiated at 815°C, and, after 1.5 at.% burnup, the $R/B$ values are still about $10^{-3}$. This is the columnar pyrolytic carbon-coated $UO_2$, which has an inner layer of $Al_2O_3$ to prevent infiltration of carbon into the porous $UO_2$ during the application of the pyrolytic carbon coating.

*Carbide-Base Fuel.* Irradiations of carbide fuel particles coated with the duplex type of pyrolytic carbon have continued at Oak Ridge.[44,45] The good performance of this type of coating is shown by the data in Table I-12. No detectable fission-gas release was found for one specimen after irradiation to 3 at.% burnup at 815°C. This specimen was a 1.5-in.-diameter graphite ball containing the coated particles.

Superior performance of the duplex coatings is also being found at Battelle. No failure was observed after 0.8 at.% burnup in an 815°C irradiation, which is still in progress. In an experiment at 850°C with a specimen having a thick (113 $\mu$) monolithic pyrolytic carbon coating, however, considerable failure occurred. The large increase in fission-gas release coincided with a reactor shutdown during which the specimen temperature dropped 250°. A specimen of the duplex type, irradiated statically in this same capsule, showed very little failure.

A topical report[47] was recently issued summarizing Battelle's irradiation evaluations of pyrolytic carbon coatings. Two major problems are discussed in this report: (1) rapid coating failure at low temperature and (2) the loss of coating integrity during thermal cycling at elevated temperatures. The low-temperature (100°C) failure occurred with coatings thinner than 70 $\mu$ but not with those thicker than 110 $\mu$. The $UC_2$ particles were 200 $\mu$ in diameter. Data in Table 1 of Ref. 47 show that 93-$\mu$ coatings also fail to some extent at 100°C and that, with larger (300 $\mu$) $UC_2$ particles, 115 $\mu$ is not sufficient to prevent cracking of the coatings.

A report was issued by Oak Ridge[48] which presents mathematical relations for calculating fission-gas release from coated particles and fuel elements containing them. Both intact and cracked coatings are considered, and the release mechanisms employed include fission recoil, diffusion from the fuel particles, diffusion through the coatings, and diffusion through the matrix. Equations are also given for calculating

Table I-12 SUMMARY OF FISSION-GAS-RELEASE DATA FROM COATED-PARTICLE FUELS IN SWEEP-GAS EXPERIMENTS[31,43-46]

| Specimen | | | | Irradiation capsule | Nominal irradiation temp., °C | Estimated burnup, at.% U | R/B† | | |
|---|---|---|---|---|---|---|---|---|---|
| Lot | Fuel | Coating* | Matrix | | | | $Kr^{85m}$, $Kr^{87}$, and $Kr^{88}$‡ | $Xe^{135}$ | $Xe^{133}$ |
| BMI-715A-HT | 127-μ $UO_2$ (98% dense) | 42-μ $Al_2O_3$ | Graphite | BMI-CFP-17 | 1100 | 6.0 | $7 \times 10^{-9}$ | $8 \times 10^{-9}$ | $2 \times 10^{-8}$ |
| | | | | | 1100 | 7.0 | $1 \times 10^{-8}$ | $1 \times 10^{-8}$ | $2 \times 10^{-8}$ |
| | | | | | 1100 | 8.0 | $1 \times 10^{-8}$ | $3 \times 10^{-8}$ | |
| | | | | | 1100 | 9.0 | $9 \times 10^{-9}$ | $5 \times 10^{-9}$ | $7 \times 10^{-8}$ |
| | | | | | 1100 | 10 | $1 \times 10^{-8}$ | $9 \times 10^{-9}$ | $1 \times 10^{-8}$ |
| BMI-761D | 127-μ $UO_2$ (80% dense) | 63-μ $Al_2O_3$ | None | BMI-CFP-28 | 100 | 2.5 | | $3 \times 10^{-8}$ | $8 \times 10^{-9}$ |
| | | | | | 100 | 3.5 | | $1 \times 10^{-8}$ | $7 \times 10^{-8}$ |
| BMI-764D | 127-μ $UO_2$ (98% dense) | 68-μ $Al_2O_3$ | None | BMI-CFP-35 | 100 | 0.01 | $3 \times 10^{-8}$ | $8 \times 10^{-9}$ | $2 \times 10^{-7}$ |
| | | | | | 100 | 0.07 | $8 \times 10^{-6}$ | $1 \times 10^{-5}$ | $1 \times 10^{-5}$ |
| BMI-765C | 200-μ $UO_2$ (92% dense) | 65-μ $Al_2O_3$ | None | BMI-CFP-36 | 100 | 0.01 | | $<4 \times 10^{-8}$ | |
| | | | | | 100 | 0.09 | $4 \times 10^{-6}$ | $5 \times 10^{-6}$ | $4 \times 10^{-6}$ |
| BMI-763B | 127-μ $UO_2$ (80% dense) | 21-μ BeO<br>43-μ $Al_2O_3$ | None | BMI-CFP-39 | 100 | 0.9 | $1 \times 10^{-8}$ | $1 \times 10^{-8}$ | $5 \times 10^{-8}$ |
| BMI-735D | 127-μ $UO_2$ (93% dense) | 16-μ $Al_2O_3$<br>65-μ laminar PyC | None | BMI-CFP-34 | 100 | 0.9 | $4 \times 10^{-10}$ | $3 \times 10^{-10}$ | ND |
| BMI-1039B | 200-μ $UO_2$ (92% dense) | 5-μ $Al_2O_3$ | None | BMI-CFP-40 | 100 | 0.9 | ND | $2 \times 10^{-10}$ | ND |
| | | 118-μ columnar PyC | None | BMI-CFP-40 | 100 | 0.9 | ND | $2 \times 10^{-10}$ | ND |
| BMI-1039B | 200-μ $UO_2$ (92% dense) | 5-μ $Al_2O_3$<br>118-μ columnar PyC | None | BMI-CFP-41 | 815 | 0.8 | $2 \times 10^{-9}$ | $2 \times 10^{-9}$ | ND |
| | | | | | | 1.5 | $2 \times 10^{-9}$ | $1 \times 10^{-9}$ | ND |
| NCC-AD | 244-μ $UC_2$ | 20-μ laminar PyC<br>80-μ columnar PyC | None | ORNL-B9-10 | 1150 | 3.8 | $1 \times 10^{-6}$ to $7 \times 10^{-6}$ | | |
| NCC-208-2 | 200-μ $(U,Th)C_2$ | 120-μ duplex PyC | None | ORNL-B9-11 | 1120 | 8 | $8 \times 10^{-7}$ | $5 \times 10^{-7}$ | $2 \times 10^{-6}$ |
| NCC-208 | 200-μ $(U,Th)C_2$ | 100-μ duplex PyC | Graphite | ORNL-06Z6 | 815 | 3 | ND | ND | ND |
| BMI-1020B | 200-μ $UC_2$ | 113-μ columnar PyC | None | BMI-CFP-32 | 850 | 0.6 | $2 \times 10^{-9}$ | $3 \times 10^{-9}$ | $1 \times 10^{-8}$ |
| | | | | | 850 | 0.8 | $1 \times 10^{-5}$ | $1 \times 10^{-5}$ | $3 \times 10^{-4}$ |
| | | | | | 850 | 3 | $5 \times 10^{-5}$ | $5 \times 10^{-5}$ | $2 \times 10^{-4}$ |
| BMI-1020B | 200-μ $UC_2$ | 113-μ columnar PyC | Graphite | BMI-CFP-33 | 1200 | 0.7 | $6 \times 10^{-8}$ | $4 \times 10^{-8}$ | $6 \times 10^{-8}$ |
| | | | | | 1200 | 1.2 | $8 \times 10^{-8}$ | $4 \times 10^{-8}$ | $7 \times 10^{-8}$ |
| | | | | | 1200 | 1.7 | | $6 \times 10^{-3}$ | $7 \times 10^{-2}$ |
| BMI-1031C | 200-μ $UC_2$ | 37-μ porous PyC<br>68-μ columnar PyC | None | BMI-CFP-44 | 815 | 0.8 | $3 \times 10^{-9}$ | $2 \times 10^{-9}$ | $2 \times 10^{-8}$ |
| BMI-1031C | 200-μ $UC_2$ | 37-μ porous PyC<br>68-μ columnar PyC | None | BMI-CFP-30 | 100 | 4 | ND | $7 \times 10^{-9}$ | $1 \times 10^{-8}$ |
| BMI-1034B | 300-μ $UC_2$ | 115-μ columnar PyC | None | BMI-CFP-37 | 100 | 0.05 | $1 \times 10^{-9}$ | $2 \times 10^{-9}$ | ND |
| | | | | | 100 | 0.3 | $1 \times 10^{-6}$ | $2 \times 10^{-6}$ | $9 \times 10^{-6}$ |
| | | | | | 100 | 0.8 | $2 \times 10^{-5}$ | $4 \times 10^{-5}$ | $1 \times 10^{-4}$ |
| BMI-1036B | 200-μ $UC_2$ | 93-μ columnar PyC | None | BMI-CFP-38 | 100 | 0.4 | $3 \times 10^{-9}$ | $2 \times 10^{-9}$ | ND |
| | | | | | 100 | 0.9 | $2 \times 10^{-7}$ | $4 \times 10^{-7}$ | $2 \times 10^{-6}$ |
| | | | | | 100 | 1.6 | $3 \times 10^{-7}$ | $6 \times 10^{-7}$ | $3 \times 10^{-6}$ |

*Coatings are listed in order of preparation in the case of multiple coatings.
†ND = none detected in the sample.
‡Data are an average of the release fractions of the three krypton isotopes.

fission-gas pressures and the resulting stresses as a function of burnup. (C. W. Townley)

## Coated-Particle Fuel Materials Compatibility

In order that one of the objectives of coated particles (retention of fission products) be met, it is necessary that uranium and thorium (for breeder reactors) be retained by the coating. Consequently, several workers have studied the diffusion of uranium and thorium in pyrocarbon coatings. Using bulk pyrolytic carbon, Oak Ridge[49] studied diffusion of thorium in pyrolytic carbon by coating the carbon with $Th^{232}$ by ion bombardment, heat-treating the specimen, and then subjecting it to neutron activation. Precision lapping techniques were used to obtain samples for analyses, and the diffusion coefficients, shown in Table I-13, were calculated.

Studies have also been conducted[49] to show the effect of rapid thermal cycling on the exposure of uranium in carbon-coated $UC_2$ particles. The specimens were heated to 2500°C in 10 sec and cooled to 900°C in 10 sec after holding at tem-

Table I-13 DIFFUSION COEFFICIENTS FOR THORIUM IN THE *C*-DIRECTION OF PYROLYTIC CARBON AT VARIOUS TEMPERATURES[49]

| Temp., °C | Diffusion coefficient ($D$), $cm^2/sec$ |
|---|---|
| 2280 | $2.09 \times 10^{-10}$ |
| 2000 | $5.48 \times 10^{-11}$ |
| 1720 | $5.60 \times 10^{-12}$ |
| 1340 | $3.32 \times 10^{-13}$ |

perature for 120 to 140 sec. As shown in Fig. I-16, cycling to very high temperatures damages the particles. However, the thick duplex coatings were resistant to thermal shock at temperatures to 2600°C. All the materials were resistant to damage at temperatures of 1800°C. Also, an attempt was made to remove uranium contamination from carbon coatings by treating with chlorine at temperatures to 1000°C. It was indicated that surface contamination was lowered appreciably but that interior contamination of particles persisted.

Oak Ridge has also tested carbon-coated particles in steam and has concluded that rapid failure can be expected when the coatings are exposed to steam at 1100°C.

On the basis of uranium diffusion data, workers at General Atomic[50] have estimated uranium solubility in pyrocarbon which varies from 0.035 wt.% at 1600°C to 0.21 wt.% at 2200°C.

The migration of uranium into carbon coatings of $UC_2$ particles is also being studied. The results for two lots of carbon-coated $UC_2$ particles are shown in Tables I-14 and I-15. Conclusions were as follows. The rate of migration decreases with time, yielding two migration curves (shallow and deep penetration) indicative of two different types of uranium transport; data obtained at high (1850 to 2300°C) temperatures do not accurately predict migration rates at lower temperatures; and migration rates vary between lots of supposedly similar coated particles. These results suggest that more than one mechanism is responsible for the observed migration and that the structure of the coating itself may have a profound influence on the migration. Investigations are now in progress to define the mechanisms of migration and determine the influence of coating structure.

Although not specifically for coated-particle work, the diffusion of uranium in graphite and pyrocarbon has been measured by workers at Livermore.[51] They obtained the following equations:

1. Uranium in pyrocarbon *a* direction

$$D = 6.8 \times 10^3 \exp(-115{,}000/RT)$$

2. Uranium in pyrocarbon *c* direction

$$D = 385 \exp(-129{,}000/RT)$$

3. Uranium in ZTA graphite

$$D = 6.2 \times 10^5 \exp(-135{,}000/RT)$$

4. Uranium in Spears 700 graphite

$$D = 9.3 \times 10^5 \exp(-136{,}000/RT)$$

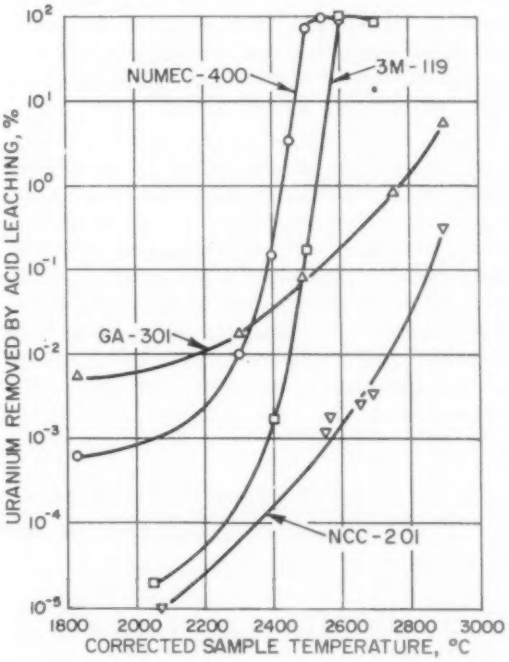


| Sample | Fuel particle | Coating type | Average coating thickness, $\mu$ | Exposed uranium as received, % |
|---|---|---|---|---|
| △, GA-301 | $(U,Th)C_2$ | Laminar | 91 | $2.9 \times 10^{-3}$ |
| □, 3M-119 | $(U,Th)C_2$ | Laminar | 97 | $<0.4 \times 10^{-4}$ |
| ▽, NCC-201 | $UC_2$ | Duplex | 106 | $2.4 \times 10^{-3}$ |
| ○, NUMEC-400 | $UC_2$ | Laminar | 44 | $0.5 \times 10^{-3}$ |

Fig. I-16 The effect of rapid thermal cycling on damage to pyrolytic carbon-coated particles. Samples held at temperatures indicated for 120 to 140 sec.[49]

They concluded that diffusion proceeds solely along defects and indicated that interstitial volume diffusion did not occur.

Also, a report has been issued[52] on the oxidation resistance of $Al_2O_3$-, BeO-, and MgO-coated $UO_2$ particles. At temperatures below 1500°C, oxidation of $Al_2O_3$-coated particles occurred by diffusion of oxygen through the coatings, partial oxidation to $U_3O_8$, and subsequent cracking and complete oxidation. Oxidation resistance of $Al_2O_3$ particles coated at 1300 and 1400°C was superior to that of particles coated at 1000°C. Extrapolation of the measured data indicated that the particles coated at 1300 and 1400°C should have satisfactory oxidation resistance for several thousand hours at temperatures of 1100°C and lower. Beryllia-coated particles were also found to have good oxidation resistance at 1100°C, but BeO-coated particles are more sensitive to thermal stresses than $Al_2O_3$-coated particles. Magnesia-coated particles failed due to thermal stresses at 800 to 900°C.

Additional data obtained at Battelle[43] show that $Al_2O_3$-coated $UO_2$ exposed to 1 atm oxygen for 6000 hr at 1100°C had good oxidation resistance—the oxygen-to-uranium ratio of the $UO_2$ was 2.014 after test. Similar tests with BeO showed little damage to sound particles after 2000 hr at 1100°C, but about 20% of the particles cracked. No damage to BeO coatings was observed after 3000 hr at 1000°C. Compatibility of the oxide coatings with graphite is also being studied.

Table I-14 MIGRATION OF URANIUM INTO PYROLYTIC CARBON COATINGS UNDER VARIOUS ANNEALING CONDITIONS[50]

(Coated-Particles Lot L1985-135NCR)

| Temp., °C | Time, hr | Migration distance, μ | Temp., °C | Time, hr | Migration distance, μ |
|---|---|---|---|---|---|
| 1700 | 81 | 1 | 2150 | 1.5 | 11 |
| | 196 | 9 | | 2.5 | 11 |
| | 356 | 9 | | 4.5 | 15 |
| | 569 | 11 | | 6.5 | 14 |
| 1850 | 4 | 5 | 2300 | 0.5 | 5 |
| | 9 | 7 | | 1.0 | 11 |
| | 16 | 10 | | 2.0 | 12 |
| | 25 | 14 | | 3.0 | 12 |
| 2000 | 2 | 5 | 2500 | 0.2 | 33 |
| | 4 | 5 | | | |
| | 7 | 14 | | | |
| | 10 | 14 | | | |

Table I-15 MIGRATION OF URANIUM INTO PYROLYTIC CARBON COATINGS UNDER VARIOUS ANNEALING CONDITIONS[50]

(Coated-Particles Lot L1985-147NC)

| Temp., °C | Time, hr | Migration distance, μ | Temp., °C | Time, hr | Migration distance, μ |
|---|---|---|---|---|---|
| 1700 | 81 | 8 | 2150 | 0.5 | 10 |
| | 196 | 11 | | 1.0 | 9 |
| | 361 | 13 | | 2.0 | 12 |
| | | | | 3.3 | 11 |
| 1850 | 4 | 6 | | 4.8 | 13 |
| | 9 | 9 | | 6.8 | 13 |
| | 16 | 10 | | 9.0 | 12 |
| | 25 | 12 | | 11.5 | 13 |
| | 36 | 11 | | | |
| | 49 | 13 | 2300 | 0.5 | 11 |
| | 64 | 13 | | 1.0 | 11 |
| | 81 | 13 | | 1.5 | 11 |
| | | | | 2.0 | 12 |
| 2000 | 1.5 | 7 | | 2.5 | 12 |
| | 2.5 | 10 | | 3.3 | 13 |
| | 4.5 | 12 | | 4.0 | 12 |
| | 6.5 | 11 | | 4.8 | 14 |
| | 8.5 | 12 | | | |
| | 11.0 | 12 | 2500 | 0.2 | 31 |
| | 14.0 | 12 | | | |
| | 17.0 | 12 | | | |

Experiments with BeO and graphite indicated that no reaction occurred in 4000 hr at temperatures to 1400°C, nor in short-time tests (up to 25 hr) at 1600°C. Metallographic examinations of specimens of MgO and graphite, heated for 3000 hr at 900°C, indicated that no observable reaction occurred. However, specimens heated for a similar time period at 1000°C exhibited a small amount of reaction. Samples of $ZrO_2$ and graphite, heated for 2000 hr at 800°C, have shown no signs of reaction.

The compatibility of oxide coatings with coolant atmospheres containing $H_2O$ and either hydrogen or oxygen is also being studied at Battelle[44] by transpiration techniques.

These studies have shown that water vapor increases the volatility of MgO and uranium oxides and that hydrogen increases the volatility of $ZrO_2$. No effect of enhanced volatility was observed in the case of alumina. The vapor pressure over zirconia, even with a hydrogen atmosphere, was negligible at temperatures to 2000°K. Calcium oxide behaved much as MgO but was less volatile by a factor of 100.

Final analysis of the data obtained for MgO indicated that gaseous $Mg(OH)_2$, MgO, and magnesium, in that order of importance, were present in the transpiration determinations

using water vapor in oxygen as the carrier gas. Using existing thermodynamic data to assess the importance of magnesium and the data obtained in this investigation for $Mg(OH)_2$, it has been possible to determine experimental values for the reaction

$$MgO(c) = MgO(g)$$

It has been found that

$$\Delta G_s^\circ = 135{,}000 - 36.33T \text{ cal/mole}$$

over the temperature range from 1780 to 2010°K. These data, when combined in a thermodynamic cycle, indicate the dissociation energy of gaseous MgO to gaseous elements at 0°K to be 4.1 ev.

(G. W. Cunningham)

# Refractory Fuel and Fertile Materials

## Properties and Behavior of Uranium Oxide Fuels

A paper by Robertson[53] of Chalk River reviews the influence of excess oxygen on the irradiation performance of $UO_2$. In-pile irradiation studies indicated that the thermal conductivity of $UO_{2.15}$ is about 0.8 times that of $UO_{2.00}$, whereas the corresponding value for $UO_{2.19}$ is 0.4. It is concluded that, generally, for most reactor fuel systems, oxygen-to-uranium ratios greater than 2.01 should be avoided.

In-pile measurements of the thermoelectric power of $UO_2$ were performed at Hanford.[20] A change from $p$ to $n$ type conductance was observed when the centerline temperature of a cylindrical specimen increased from 1000 to 2000°C. An average thermal electromotive force of 500 $\mu$v/°C was observed at 1000°C. Greater thermoelectric power levels may be achieved by varying the oxide composition. In other work at Hanford,[30] the infrared absorption coefficient was measured for single-crystal $UO_2$ at room temperature. Values of the absorption coefficient vary from 100 cm at 2 $\mu$ to 1 cm at 11 $\mu$. Between 3 and 13 $\mu$, there is a large optical window with minimum absorption at 11 $\mu$. The specific volume of single-crystal $UO_{2.00}$ between 0°C and the melting point (2800°C) can be expressed by $V_T = V_0 (1 + 9 \times 10^{-6}\ T + 6 \times 10^{-9}\ T^2 + 3 \times 10^{-12}\ T^3)$, where

$T$ = temperature, °C
$V_T$ = specific volume at temperature $T$, g/cm$^3$
$V_0$ = specific volume at 0°C

Above the melting point to 3100°C,

$$V_T = V_{2800^\circ} (1 + 1 \times 10^{-4}\ T)$$

At Lewis Research Center,[54] the compatibility of molten $UO_2$ with tungsten, tantalum, $TaB_2$, TaC, and HfC was determined at 2882°C for test periods of 15 min in static argon. Reactions were observed in all cases; however, the use of tungsten, tantalum, or HfC in contact with molten $UO_2$ appears feasible for short-time applications.

The Russians[55] have measured the magnetic moments of uranium atoms in $UO_2$, $U_2O_5$, and $U_3O_8$. The values of the magnetic moments were 3.01, 1.74, and 1.59 for $UO_2$, $U_2O_5$, and $U_3O_8$, respectively. These results suggest that the uranium is pentavalent in both the $U_2O_5$ and $U_3O_8$ structures.

Studies of substoichiometry in $UO_2$ have been reported by Robins.[56] $UO_2$ compacts containing uranium-metal additions were heated at temperatures up to 2500°C and then either cooled or quenched rapidly. The quenched specimens showed no second phase, whereas the compacts that were cooled slowly showed a fine uranium precipitate. Single-crystal electrolytic $UO_2$ when annealed at 1800°C showed uranium precipitation on both the surface and in the interior of the crystal.

(R. H. Barnes)

## Properties of Uranium Carbides, Nitrides, and Sulfides

Studies of the uranium-carbon-oxygen system are in progress in Japan, England, France, and the United States. As might be expected for measurements in a system where the equilibrium partial pressures of CO have not been reported in detail as a function of composition and temperature, the results show considerable disagreement. Results obtained by Stoops and Hamme[57] suggest that the UC-U(C,O) solid solution extends to $U(C_{0.75}O_{0.25})$ at 1800°C.

The UC-PuC system is known to be a solid-solution system, but since UC contains 50 at.% carbon and PuC contains less than 48 at.% carbon, the solid solutions must deviate from ideal stoichiometry at some point. According to studies by Rosen and Nevitt,[58] this point occurs at

approximately 70 mole % PuC (35 at.% plutonium).

Data obtained in England show that the solidus temperature on the $UC_2$-$UFeC_2$ tie line is at 1615°C. Between 1500°C and 1615°C, graphite, $UC_2$, and $UFeC_2$ exist in equilibrium. Below 1500°C, graphite, $U_2C_3$, and $UFeC_2$ are in equilibrium. Studies in the uranium-chromium-carbon system show that $UCrC_2$ melts incongruently at 1625°C and suggest that a compound exists near the composition $U_2CrC_4$. UC, $Cr_{23}C_6$, and chromium form a ternary eutectic at 1315°C. UC, $Cr_7C_3$, and $Cr_{23}C_6$ are in equilibrium below a peritectic temperature of 1430°C.

Atomics International[59] reports that, when as-cast uranium carbides containing more than 50 at.% carbon are bonded to stainless steel with liquid sodium, the sodium acts to transfer carbon from the $UC_2$ phase in the carbide to the austenitic solid solution. The sodium attacks the $UC_2$ phase, producing a zone depleted of $UC_2$ near the surface of the carbide. The depleted zone consists of residual tetrahedral particles of UC and is relatively weak and friable. The rate of decarburization of as-cast hyperstoichiometric uranium carbides by sodium in the presence of stainless steel is shown in Fig. I-17 as a function of time and temperature. The stainless steel absorbs all the carbon available to it, so that the carbon content of the stainless steel at any time depends on the above decarburization rate and the amount of excess carbon in the carbide. Sodium attacks $U_2C_3$ in hyperstoichiometric uranium carbide much more slowly than it attacks $UC_2$, so that heat-treated carbides are expected to show much less carburization of stainless steel than as-cast carbides when sodium bonded to stainless steel.

Twenty technical talks were presented at the Fourth Uranium Carbide Conference[60] sponsored by the U. S. Atomic Energy Commission. W. Chubb reported that the diffusion coefficient for diffusion of carbon in uranium monocarbide in the presence of a chemical concentration gradient was: $D = 0.0002 \exp(-22{,}000/RT)$. Hot-hardness data were presented which show that, above 800°C, hypostoichiometric UC softens much more rapidly than hyperstoichiometric UC. A. Accary presented X-ray data which suggest that the UC-U(C,O) solid solution extends to $U(C_{0.63}O_{0.37})$. A. Boltax obtained a thermal conductivity of 0.018 cal/(sec)(cm)(°C), on a 98% dense sample of UC–80 wt.% NbC alloy. No drastic changes were noted when this material was irradiated at a central temperature of about 2500°C for 10 min. A. Auskern presented fission-gas-release data for UC and suggested that the "burst" phenomenon was related to fission gas contained in the first four atomic layers from the surface of the fuel.

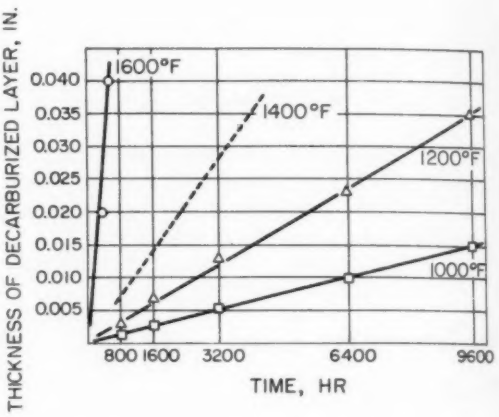


Fig. I-17 Decarburization of hyperstoichiometric UC vs. time.[59]

B. R. T. Frost observed no gross effects of irradiation on hypostoichiometric UC and UC-PuC alloys after irradiations at low temperatures and moderate burnups. W. Hayes stated that, at a maximum surface temperature of 850°C and a burnup of about 16,000 Mwd/ton, a uranium–4.2 wt.% carbon alloy swelled and split its cladding. Metallographic studies showed that the free uranium in the alloy migrated toward the surface of the fuel and reacted with and embrittled the stainless-steel cladding. No evidence of eutectic melting was observed, however. J. P. Hammond found that $UAl_2$, UC, and liquid uranium metal exist in equilibrium from 1200 to 1400°C. W. Witteman placed the melting point of UC at 2560°C and the minimum melting point between UC and $UC_2$ at 2450°C and 60 at.% carbon and found a eutecticlike thermal arrest between $UC_2$ and carbon at 2450°C. The two-phase region, UC plus $UC_2$, was found to extend into the solid-solution region to 2050°C at 57 at.% carbon. The solubility of carbon in UC at 1800°C was reported to be less than 51.7 at.%, and the solubility limit for uranium in $UC_2$ at 1800°C occurred at 62 at.% carbon. M. Bowman analyzed the thermodynamic data on uranium carbides and noted that the activity of carbon in

the system is very nearly constant from graphite to UC. L. Grossman reported that the thermal conductivity of $UC_2$ is 0.035 cal/(sec)(cm)(°C). It was noted that resistivity data as a function of temperature suggest a change in state in $ThC_2$ at 1280°C.

A summary and review of irradiation, compatibility, and property data generated at Atomics International in connection with reactors operating at fuel surface temperatures of about 600°C has been prepared by Hahn.[61]

Argonne[62] has irradiated 8 PuC and 23 UC–20 wt.% PuC specimens at central temperatures up to 650°C and burnups up to 810 Mwd/metric ton. Dimension and density changes were slight. A cast specimen released 0.24% of its fission gases, whereas sintered specimens released from 10 to 20% of their fission gases.

According to data obtained by Shaked,[63] the diffusion coefficient for $Xe^{133}$ in large-grained castings of UC is expressed by

$$D = 1.17 \times 10^{-6} \exp(-54{,}900/RT)$$

This expression is valid from 1000 to 2040°C for material having a grain size over 700 μ. Little or no effect of grain sizes smaller than 700 μ was noted above 1500°C, but an appreciable effect was noted at 1000 and 1200°C.

The UN-iron and UN-chromium systems are pseudo-binary systems with eutectics at 48 wt.% iron and 1450°C and at 37 wt.% chromium and 1720°C, respectively. No liquid or solid solubility has been found in the UN-copper system.

PuN melts at 2750°C under 1 atm of nitrogen pressure. $Pu_2S_3$ melts at 1725°C (Ref. 27).

$US_{0.98}$ having an initial hardness of 200 kg/mm² was subjected to two short neutron exposures. After $3 \times 10^{16}$ fissions/cm³, the sulfide showed a lattice expansion of 0.09% and increased in hardness to 340 kg/mm². After $6 \times 10^{16}$ fissions/cm³, the hardness increased[64] to 390 kg/mm². (W. Chubb)

### Fabrication of Refractory Fuels Other Than Uranium Oxides

Uranium monophosphide (UP) powder prepared by reacting uranium with phosphine gas had about one-fifth as much oxygen contamination as UP prepared by reacting the elemental powders. The UP powder made by the phosphine reaction was sinterable. Cold-pressed pellets sintered in vacuum at 2000°C densified to about 90% of the theoretical density.[65]

Argonne will study the US-UOS system in some detail since the main secondary phase found[65] in US is UOS. About 7% higher densities are obtained when US prepared from uranium powder and $H_2S$ are sintered in argon instead of in vacuum. It is hypothesized that, in a vacuum, UOS decomposes to $UO_2$ before a US-UOS eutectic temperature is reached; in argon the volatilization of the UOS phase is suppressed and liquid-phase sintering occurs, which leaves UOS as a gray intergranular phase.[66]

Dell and Allbutt[67] have compiled a fairly extensive summary of the literature published before the end of 1962 on the nitrides and sulfides of uranium, thorium, and plutonium. Although primarily a summary of chemical and physical-property data, this review includes reported fabrication studies of the above-mentioned compounds. (E. O. Speidel)

## Mechanism of Corrosion of Fuel Alloys

Argonne[68–70] has reported on the burning temperature and burning velocities of uranium and zirconium in air and the effect of halogenated hydrocarbons on the burning of these materials. Burning temperatures were calculated on the assumption that the metal-oxygen reaction was controlled by diffusion of oxygen through a nitrogen-rich gaseous boundary layer at the metal surface. The calculations were found to correctly describe the variation of burning temperature with the width of foils, thus providing evidence for the proposed model of burning. Measurements made on various sized foils, using a high-speed motion-picture camera or a specially constructed two-slit electronic pyrometer, confirmed the assumption that the rate of propagation of combustion along the foil was determined by the rate of conduction of heat through the foil. The addition of several percent of halogenated hydrocarbons to air markedly lowered the maximum burning temperature and burning propagation velocity of foils. The effect was attributed to a lowered heat-generation rate rather than to an increased heat-loss rate. The means by which this occurred were believed to be simple dilution, competition between the metal and organic for oxygen in the nitrogen-

rich diffusion boundary layer, or a reduced rate of chemical reaction as a result of contamination of the oxide surface.

Atomics International[71] has studied the oxidation of "reactive" uranium carbide (freshly melted material exposed to laboratory air containing moisture). Ignition in oxygen occurred at 275 to 350°C, depending on pressure, and in air at about 350°C. The oxidation was found to be a two-step process which produced two different reaction rates. The product during the first step was $UO_2$ at 10-mm oxygen pressure or $U_3O_7$ at higher pressures, whereas $U_3O_8$ was formed during the final oxidation.

(W. E. Berry)

### Fabrication of $UO_2$-Containing Ceramics

At Combustion Engineering,[72] densities above 90% of theoretical have been achieved in the fabrication of 3-ft-long vibratorily compacted fuel elements of fused $UO_2$. Approximately 25 wt.% segregation of the −200-mesh fraction was noted and was considered to be one of the primary problems to be solved in achieving higher compaction density. A difference has been noted in some of the physical properties of samples of fused $UO_2$ from two vendors. One material consisted primarily of single crystals containing small colonies of fine, shiny second phase; the other material was fine grained with relatively large amounts of fine, shiny phase in a random dispersion.

In a joint program at Hanford[27] and Battelle, $UO_2$ rods in thin-walled stainless steel were fabricated by swaging and hydrostatic pressing (1000°C, 10,000 psi). Mixtures of 70 wt.% fused $UO_2$ and 30 wt.% micronized $UO_2$ were used. Some of the results obtained in this study are given in Table I-16. The method may be satisfactory for preparing fuel elements having high-density core material and thin cladding of high integrity. The principal problem noted was the agglomeration of the micronized $UO_2$.

Table I-16 SWAGED AND ISOSTATICALLY PRESSED FUEL ELEMENTS[27]

| Fused $UO_2$ mesh size | Fabrication method | Swaged density, % of theoretical | Final average density, % of theoretical | O/U (av.) |
|---|---|---|---|---|
| −100 +200 | Hot swaging (800°C) | 83 | 94.2 | 2.011 |
| −65 +100 | Hot swaging | 85 | 93.7 | 2.010 |
| −35 +65 | Cold swaging | 81 | 93.6 | 2.004 |
| −20 | Hot swaging | 83 | 96.3 | 2.009 |

Table I-17 EFFECT OF SIZE DISTRIBUTION IN THE FINE (−200 MESH) FRACTION ON BULK DENSITY OF VIBRATION-COMPACTED RODS* CONTAINING FUSED $UO_2$ (REF. 27)

| Fine-fraction designation | Apparent Stokes diameter,† ($d_{ms}$), μ | Bulk density, % of theoretical |
|---|---|---|
| A | 29 | 87.5 ± 0.2 |
| C | 24 | 89.2 ± 0.1 |
| B | 23 | 88.5 ± 0.1 |
| G | 20 | 88.8 ± 0.2 |
| D | 17 | 88.7 ± 0.3 |
| E | 15 | 89.5 ± 0.3 |
| F | 11 | 89.3 ± 0.1 |

*Particle-size distribution: 60 wt.%, −10 +16 mesh; 15 wt.%, −70 +100 mesh; 25 wt.%, −200 mesh.
†Determined by sedimentation techniques.

In vibratory compaction studies with fused $UO_2$ at Oak Ridge,[73] the effect of size distribution within the fine fraction (−200 mesh) on the compaction density was investigated. Some of the results of this investigation are given in Table I-17.

A status report has been issued by Hanford[74] concerning the electrolytic growth of dense self-supported $UO_2$ shapes.

Australian workers[75] have developed a self-abrading process for the small-scale production of 150- to 200-μ spherical particles of $UO_2$-$ThO_2$.

(D. E. Rhodes)

## Basic Studies of Irradiation Effects on Fuel Materials

### Metallic Fuels

Uranium metal, after a thermal treatment of 24 hr at 620°C, contained krypton gas in bubbles having diameters from 50 to 400 A and in a concentration of $10^6/cm^3$, the volume representing about 1% of the metal volume.[76] The bubbles are reported to be at their equilibrium pressure (several tons per square centimeter).

There is no decrease in bubble concentration at the grain boundaries or at twin boundaries, but the bubbles seem to decorate the dislocations. It appears likely that the bubbles in uranium are not spherical. Although the bubbles are too small to show the planes which limit them,

the authors are confident that the dense planes of weak surface energy, namely, {0 1 0}, {1 1 0}, {0 2 1}, and {0 0 1}, are limiting.

Recent work at Hanford[77] indicates that overall volume change in irradiated high-purity uranium is the sum of volume change due to tearing (brought about by the fissioning) which decreases with increasing temperature and the volume change due to fission-gas porosity which increases with increasing temperature. The net effect is an apparent maximum volume increase at 400°C.

Thermal expansion and resistivity, measured in uranium fuel bars on longitudinal specimens from core and rim positions, are used to predict the irradiation growth rates at these positions as percentages of the growth rate of a single crystal.[78] The assumptions adopted to make these predictions are explained. Errors of the order of ±20% are expected in the absolute prediction of growth rate, and comparisons between specimens can give relative growth rates within ±4.8% of the single-crystal growth rate. The cores of the uranium bars examined are expected to shrink on irradiation relative to the rims at rates between 3.5 and 14.1% of the single-crystal growth rate.

The possibility of breakaway swelling in nuclear fuels being due to coalescence of fission-gas bubbles has been examined by the French.[79] Several possible methods of calculation are given. The results that agree best with experiments are obtained by considering the bubbles to be distributed randomly in the fuel, to grow by gas absorption proportionally to their surface area, and to merge without an increase of nucleation sites. Curves are given showing the swelling as a function of the irradiation and the distribution of the bubble diameters in the breakaway swelling zone.

Observations of others on elliptical dislocations in thin foils of irradiated alpha uranium are discussed in an article by Crocker.[80] The energy of a dislocation loop is considered and a plot of energy vs. $b/a$ (ratio of semiminor and semimajor axes of elliptical loop) is given for various ratios of minimum and maximum dislocation energies per unit length. The error of assuming an elliptical loop to be a circle is given, and it is believed that loops of a wide range of shapes are likely to arise in nonisotropic materials. Grouping of the reduced loop planes around {1 1 0} and {0 2 3} is discussed.

## Ceramic Fuels

Sintered $UO_2$ specimens with densities of 82, 92, and 99% of theoretical were irradiated, and the fission gases released during irradiation were collected and analyzed.[81] For in-pile release in the range 1000 to 1650°C, the diffusion coefficients for $Xe^{133}$, $Xe^{135}$, and $Kr^{85m}$ were

$$D = D_0 \exp Q/RT$$

where $D_0 = 2.0 \times 10^{-3}$ to $4.6 \times 10^{-3}$ cm$^2$/sec and $Q$ = 87 to 92 kcal/mole. Release below 1000°C was not so temperature dependent, indicating with other details that diffusion was not the principal mechanism of release in this range. The authors believe correspondence of in-pile and out-of-pile data indicates that, at low burnups, adequate diffusion data are obtained by postirradiation annealing.

Progress in the study of fission-gas release from $UO_2$ is covered in quarterly reports, such as that of Ref. 82, which may be of interest to those wishing to be familiar with the current literature.

Much practical information concerning fission-product release is available in a document that contains the papers presented at the Third Conference on Nuclear Reactor Chemistry.[83] Of particular interest are most of the papers in a session on Particle and Fission-Product Behavior in Nuclear Reactor Accidents. Some of the papers included are: "Parametric Studies of Fission-Product Realease from $UO_2$ Fuels," "Release of Fission Products by the In-Pile Destruction of Fuel," "Studies of Fission-Gas Release from In-Pile Tests, II," "Corrosion Induced Loss from BeO Ceramic Fuel Elements," "Particulates Generated During the Air-Oxidation of Uranium," "Interactions Between Radionuclides and Aerosols in the Respirable Size Range," "Characterization of Millimicron Radioactive Aerosols and Their Removal from Gases," "BeO Ceramic Fuel Meltdown Experiments Using a Plasma Jet," and "The Chemical and Physical Behavior of Released Fission Products." (F. A. Rough)

## References

1. W. Klement, Jr., A. Jayaraman, and G. C. Kennedy, High-Pressure Investigations of Group III Elements. Part II. Phase Transformations in Uranium at High Pressures, USAEC Report UCRL-

7128, University of California Lawrence Radiation Laboratory, November 1962.

2. J. R. Kench, J. Chamberlain, and A. G. Young, Incremental Collapse in Alpha-Uranium Subjected to Thermal Cycles While Undergoing Creep, *J. Nucl. Mater.*, 7: 165-181 (November 1962).
3. G. W. Greenwood and R. H. Johnson, An Analysis of Stress-Induced Permanent Dimensional Changes in Uranium Fuel Bars with a β-Core, *J. Nucl. Energy: Pts. A & B*, 16: 473-476 (October 1962).
4. J. W. Weber, Irradiation of Zircaloy-2-Clad Uranium Rods in NaK-Filled Capsules, GEH 3-31, 32, 57, 58, and 59, USAEC Report HW-67072, Hanford Atomic Products Operation, October 1962.
5. H. L. Dunegan, Grain Size Measurements in Uranium by Use of Ultrasonics, USAEC Report UCRL-6984, University of California Lawrence Radiation Laboratory, July 2, 1962.
6. R. S. Sharpe and S. Aveyard, The Visualization of an Ultrasonic Extinction Network in Coarse Grained Uranium, *Appl. Mater. Res.*, 1: 170-176 (October 1962).
7. E. S. Hodge, R. J. Carlson, E. G. Bodine, and E. G. Smith, Jr., Measurement of the Coefficient of Friction Between Uranium and Steel at High Alpha-Uranium Temperatures, USAEC Report BMI-X-226, Battelle Memorial Institute, Apr. 9, 1963.
8. G. L. Kehl and E. Mendel, A Study of Inclusions in Uranium, USAEC Report NYO-10354, Columbia University, March 1963.
9. R. F. Hills, B. W. Howlett, and B. R. Butcher, Further Studies on the Decomposition of the Gamma Phase in Uranium–Low Molybdenum Alloys, British Report AERE-M-1142, December 1962.
10. C. Collot and R. Faivre, Micrographic and Radiocrystallographic Study of Uranium-Niobium Alloys with 2.5 and 5 At.% Niobium Tempered from the Gamma Region (in French), *Compt. Rend.*, 256: 661-663 (January 1963).
11. C. Collot and R. Faivre, Effect of the Cooling Rate on the Temperature for the Onset of the Gamma-Beta Transformation of Uranium-Niobium Alloys Cooled in the Gamma Range (in French), *Compt. Rend.*, 256: 151-152 (January 1963).
12. M. Degois and R. Faivre, Determination by Isothermal Dilatometry of Curves for the Beginning and End of Transformation of Uranium-Chromium Alloys Tempered from the Beta Region (in French), *Compt. Rend.*, 255: 3185-3186 (December 1962).
13. P. Wynblatt and A. Bar-Or, Grain Refinement of Dilute Uranium-Chromium Alloys, Israeli Report IA-744, September 1962.
14. P. Wynblatt and A. Bar-Or, Grain Growth in a Uranium–0.45 At.% Chromium Alloy, Israeli Report IA-787, January 1963.
15. G. Petzow and R. Tank, The Phase Relations in Uranium-Aluminum-Iron Alloys of the Range Portion Uranium-$UAl_2$-$UFe_6$ (in German), *Z. Metallk.*, 54: 91-98 (February 1963).
16. H. M. Green and W. B. Nowak, Irradiation Behavior of Metastable Beta Phase Uranium Alloys, USAEC Report NMI-1255, Nuclear Metals, Inc., Dec. 13, 1962.
17. P. E. Repas, R. H. Goodenow, and R. F. Hehemann, An Investigation of Transformation Characteristics of Three Uranium Base Alloys, Report AMRA-CR-63-02/1(F), Case Institute of Technology, January 1963.
18. Orientation of Oxide Films Formed on Gamma Phase Uranium Alloys, *J. Nucl. Mater.*, 7: 125-132 (November 1962).
19. Argonne National Laboratory, Reactor Development Program Progress Report, May 1963, USAEC Report ANL-6739, June 15, 1963.
20. Hanford Atomic Products Operation, Reactor and Fuels Laboratory Monthly Report, March 1963, USAEC Report HW-77046A, Apr. 15, 1963. (Classified)
21. Los Alamos Scientific Laboratory, Quarterly Status Report on LAMPRE Program for Period Ending February 20, 1963, USAEC Report LAMS-2875, March 1963.
22. L. V. Jones and L. J. Wittenberg, Reactor Fuels and Materials Development, Plutonium Research, January–March 1963, USAEC Report MLM-1156, Mound Laboratory, May 29, 1963.
23. J. F. Eichelberger, G. R. Grove, L. V. Jones, and E. A. Rembold, Mound Laboratory Progress Report for November 1962, USAEC Report MLM-1145, Nov. 30, 1962.
24. G. R. Grove, F. D. Lonadier, and R. E. Vallee, Quarterly Report on Isotopes Development, January–March 1963, USAEC Report MLM-1153, Mound Laboratory, Apr. 30, 1963. (Classified)
25. G. R. Grove, L. V. Jones, J. F. Eichelberger, and E. A. Rembold, Mound Laboratory Progress Report for October 1962, USAEC Report MLM-1144, Mound Laboratory, Oct. 31, 1962.
26. Nuclear Materials & Equipment Corp., May 10, 1963. (Unpublished)
27. Hanford Atomic Products Operation, Ceramics Research and Development Operation Quarterly Report, October–December 1962, USAEC Report HW-76300, January 1963.
28. Centre d'Étude de l'Énergie Nucléaire, Use of Plutonium as a Fuel in Nuclear Reactors, Quarterly Report No. 8, April 1–June 30, 1962, USAEC Report EURAEC-408, July 1962.
29. Centre d'Étude de l'Énergie Nucléaire and Société Belge pour l'Industrie Nucléaire, Use of Plutonium as a Fuel in Nuclear Reactors, Quarterly Report No. 9, July 1–September 30, 1962, USAEC Report EURAEC-490, October 1962.
30. Hanford Atomic Products Operation, Reactor and Fuels Laboratory Monthly Report, May 1963,

USAEC Report HW-77709A, June 15, 1963. (Classified)

31. R. W. Dayton and R. F. Dickerson, Progress Relating to Civilian Applications During April 1963, USAEC Report BMI-1630, Battelle Memorial Institute, May 1, 1963. (Classified)
32. Argonne National Laboratory, Reactor Development Program Progress Report, March 1963, USAEC Report ANL-6705, Apr. 15, 1963.
33. F. Anselin and R. Pascard, The Volatility of Plutonium Carbide and Plutonium Nitride, British Translation NP-990 [translated from *Compt. Rend.*, 225: 698-700 (1962)].
34. Hanford Atomic Products Operation, Reactor and Fuels Laboratory Monthly Report, April 1963, USAEC Report HW-77397A, May 15, 1963. (Classified)
35. M. M. Hendrickson and J. K. Green (Eds.), Research and Development Programs Executed for the Division of Reactor Development, Quarterly Progress Report, October–December 1962, USAEC Report HW-76559, Hanford Atomic Products Operation, January 1963.
36. M. S. Farkas, A. A. Bauer, and R. F. Dickerson, in Proceedings of the Thorium Fuel Cycle Symposium, Development of Thorium-Uranium and Thorium-Uranium Base Alloys for Breeder Applications, USAEC Report TID-7650 (Book II), pp. 468-497, December 1962.
37. General Electric Company, Flight Propulsion Laboratory Department, High-Temperature Materials and Reactor Component Development Programs, Second Annual Report, USAEC Report GEMP-177A, Feb. 28, 1963.
38. S. A. Rabin, M. M. Martin, A. L. Lotts, and J. P. Hammond, Fabrication Development of U-Mo-$UO_2$ and U-Mo-UC Dispersion Fuels for the Enrico Fermi Fast-Breeder Reactor, USAEC Report ORNL-3437, Oak Ridge National Laboratory, June 24, 1963.
39. Phillips Petroleum Co., Materials Testing Reactor, Engineering Test Reactor Technical Branches Quarterly Report, October 1–December 31, 1962, USAEC Report IDO-16857, Mar. 29, 1963.
40. H. Oxley, Recent Developments with Coated-Particle Fuel Materials, *Reactor Mater.*, 6(2): 1-14 (May 1963).
41. David E. Goslee, Improving Performance of Stainless Steel–$UO_2$ Cermet Fuels, *Nucleonics*, 21(7): 48-52 (July 1963).
42. Oak Ridge National Laboratory, Reactor Chemistry Division Annual Progress Report for Period Ending January 31, 1963, USAEC Report ORNL-3417, May 1, 1963.
43. Battelle Memorial Institute, Progress Relating to Civilian Applications During May 1963, USAEC Report BMI-1632, June 1963. (Classified)
44. Oak Ridge National Laboratory, May 8, 1963. (Unpublished)
45. Oak Ridge National Laboratory, Apr. 8, 1963. (Unpublished)
46. Battelle Memorial Institute, Progress Relating to Civilian Applications During March 1963, USAEC Report BMI-1624, Apr. 1, 1963. (Classified)
47. R. J. Burian, N. E. Miller, R. L. Ritzman, and C. W. Townley, Initial Irradiation Evaluation of Experimental Pyrolytic-Carbon-Coated $UC_2$ and $UO_2$, USAEC Report BMI-1628, Battelle Memorial Institute, Apr. 25, 1963.
48. J. W. Prados and J. L. Scott, Models for Fission-Gas Release from Coated Fuel Particles, USAEC Report ORNL-3421, Oak Ridge National Laboratory, June 20, 1963.
49. Oak Ridge National Laboratory, 1963. (Unpublished)
50. W. V. Goeddel and L. R. Zumwalt, General Atomic Division, General Dynamics Corp., June 3, 1963. (Unpublished)
51. R. J. Borg et al., The Self-Diffusion of Uranium in Pyrographite, USAEC Report UCRL-6827-T, University of California Lawrence Radiation Laboratory, March 1962.
52. G. W. Cunningham, W. H. Pfeifer, D. C. Carmichael, and E. S. Hodge, Oxidation Resistance of Oxide-Coated $UO_2$ Microspheres, USAEC Report BMI-1625, Battelle Memorial Institute, Apr. 2, 1963.
53. J. A. L. Robertson, Some Consequences of Excess Oxygen in $UO_2$, paper presented at Symposium on Radiation Effects in Refractory Fuel Compounds, American Society for Testing Materials, Philadelphia, 1962.
54. W. A. Sanders and I. L. Drell, Compatibility of Molten Uranium Dioxide with Five Refractory Materials, Report NASA-TN-D-1442, National Aeronautics and Space Administration, Lewis Research Center, January 1963.
55. N. I. Blinova et al., Magnetic Properties of $U_2O_5$, *Dokl. Akad. Nauk SSSR*, 147: 1112-1113 (Dec. 11, 1962).
56. R. G. Robins, The Precipitation of Uranium Metal in Uranium Dioxide Single Crystals, *J. Nucl. Mater.*, 7: 218-219 (November 1962).
57. R. F. Stoops and J. V. Hamme, Uranium Interstitial Phases, Quarterly Progress Report, USAEC Report NCSC-2663-10, North Carolina State College, December 1962.
58. S. Rosen, M. J. Nevitt, and A. W. Mitchell, The Uranium Monocarbide–Plutonium Monocarbide System, *J. Nucl. Mater.*, 9(2): 137 (1963).
59. B. A. Webb, Carburization of Austenitic Stainless Steel by Uranium Carbides in Sodium Systems, USAEC Report NAA-SR-6246, Atomics International, May 31, 1963.
60. W. Chubb, Notes from the Fourth Uranium Carbide Conference at East Hartford, Conn., May 20–21, 1963.
61. R. D. Hahn, A Study of Uranium Carbide and Cladding Materials for High-Temperature So-

dium-Cooled Reactors, USAEC Report NAA-SR-7696, Atomics International, Mar. 15, 1963.

62. J. H. Kittel, R. Carlander, L. A. Neimark, O. L. Kruger, and R. C. Lied, Preliminary Irradiations of PuC and UC-PuC, USAEC Report ANL-FGF-399, Argonne National Laboratory, November 1962.
63. H. Shaked, Diffusion of Xenon in Uranium Monocarbide, USAEC Report UCRL-10462, University of California Lawrence Radiation Laboratory, Nov. 7, 1962.
64. Hanford Atomic Products Operation, Reactor and Fuels Laboratory Monthly Report, February 1963, USAEC Report HW-76596A, Mar. 15, 1963. (Classified)
65. Argonne National Laboratory, Reactor Development Program Progress Report, April 1963, USAEC Report ANL-6717, May 15, 1963.
66. P. D. Shalek, Preparation and Properties of Uranium and Thorium Monosulfides, *J. Am. Ceram. Soc.*, 46(4): 155-161 (Apr. 21, 1962).
67. R. M. Dell and M. Allbutt, The Nitrides and Sulphides of Uranium, Thorium, and Plutonium: A Review of Present Knowledge, British Report AERE-R-4253, March 1963.
68. E. M. Mouradian and L. Baker, Jr., Burning Temperatures of Uranium and Zirconium in Air, *Nucl. Sci. Eng.*, 15(4): 388-394 (April 1963).
69. L. Liebowitz, L. Baker, Jr., J. G. Schnizlein, L. M. Mishler, and J. F. Bingle, Burning Velocities of Uranium and Zirconium in Air, *Nucl. Sci. Eng.*, 15(14): 395-403 (April 1963).
70. L. Liebowitz, J. G. Schnizlein, and L. W. Mishler, The Effect of Halogenated Hydrocarbons on the Burning of Uranium and Zirconium in Air, *Nucl. Sci. Eng.*, 15(4): 404-410 (April 1963).
71. E. W. Murbach, The Oxidation of "Reactive" Uranium Carbide, *Trans. AIME*, 227(2): 488-491 (April 1963).
72. B. E. Murtha and W. P. Chernock, The Development and Testing of $UO_2$ Fuel Systems for Water Reactor Application, Progress Report for Period Ending Dec. 31, 1962, USAEC Report CEND-172, Combustion Engineering, Inc., January 1963.
73. Oak Ridge National Laboratory, Maritime Reactor Program, Annual Progress Report for Period Ending November 30, 1962, USAEC Report ORNL-3416, Apr. 4, 1963.
74. F. A. Scott, The Electrolytic Growth of Dense Self Supported Uranium Dioxide Shapes, USAEC Report HW-74784, Hanford Atomic Products Operation, Oct. 5, 1962.
75. K. D. Reeve and K. A. Jones, The Preparation of Spheroidal $UO_2$–$ThO_2$ Particles, Australian Report AAEC/E-104, March 1963.
76. J. Leteurtre and G. Brebec, Study of Electron Microscopy of Uranium Containing Krypton, *J. Nucl. Mater.*, 6: 342-345 (1962).
77. Hanford Atomic Products Operation, Metallurgy Research Operation Quarterly Progress Report, January–March 1963, USAEC Report HW-77052, Apr. 15, 1963.
78. B. Pawelski and J. J. Stobo, The Prediction of Irradiation Growth Rates in Uranium by Resistivity and Expansion Measurements, *J. Nucl. Energy: Pts. A & B*, 16: 477-481 (October 1962).
79. Y. Quere, F. Pham, and J. Blin, On the Breakaway Swelling in Nuclear Fuels (in French), *J. Nucl. Energy: Pts. A & B*, 17: 15-24 (January 1963).
80. A. G. Crocker, On the Orientation of Dislocation Loops in Alpha-Uranium, *J. Inst. Metals*, 91: 242-243 (March 1963).
81. J. B. Melehan, R. H. Barnes, J. E. Gates, and F. A. Rough, Release of Fission Gases from $UO_2$ During and After Irradiation, USAEC Report BMI-1623, Battelle Memorial Institute, Mar. 26, 1963.
82. FIAT. Sezione Energia Nucleare, Turin, Fission Gas Release from Uranium Dioxide, Quarterly Progress Report No. 8, October–December 1962, USAEC Report EURAEC-568, Jan. 31, 1963.
83. The Third Conference on Nuclear Reactor Chemistry, held at Gatlinburg, Tenn., October 9–11, 1962, USAEC Report TID-7641.

Section II

Reactor Materials

# Moderator Materials

## Graphite

In studies related to Molten-Salt Reactor Experiment (MSRE) design, additional data have been obtained on the effect of temperature and heating rates on moisture removal from AGOT and ETL graphites by helium purging.[1] The predominant characteristics noted in Figs. II-1 and II-2 are the removal of physically absorbed moisture at temperatures up to 150°C and the removal of what appears to be chemisorbed moisture over the temperature interval 200 to 400°C.

In several experiments graphite specimens were presaturated with water vapor by exposure to moist helium. The moisture-removal curves were similar to those shown in the previously noted figures, and the reproducibility of the moisture-removal pattern for the same graphite was qualitatively good.

Because of the upper concentration limit (1000 ppm) of the moisture analyzer used for these experiments, the relatively large quantity of physically held water in as-received ETL graphite was not accurately measured. In two experiments more than 25 $cm^3$ [standard temperature and pressure (STP)] of water vapor for 100 $cm^3$ of graphite was noted. The quantities of chemisorbed water in both as-received and presaturated pieces of ETL graphite are listed in Table II-1. The temperature at which the chemisorbed moisture evolution reached a maximum value was found to increase from about 270 to 400°C as the heating rate was increased from 5 to 65°C/hr.

A process for treating commercial graphite to lower its permeability to the order of $1 \times 10^{-5}$ $cm^2/sec$ by a series of impregnations with furfuryl alcohol type monomer has been reported in detail.[2] The experimental procedure and equipment and the effect of the process on the graphite properties are given. Graphites with maximum pore diameters up to 40 $\mu$, as measured by mercury porosimetry, can be treated, and, since the impregnant is heated to >2650°C in the process, the treated material is suitable for high-temperature applications. Tubes of HLM-85 graphite, 4 ft long, $3\frac{1}{2}$ in. in outside diameter, and $\frac{3}{8}$ in. in wall thickness, have been treated to yield permeabilities of $< 1 \times 10^{-6}$ $cm^2/sec$ by the process.

Two types of graphite have been examined by electron microscopy before and after irradiation.[3] Replicas of identical areas were taken before and after irradiation of a sample prepared with a natural-flake graphite filler and coal-tar pitch binder. This sample was irradiated at 700°C to an exposure of $1.1 \times 10^{21}$ nvt, $E > 0.18$ Mev.

In addition to microcrack broadening, a series of steps arranged in echelon across the sample surface developed during irradiation. The surfaces exposed on the steps were parallel to the well-developed, layered structure in the natural-flake filler. Shadowing on the step faces suggested that these surfaces intercepted the polished surface of the sample at an angle approximating the shadow angle of 35°. Therefore the step displacements measured would be of the order of 80% of the actual displacements. Average displacements measured were 3 $\mu$, with a maximum of 4 $\mu$ observed.

Thin sheets of binder material separating the natural-flake particles were readily detected on the preirradiation replicas. The displacements, which produced steps during irradiation, occurred at these binder-filler interfaces. A sample of CSF graphite having a petroleum-coke filler and coal-tar pitch binder also examined by this technique showed broadening of microcracks in the coke-filler particles during irradiation.

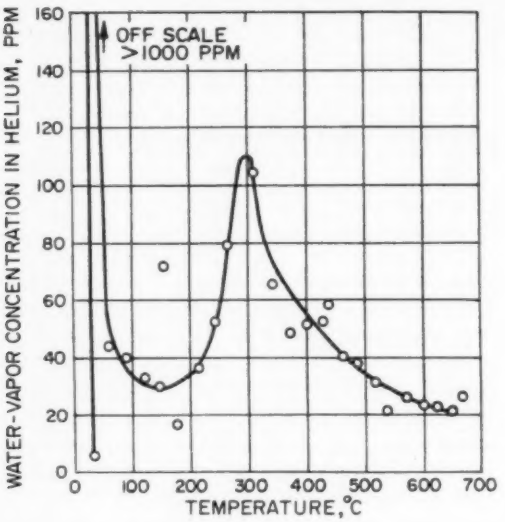


Fig. II-1 Removal of moisture from AGOT graphite by helium purging.[1] Graphite weight, 695 g; volume, 418 $cm^3$; gas volume, 2.96 liters (STP); gas flow rate, 3 liters/min; temperature rise, 30°C/hr.

The presence of large displacements in the natural-flake graphite and their absence in petroleum–coke-base graphite can be attributed to several factors. Structural differences between binder and filler materials and the associated differences in radiation-induced contraction are greater in the graphite made from natural-flake graphite and coal-tar pitch than in the petroleum–coke–coal-tar pitch system. Stresses at binder-filler boundaries therefore increase with radiation dose at a higher rate in the natural-flake graphite. A low concentration of pinning sites at binder-filler boundaries provides the freedom necessary for large internal displacements when slip does occur, and these displacements are not transmitted from particle to particle as readily as in petroleum–coke-base graphites having many more pinning sites.

The relation of these observations to theories explaining bulk dimensional changes during irradiation is being explored. The accommodation of slip in highly ordered binder-filler graphite systems suggests that lower internal stress exists in these graphites after manufacture because slip allows relief of some of the differential thermal contraction produced in cooling from graphitization temperatures. Since ordered graphites contract at lower rates than disordered graphites, the theory that bulk contraction is, in part, a process of stress relief is consistent with microscopic observations.

Information on graphite–water-vapor reaction under gamma irradiation has been supplemented by further study at Hanford.[4] A TSX graphite sample weighing approximately 8 g was employed. At sample temperatures of 600 to 680°C and a helium flow rate of 0.5 cu ft/hr, oxidation rates obtained at a dose rate of $3.04 \times 10^6$ r/hr were $2.2 \times 10^{-6}$ $hr^{-1}$ and were independent of water-vapor concentration (200 to 6000 ppm) and temperature. A comparison of the present data with those obtained previously for TSX graphite but at a lower dose rate, about $8.1 \times 10^5$ r/hr, indicates that the oxidation rate is approximately proportional to the dose rate.

The radiation chemistry of CO exposed to nuclear and gamma irradiation has been examined in preliminary experiments[3] at about 550°C and at pressures more nearly typical of gas-cooled reactors than those for previous investigations. The CO was contained in sealed quartz capsules at test pressures in the 1- to 18-atm range. Seven capsules comprised this series. Following irradiation, the capsules were opened and changes in gas pressure and composition were determined.

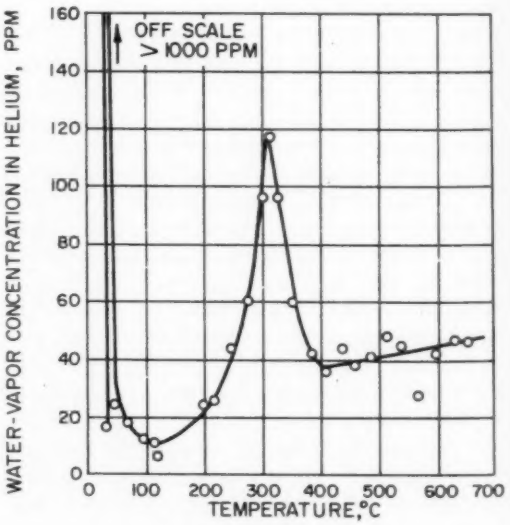


Fig. II-2 Removal of moisture from ETL graphite by helium purging.[1] Graphite weight, 1.22 kg; volume, 620 $cm^3$; gas volume, 2.88 liters (STP); flow rate, 3 liters/min; temperature rise, 30°C/hr.

In all the capsules there was a decrease in the initial quantity of CO, accompanied by the formation of $CO_2$ and deposition of solids on the capsule walls. The formation of $CO_2$ was proportional to the CO pressure and did not reach a limiting value. The average $CO_2$:CO ratio and standard deviation were $0.42 \pm 0.07$.

Table II-1 CHEMISORBED WATER CONTENT OF ETL GRAPHITE[1]

| Graphite specimen condition | Chemisorbed water removed, mg | Water content of graphite | |
|---|---|---|---|
| | | $Mg/cm^3$ | Mg/g |
| As received | 23.5 | 0.075 | 0.142 |
| 30-min saturation with moist He | 14.0 | 0.047 | 0.089 |
| As received | 19.4 | 0.063 | 0.119 |
| 2-hr saturation with moist He | 23.3 | 0.075 | 0.142 |
| 2-hr saturation with moist He | 20.2 | 0.065 | 0.123 |
| 2-hr saturation with moist He | 22.7 | 0.073 | 0.138 |
| 2-hr saturation with moist He | 29.2 | 0.094 | 0.178 |
| 2-hr saturation with moist He | 21.8 | 0.070 | 0.133 |

This value indicates an overall reaction represented approximately by the equation $5CO \rightarrow 2CO_2 +$ solids.

As shown by the equation, there was an oxygen deficiency in the gas. From 71 to 84% of the original amount of oxygen was recovered from the gas at room temperature; however, the recovery improved to more than 90% after degassing the capsule at 1000°C under vacuum. Thus the deposit probably contained polymerized carbon suboxides (the monomer, $C_3O_2$, is unstable at the test temperature) and chemisorbed oxygen or carbon dioxide.

As suggested by previous investigators, the reaction mechanism probably involves one or more of the carbon suboxide homologues, $C_2O$, $C_3O_2$, or $C_4O_3$, as intermediates in transporting carbon to the capsule wall. The first step involves the radiolysis of a molecule of CO. Carbon suboxides form, polymerize, and then partially decompose to yield $CO_2$, C, and a lower suboxide homologue.

The thermal decomposition of CO was not studied in this investigation. However, it is generally believed that a catalyst is required for this reaction to occur at an observable rate below 700 to 1000°C.

Hanford[4] has reported additional data on the effect of additives on the dimensional stability of graphite under irradiation. After a second exposure at 600 to 650°C, the rates of contraction between 1745 and 4200 Mwd/$AT_K$ for transverse samples of the 17 additive systems were in every case equal to or less than the 0.005% contraction per 1000 Mwd/$AT_K$ observed for the transverse control that contained no additive. Significant reduction of contraction rate was observed in the following samples.

| Additive (1 wt.% original mix) | Contraction rate, %/1000 Mwd/$AT_K$ |
|---|---|
| $Fe_3O_4$ | 0.0004 |
| $V_2O_3$ | 0.0004 |
| $CrCl_3 \cdot 6H_2O$ | 0.001 |
| $Al_4C_3$ | 0.002 |

The comparatively low contraction rates for all samples reflect the transition from growth through nonlinear contraction to linear contraction, which occurs during the exposure interval in which data were obtained. Comparison of rates at this point should be indicative of the relative rates for linear contraction at higher exposure; however, it is expected that the ultimate linear rates will be higher than those determined above. Irradiation of these samples will be continued. Additional samples will also be tested to provide information on additive effects in graphites which are of interest in ap-

plications requiring high strength or impermeability but which have the disadvantage of high contraction rates.

The room-temperature flexural strength of a carbon-rich alloy of zirconium pyrocarbide is reported[5] to average $92.9 \times 10^3$ psi. Specimens tested had a composition of 78 wt.% carbon, compared with 12 wt.% in carbon in stoichiometric ZrC. The strength of this composition is much higher than that of either pyrolytic graphite (about $22 \times 10^3$ psi) or pyrolytic ZrC (about $9 \times 10^3$ psi). Examination of the microstructure of the 78 wt.% carbon alloy offered no apparent explanation for its remarkable strength since it was indistinguishable from pyrolytic graphite. It was speculated that the dispersion of ultrafine carbide particles as a second phase in the graphite matrix may result in a type of precipitation-hardened alloy. The effect of composition on strength is to be studied further.

(M. C. Brockway)

# Beryllium Metal and Alloys

Commercial beryllium is not a relatively pure metal but a very complex alloy, says Dr. Bunshah of Lawrence Radiation Laboratory.[6] The effects of purification strongly suggest that impurities in commercial beryllium cause brittleness and limit its potential applications. He suggests that future research should be conducted to (1) improve commercial beryllium and (2) produce a superpure metal (99.995+% pure) to see whether the brittleness problems can be solved, to be followed by a study of the "pure" alloys.

## Melting, Casting, and Purification of Beryllium

Vacuum-induction melting of beryllium appears to offer a promising means of producing beryllium sheet.[7] Ingots of domestic purity up to 6 in. in diameter are cast without centerline defects. (Ingots up to $13\frac{1}{2}$ in. in diameter have been produced by Pechiney by vacuum-arc remelting.) Additions of up to 0.1% iron to the beryllium melts lead to a substantial improvement in elevated-temperature ductility after aging. Apparently the iron (and possibly silicon) diffuses to the grain boundaries to form a complex, solid phase with aluminum. Iron also precipitates and agglomerates within the grains. The cast material has fewer nonmetallics than does hot-pressed material. The cast ingots can be extruded and forged or rolled. Rolling has produced sheet with tensile and yield strengths of 48,000 and 37,000 psi and 4% elongation in both directions in the plane of the sheet. The authors suggest that these values probably can be increased about 50% by additional grain refinement. The elevated-temperature ductility of sheet rolled from arc-melted ingots is considerably greater than that rolled from hot-rolled powder, as shown by Fig. II-3.

Limited studies[8] were carried out on two possible techniques for producing spherical particles of beryllium metal of 5 to 13 mils in diameter: (1) a salt-bath technique whereby molten beryllium droplets fall into molten salt and (2) a shot-tower technique in which molten beryllium is dropped against a refractory oxide disk rotating at high speed. The salt-bath technique (which was studied by using the Wood's metal–water system) produced a maximum yield of perfect spheres of about 50%.

A process apparently similar to that developed at the U. S. Bureau of Mines was used by Boisde et al.[9] to electrorefine $BeCl_2$ in a KCl-LiCl bath to obtain highly purified beryllium, except for oxygen. The following analysis, in parts per million, was reported: Al, ≤10; Cr, <3; Cu, ≤5; Fe, ≤5; K, 50–100; Li, 20–40;

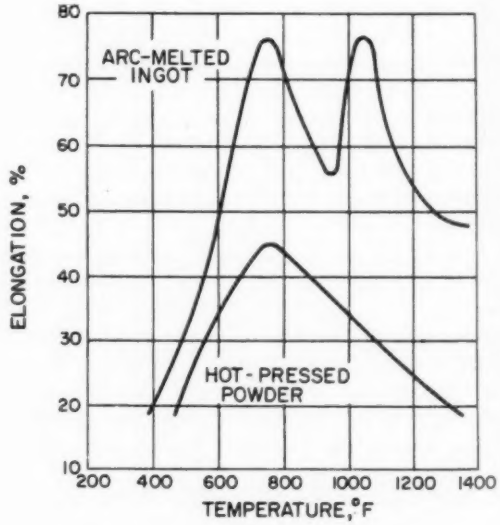


Fig. II-3 Ductility of beryllium sheet.[7] Before testing, specimens were heat-treated for 24 hr at 1300°F and cooled slowly.

Mg, ≤6; Mn, <3; Cl, 300–100; Ni, ≤3; Si, ≤15; Sn, ≤15; O, 100–300. After fusion, potassium, lithium, and chlorine were reduced to a few parts per million.

In the United States, beryllium of very high purity was produced by distillation.[10] Iron, nickel, and chromium contents were each reduced to below 5 ppm, and manganese and silicon, to below 15 ppm. Aluminum content of the distilled beryllium appeared variable and possibly unevenly distributed, with a spread from 30 to 65 ppm reported on one sample. A few analyses for copper and nitrogen showed 7 ppm of each. Three analyses for carbon showed a spread from 25 to 35 ppm, but the analytical technique was not considered completely reliable. Oxygen was not reported since the available analytical technique was unreliable at the oxygen level in question. Although the distilled beryllium was pure, it had much lower ductility than the zone-refined beryllium produced at the Franklin Institute. Small spherical particles of precipitate were observed on the fracture surfaces of the distilled, but not on the zone-refined, metal. These particles are believed to be linked with the low ductility. They were found to contain silicon, iron, and sulfur in the approximate proportions by weight of 3 : 3 : 1. Some of the particles also contained aluminum and occasionally other elements. The precipitated particles could not be redissolved by annealing at 1000°C for 1 hr.

## Fabrication of Beryllium

Research on free-standing plasma-arc shapes disclosed that sprayed and sintered forms of beryllium have a density only a little lower than hot-pressed and sintered material.[11] The tensile strength of the former, especially at elevated temperatures, appears to be much higher (27,000 to 30,000 psi at 1200°F). The reason for the higher strength is not obvious since the sprayed and sintered metal was reported to have an oxide content of less than 1%.

A special four-quadrant beryllium hot pressing was prepared to study the effect of powder input material on hot-press billet and sheet tensile properties.[12] Differences in hot-press billet and sheet material were traced to differences in powder input material, although the blended materials for the four quadrants had similar chemical analyses. Results of systematic testing of hot-press billet and sheet material revealed a strong correspondence of beryllium-sheet tensile properties to those of the billet material. Sheet from the best quadrant had the capacity for definitely improved resistance to triaxial stresses.

In a recently issued British patent,[13] a method for forming beryllium into shaped bodies is claimed to impart improved formability and decreased anisotropy in mechanical properties. A coarse-grained ingot of cast beryllium is worked to form a shaped body with a fibrous grain structure that is then refined.

The combination of low neutron absorption and certain desirable high-temperature properties of beryllium makes this metal attractive for use as a fuel-element cladding material in high-temperature gas-cooled nuclear reactors. Twisted-rib beryllium tubes of high quality would allow maximum advantage to be taken of those desirable properties. It was found[14] that acceptable tubes could be made by at least three different means, but the "shaped die" process offered many advantages over the others. By this method, beryllium is extruded directly to the desired shape, including the twist, over a mandrel. The tubes made showed hoop stresses approaching 100,000 psi during burst tests.

Thin, high-vacuum beryllium windows were successfully vacuum brazed to copper supports for electronic devices using small frames of indium-copper-silver brazing alloy (melting range, 630 to 705°C). The edges of the beryllium windows were coated with copper before brazing.[15]

Welding parameters affecting the integrity of tungsten-arc welds in 0.30-in. outside diameter by 0.040-in.-wall tubing were investigated at Oak Ridge.[16] On the basis of a study of three joint designs, it was determined that the edge-fusion type is better than either the butt or plug type design. To eliminate root cracking in the welds, it was necessary to obtain a very tight fit-up of the end cap and the tube by tapering the joint about 3°. Additional refinements, such as preheating the joint to 1400°F under a suitable cover gas of argon, reduced the propensity toward crack formation and propagation during welding and cooldown. An evaluation of seven lots of tubing produced by six different fabrication processes showed that the welds in extruded tubing exhibited a tendency to be porous, whereas the welds in machined tubing did not. All the tubing produced welds having shear strengths of the order of 20,000 psi at room tempera-

ture and 10,000 psi at 1100°F (593°C). No service failures attributable to defective welds were reported from approximately 300 tube-burst specimens tested in or out of the reactor.

Beryllium blocks, plated on one side with 0.0005 in. of silver, were furnace brazed to each other at 900°C while they were held in contact with a pressure of 100 or 200 psi (40 psi was said to be sufficient) for periods of 1 to 5 min. Tensile specimens were then cut with the brazed joint normal to the axis of tension. The as-brazed joint strengths varied from 27,000 to 41,000 psi. MacPherson et al.[10] reported that holding the joints at 600°C for 6 hr or 1 week produced marked increases (about 18%) in room-temperature tensile strengths, whereas 6 hr at 800°C lowered it drastically. However, after 1 week at 800°C, the tensile strength at room temperature was slightly higher than it had been at the start. Except for the heat-treatment at 800°C for 1 week, the heat-treatments had little or no effect on the elevated-temperature strengths. The presence of silver-beryllium intermetallics in a brazed joint appears to be detrimental to the strength of the joint. The heat-treatments at 600°C eliminated the intermetallics, whereas those at 800°C increased the amount of gamma phase. Several experimental silver-base brazing alloys were compared, but none were found to be as good as the commercial silver–0.2% lithium alloy for furnace brazing.

Fusion welds can be made by the TIG process by use of a bare beryllium filler wire. The properties of these welds can be definitely improved by hot rolling under controlled conditions.[5] Mechanically hot working the fusion-weld reinforcement flush with the parent metal by roll-planishing techniques produced the best microstructure. Roll-planished welds in 0.062-in. sheet having ultimate strengths in excess of 50,000 psi after a 20% reduction at 760°C could be obtained.

Resistance butt welds in beryllium rods enclosed in aluminum oxide tubes could be made with the joint practically indistinguishable in the microstructure.[10] A contributing factor to the attainment of high strengths in this operation is believed to be repeated thermal cycling between the alpha- and beta-phase fields of beryllium. Good joints made by this process have ultimate strengths in excess of 45,000 psi.

The melting behavior on hot-pressed beryllium of these metals and alloys was studied both in vacuum and in argon: liquid silver, gold, germanium, aluminum, copper, palladium–2.1 wt.% beryllium, zirconium–5 wt.% beryllium, and titanium–6 wt.% beryllium.[17] Of these, only aluminum, zirconium–5 wt.% beryllium, and titanium–6 wt.% beryllium caused little or no base-metal reaction with the beryllium. Aluminum did not wet beryllium. The zirconium–5 wt.% beryllium alloy showed some small ability to wet, and this was greater in vacuum than in argon. Only the titanium–6 wt.% beryllium alloy wetted the beryllium readily. This experiment presumably indicates that a titanium–6 wt.% beryllium alloy would be a good brazing metal for joining beryllium to itself.

## Physical Metallurgy of Beryllium

Pemsler et al.[18] estimated the solubility of nitrogen as about 60 ppm. This value appears to be temperature independent. Measurement of the growth characteristics of hydrogen bubbles formed in beryllium by proton bombardment indicated a value for the diffusion coefficient of hydrogen in beryllium of $9 \times 10^{-10}$ cm$^2$/sec at 850°C. The solubility of hydrogen in beryllium is believed to be very small. Measurement of the rate of diffusion of nitrogen in beryllium gave a result the authors considered probably unreliable. No new data concerning the beryllium-oxygen system were obtained because of the limitations of chemical analysis.

Scott[19] described several electron microscopy techniques for studying problems associated with the plastic behavior of beryllium. He attempted to explain the microstructure in terms of the mechanical properties of the metal. Theories that have been put forward to explain the brittle behavior of beryllium at 600°C are discussed, and an alternative mechanism is proposed which involves a consideration of the stacking-fault energy of the material.

X-ray diffraction and spectral analyses have been made[20] of the structure and phase composition of the beryllium-tungsten diffusion layer. It was shown that a beryllium-tungsten couple diffuses on the surface with parallel formation of intermetallic phases of various thicknesses. The phases are separated, and their boundaries correspond to a step-line concentration curve.

Optical and transmission electron microscopy studies by Bonfield and Li show[21] that annealing hot-pressed beryllium at elevated temperatures produces considerable changes in the density

and distribution of dislocations within a grain without causing any change in grain size. Annealing also results in appreciable reductions in the microscopic yield stress, defined as the stress to cause a permanent strain of $2 \times 10^{-6}$ in./in., and the rate of strain hardening in the microstrain region, which can be correlated with the observed changes in dislocation structure within a grain. From these experiments it was found that the stress ($\sigma$) in the microstrain region, both for beryllium with a dense dislocation structure and beryllium with only a few isolated dislocations within a grain, is given by:

$$\sigma = C + B\epsilon^{1/2}$$

where $\epsilon$ is the strain and $C$ and $B$ are some function of the dislocation density. Values of the stress required to move the first dislocations in beryllium can be derived from this formula.

Pronounced changes in the tensile strength and ductility of beryllium were obtained[10] by aging solution-treated beryllium rod at temperatures between 200 and 800°C. However, no significant changes were obtained in the yield strength. A yield point, although absent in the as-solution-treated material, was observed after certain aging treatments at 400°C. This yield point appeared to be sensitive to minor variations introduced in processing, presumably differences in grain size. X-ray diffractometer studies revealed that precipitation occurred during aging. It was concluded that the observed improvements in ductility and tensile strength resulted from the precipitation from solution of one or more detrimental impurities. Strain aging of beryllium occurred between 300 and 400°C.

Gross and O'Rourke[22] converted zone-refined crystals of both thermally and electrolytically reduced beryllium to polycrystalline aggregates by a combination of deformation and heat-treatment. The crystals were jacketed in steel, swaged, and drawn at 450°C. It was learned that two mechanisms must cooperate in order to convert the single crystal into a polycrystalline aggregate. Besides slip, a part of the deformation must result from twinning, and some of the twinned orientations must survive during primary recrystallization to become grains in the recrystallized aggregate. The ductility of the as-drawn wire was, in some cases, about three times that of commercially pure wire in a comparable condition. Strength levels were found to be about 50% of those of commercially pure, block-pressed beryllium. Grain growth occurred very readily during recrystallization annealing.

Weisz and Adda[23] have shown that the brittleness of beryllium, at all temperatures, is strongly dependent on the purity of the metal. Experimental results, by analogy with the effects of oxygen and nitrogen in titanium, appear to show that certain impurities block prismatic and pyramidal glide in beryllium. Although it is still impossible to make a definite pronouncement on the causes of brittleness in beryllium, the authors are convinced that one cannot consider the metal intrinsically brittle.

Intentional additions of iron were made at Nuclear Metals to a six-pass zone-refined crystal made from Pechiney SR bar.[24] Most of the specimens cracked during spark machining of tensile bars, but one containing 98 ppm iron had a critical resolved shear stress of 1180 psi. Premature failure occurred at 19% glide strain. The work-hardening rate (obtained by extrapolation) at 20% strain was 1800 psi. A control specimen with 5 ppm iron (not intentionally added) had a critical resolved shear stress of 330 psi, a glide strain of 62%, and a work-hardening rate at 20% strain of 830 psi.

Morrow and Moore[25] prepared tensile specimens from hot-extruded beryllium rod by turning and by grinding. Tests of the specimens at temperatures between 20 and 600°C showed that those prepared by grinding exhibited the same mechanical properties as those prepared by turning. However, the rate of cutting was not increased by grinding, so that no particular advantage was achieved.

King[26] presented the tensile data on forged beryllium shown in Figs. II-4 and II-5. The S-200 material is commercial hot-pressed block and the I-400 is the high-oxide "instrument" grade containing not less than 4.25% BeO. The 1.03% BeO forging with the properties shown in Fig. II-4 had the following average properties in the thickness direction: 51,300 psi ultimate tensile strength and 0.5% elongation at room temperature.

King stated that Brush Beryllium Company no longer considers fine silver a suitable brazing material for wrought beryllium. The majority of their recent work has been done with zinc, which brazes at about 800°F (425°C). Scarf joints made in 0.100-in. beryllium sheet with zinc as the brazing medium have consistently developed sheet tensile stresses of 65,000 to

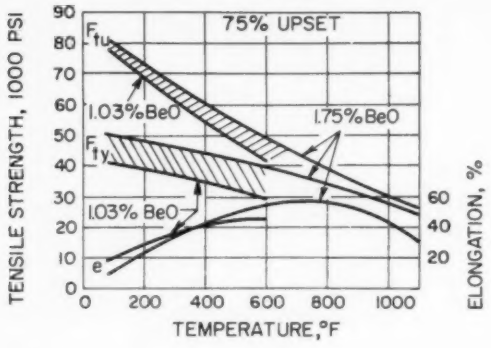


Fig. II-4 Typical mechanical properties of forged S-200C beryllium.[26]

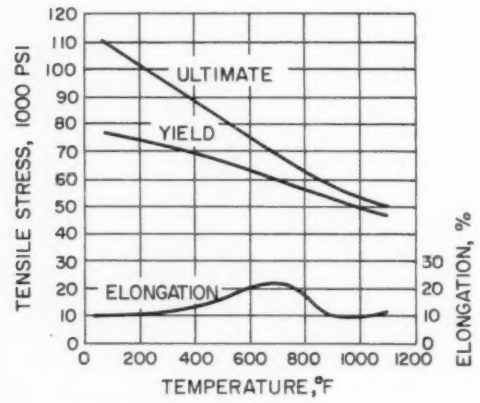


Fig. II-5 Tensile properties of forged I-400 beryllium.[26]

70,000 psi. Exploratory work was being conducted on a silver-copper braze alloy that flows at about 1150°F (620°C).

## Chemical and Nuclear Properties of Beryllium

A black chemical-conversion coating on beryllium with high emissivity and good resistance to high temperatures has been developed.[27] The coating is applied by depositing electroless copper on the beryllium surface, converting this coating to the black copper oxide in an alkaline chlorite solution, and sealing by spraying with high-temperature-resistant inorganic films.

Studies of orbital reentry burnup behavior of beryllium reflectors in SNAP reactor systems led to the conclusion that no toxic hazard will exist at ground level, even with complete reflector burnup at the lowest possible altitude.[28]

It has been conclusively shown that beryllium of greater purity than that of normal, commercial (QMV or equivalent) purity corrodes with extreme rapidity in hot water at 343°C. On the other hand, the corrosion resistance of commercial-purity beryllium in hot water is very erratic. It was found[29] that high *p*H invariably led to increased rate of attack, but lowering the *p*H would not eliminate the catastrophic failures. Likewise, it was shown that boiling of the water could accelerate the attack, but overpressure of the autoclave with argon to prevent boiling did not eliminate the sudden, unpredictable failures. Tests were under way to try to correlate the corrosion resistance with the presence of certain impurities in the beryllium.

The oxidation behavior of approximately 600 AGR beryllium tubes in $CO_2$ containing 50 ppm $H_2O$ was examined. The test temperatures covered the range 550 to 650°C at intervals of 25°C. Relatively rapid breakaway oxidation occurred at 650°C, but, at 600°C, it occurred at a markedly slower rate. At 550°C, breakaway was rarely apparent from weight-gain results prior to statistical analysis. On the other hand, very slow rates of oxidation were found in dry $CO_2$ at 600 and 650°C, with no indication of breakaway after 3832 hr (Refs. 30 and 31).

Irradiation of beryllium by neutrons leads to the formation of considerable quantities of helium. Micrographic examinations have shown no gas bubbles if the irradiation temperature is sufficiently low, and density measurements show no appreciable swelling at temperatures below 800°C. With increased temperature, bubbles are formed. The apparent activation energy of the swelling process is 45 kcal/mole. Higher temperatures cause the bubbles to grow and decrease in number. Preferential location of the bubbles is along dislocations or on grain boundaries where they have an important effect on the mechanical properties of the beryllium.[32]

## Other Beryllium Reports

A "current awareness" service was performed by the American Society for Metals for Lawrence Radiation Laboratory. It resulted in a 350-page bibliography of journals, books, technical reports, dissertations, and patents on the metallurgy, chemistry, and physics of beryllium,

together with sections on beryllium compounds and beryllium oxide. Most of the references are annotated. The bibliography covers the period from January 1961 to December 1962 inclusive.[33]

(W. Hodge)

# Beryllium Oxide

Since the characteristic crumbling of beryllium oxide to powder as a result of reactor irradiation is associated with the anisotropic lattice expansion, several investigators have considered the stresses that would result in two irradiated grains so aligned that the $c$ axis in one lies parallel to both the boundary and the $a$ axis of the other. Recently, Clarke[34] has considered this case in an idealized manner and, utilizing irradiation-induced strain data from previous work, he has related the ratio of fracture stress after irradiation, $\sigma_i$, to fracture stress of unirradiated material, $\sigma_0$, with irradiation-induced strain. It was assumed in his calculations that the strain deduced from X-ray measurements represents the actual boundary strain. Furthermore, the $c$-axis strain in the solid material was taken as an approximation to the desired but unavailable lattice strains in the powdered state. The model ignores the actual presence of other grains around the boundary, and Fig. II-6 is calculated on the assumption that one grain fracture is sufficient to cause the body to fracture. This simplified model predicts that the fracture strength will decrease rapidly within a fairly narrow range of irradiation-induced strain, and the magnitude of the strain is dependent on the inverse of the square root of the grain size. Figure II-6 is a plot of fracture-stress ratio vs. irradiation-induced strain for three different grain sizes.

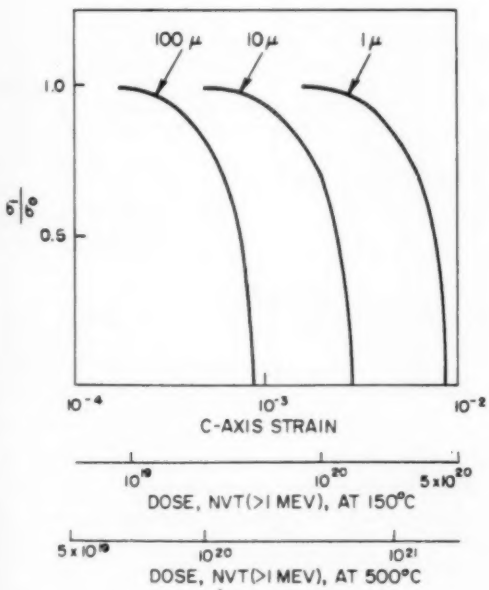


Fig. II-6 Fractional change in fracture stress, $\sigma_0$, due to irradiation for grain sizes of 100, 10, and 1 $\mu$, according to the model.[34]

An annual report[35] on BeO studies conducted at General Electric during 1962 contains the following summary observations.

The most significant aspect of radiation effects in BeO is expansion of the crystal lattice, which is reflected in the expansion of polycrystalline bodies. Expansion of the lattice is anisotropic in the two crystallographic axes, $c$-axis expansion being approximately eight times that in the $a$ axis. Estimates of the expansion rates are $0.27\%/10^{20}$ nvt for the $c$ axis and $0.03\%/10^{20}$ nvt for the $a$ axis, both dosages being for neutrons $\geq 1$ Mev.

Expansion of polycrystalline bodies is of three types:

1. Expansion corresponding to that computed from the lattice parameters, denoted by $(\Delta V/V)_L$
2. Expansion arising from porosity introduced into specimens by grain-boundary cracks that develop from stresses between grains as a result of the anisotropy of the lattice expansion
3. Expansion resulting from segregation of helium atoms into microbubbles, the helium being a transmutation product of neutron absorption in beryllium

The first two types of expansion occur at both low and elevated irradiation temperatures. The third type was observed only at irradiation temperatures greater than about 600°C, but it is expected to occur at temperatures down to about 400°C. Expansion caused by grain-boundary separation can be avoided under certain irradiation conditions; when it is avoided, the total expansion and the property changes are minimized.

The types of expansion obtained are governed by the neutron flux and temperature as defined by the relation:

$$\left(\frac{\Delta V}{V}\right)_L = \frac{K}{A}(1 - e^{-At})$$

where $K$ is the defect production rate, $A$ is the defect annealing rate, and $t$ is the time of irradiation. For specimens of 20-$\mu$ grain size,

$$K = 3.3 \times 10^{-23}\phi$$

and

$$A = 1.9 \times 10^{-4} \exp(-10{,}400/RT)$$

The symbols $K$ and $A$ are defined in terms of $(\Delta V/V)_L$/sec; $\phi$ is the neutron flux, nv $\geq$ 1 Mev; $R$ is the molar gas constant; and $T$ is the absolute temperature in degrees Kelvin. This relation is believed to apply to temperatures down to about 400°C.

Important aspects of the radiation behavior defined by this equation include the following:

1. Expansion $(\Delta V/V)_L$ at constant irradiation temperature varies with the neutron flux.
2. Saturation of the lattice expansion $(\Delta V/V)_L$ occurs and is equal to the ratio $K/A$.
3. Comparison of the saturation value of lattice expansion with the value corresponding to grain-boundary separation permits definition of the temperature and flux conditions that avoid boundary separation.
4. In different fluxes, equivalent expansion occurs at the same dosage when the irradiation temperatures are varied such that the $K/A$ ratios are equal.
5. Under irradiation conditions that prevent grain-boundary separation, the total expansion utlimately is dominated by the quantity of helium gas retained in the material. The maximum exposure that BeO can withstand will be determined by its ability to retain the helium without undue property changes or to lose the helium through diffusion to pores or free surfaces. Assuming that low density enhances loss of the helium, it is estimated that low-density BeO can withstand extended irradiation when exposed under flux and temperature conditions that avoid grain-boundary separation.

The strength and elastic constants of irradiated BeO are essentially unchanged unless grain-boundary separation occurs. Observations extend to dosages of $4 \times 10^{20}$ nvt ($\geq$1 Mev).

Preliminary observations indicate that large grain sizes may withstand the highest exposures in irradiations at temperatures greater than 400°C; below this temperature, small grain sizes ($\geq 5\mu$) appear more stable. Preliminary data also suggest that the optimum density for irradiation stability is less than 2.9 g/cm$^3$.

(M. C. Brockway)

# Solid Hydrides

## Zirconium Hydride

A literature survey on zirconium hydride covering the past 10 years has been published by Motz.[36] He also investigated portions of the zirconium-hydrogen system by X-ray diffraction and showed that the delta-phase zirconium hydride exists between 59.5 and 61.4 at.% hydrogen at room temperature. This result is in agreement with earlier phase diagrams published by Atomics International,[37] but not with that of Denver Research Institute,[38] which showed the delta phase to exist between 61.4 and 62.5 at.% hydrogen at room temperature. Motz also observed that, at temperatures above 240°C, the

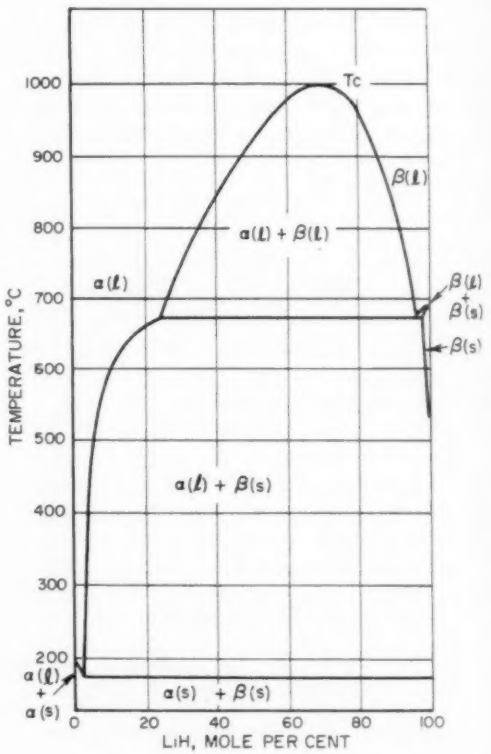


Fig. II-7 Phase diagram of the Li-LiH system.

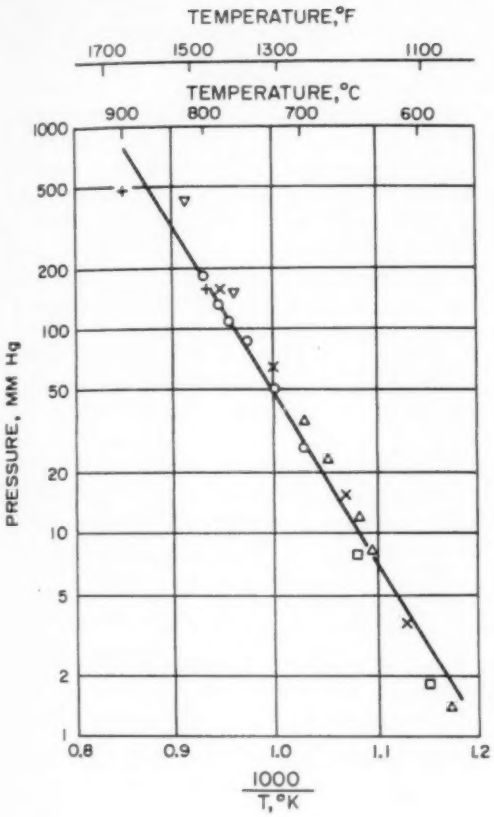


Fig. II-8 Dissociation pressure of lithium hydride. ○, F. K. Heumann and O. N. Salmon, USAEC Report KAPL-1667, Dec. 1, 1956. △, L. L. Hill, Ph. D. dissertation, University of Chicago, 1938. ▽, M. R. J. Perlow, Ph. D. Thesis, University of Chicago, 1941. □, C. B. Hurd and G. A. Moore, *J. Am. Chem. Soc.*, 57: 332 (1935). +, T. R. P. Gibb, Jr., Report NEPA-1841, Apr. 30, 1951. ×, F. H. Welch, Report XDC-61-5-67, Apr. 19, 1961.

delta phase is no longer in equilibrium with alpha zirconium but rather with the epsilon-hase zirconium hydride.

## Lithium Hydride

Information on the properties of lithium hydride has been compiled at Atomics International. The phase diagram of the Li-LiH system is presented in Fig. II-7, and other properties of lithium hydride such as dissociation pressure, specific heat, thermal conductivity, thermal expansion, and ultimate compressive strength are shown in Figs. II-8 to II-12.

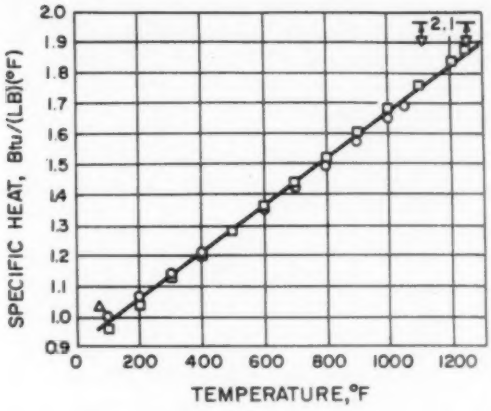


Fig. II-9 Specific heat of lithium hydride. ○, I. B. Fieldhouse, J. C. Hedge, and J. I. Lang, USAEC Report WADC-TR-38-274 (300 to 1050°F). □, Air Force LiH Panel discussion, Wright Air Development Division, Wright-Patterson AFB, February 1961, reported by Union Carbide Nuclear Company, Y-12 plant personel (210 to 1200°F). △, P. Guenther, *Ann. Physik*, 63: 476 (1920). ▽, J. W. Vogt, Report ER-4809, Oct. 15, 1961, 2.1 Btu/(lb)(°F) for 97.5% LiH (1292 to 1472°F).

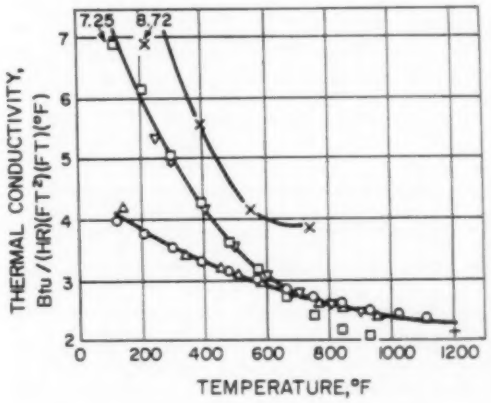


Fig. II-10 Thermal conductivity of lithium hydride. ○, F. H. Welch, Report XDC-61-5-67 (by Vetrand of Battelle for General Electric Company, Aircraft Nuclear Propulsion Department, cold-pressed compact, in $H_2$ atmosphere. □, ibid., cast crystalline in $H_2$ atmosphere. △, I. B. Fieldhouse, J. C. Hedge, and J. I. Lang, USAEC Report WADC-TR-58-274, cold-pressed compact. ▽, D. J. McKee, Report DC-61-1-22, cast crystalline, averaged three tests measured in hydrogen, argon, and in vacuo. +, Air Force LiH panel discussion, February 1961, reported by Thompson Ramo Wooldridge, Inc., personnel. ×, Y-12 data.

There is considerable scatter in the data for thermal conductivity and somewhat less for thermal expansion.

## Ternary Hydrides

General Dynamics[39] has been granted a patent on the process for hydriding massive speci-

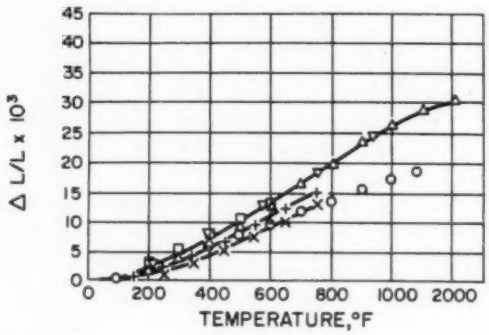


Fig. II-11 Thermal expansion of lithium hydride. ○, F. H. Welch, Report XDC-61-5-67, determined by Union Carbide Nuclear Company, Y-12 personnel, for General Electric Company, Aircraft Nuclear Propulsion Department, for cold-pressed LiH. Δ, I. B. Fieldhouse, J. C. Hedge, and J. I. Lang, USAEC Report WADC-TR-58-274. □, Pratt & Whitney data reported at meeting, March 1961 (F. H. Welch, Report DC-61-3-73). ▽, A. Zalkin, USAEC Report UCRL-4289, single-crystal X-ray diffraction study. + and ×, Y-12 data.

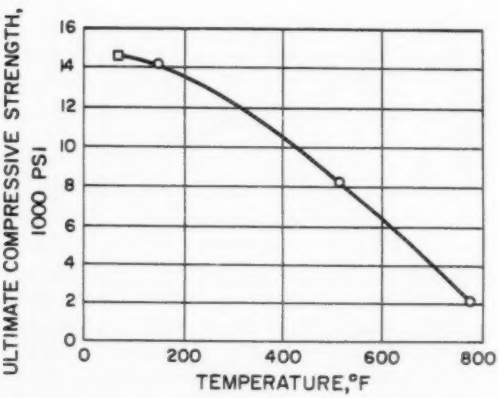


Fig. II-12 Ultimate compressive strength of lithium hydride. □, F. H. Welch, Report XDC-61-5-67, May 1961, cold-pressed LiH, by Union Carbide Nuclear Company, Y-12 personnel. ○, Atomics International-determined values.

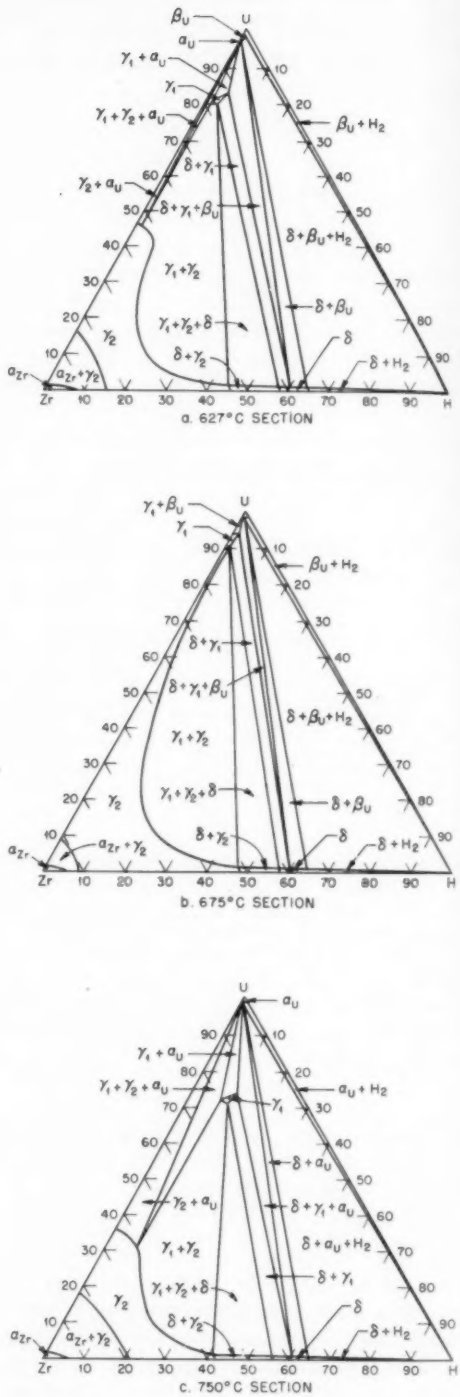


Fig. II-13 Proposed zirconium-hydrogen-uranium phase diagrams.[40]

mens of zirconium alloys without cracking. The process is claimed to be applicable for alloys containing more than 50 wt.% zirconium. Initial hydriding of the alloy is carried out at 700°C, after which the hydrogen pressure is maintained equal to the dissociation pressure of beta-phase zirconium hydride, as the specimen is cooled.

Proposed ternary diagrams for the zirconium-hydrogen-uranium system at 627, 675, and 750°C have been published by Battelle.[40] Hydrogen absorption isotherms and high-temperature X-ray diffraction data published previously[41] were combined with information from the phase diagrams of the binary systems involved to construct the ternary diagrams, which are shown in Fig. II-13.

The hydriding of a zirconium-titanium alloy containing 55 at.% zirconium has been studied by the British.[42] Four major crystalline phases have been identified:

Alpha$_1$—hexagonal close-packed, isomorphous with alpha zirconium and alpha titanium

Beta—body-centered cubic phase, isomorphous with beta zirconium and beta titanium

Delta—face-centered cubic phase, similar to delta zirconium hydride, which appears in the composition range (Zr,Ti)$H_{1.25}$ to (Zr, Ti)$H_{1.95}$

Alpha$_2$—hexagonal phase, not close packed, which appears at 36 at.% hydrogen and has a smaller *c* axis and a larger *a* axis than the alpha$_1$ phase

Hydrides of titanium-niobium alloys have also been investigated by the British.[43] A face-centered cubic hydride phase was found from pure titanium to 67 at.% niobium. Between 67 and 74 at.% niobium, both face-centered cubic and body-centered cubic hydrides exist. Above 74 at.% niobium, a distorted body-centered cubic hydride occurs. Over the face-centered region, the hydrogen-to-metal atom ratio is 2.0; in the two-phase region, this ratio drops sharply to 1.4 and finally becomes 0.9 for pure niobium. This study confirms the composition $NbH_{0.9}$ as the maximum hydrogen content for this hydride. (H. H. Krause)

## References


1. Oak Ridge National Laboratory, Molten-Salt Reactor Program. Semiannual Progress Report for Period Ending January 31, 1963, USAEC Report ORNL-3419, June 3, 1963.
2. G. R. Tully, Jr., and B. F. Disselhorst, A Process for Making Graphite Less Permeable to Gases at High Temperatures, USAEC Report GA-2318, General Atomic Division, General Dynamics Corp., Feb. 1, 1963.
3. Hanford Atomic Products Operation, Reactor and Fuels Laboratory Monthly Report, USAEC Report HW-77397A, May 15, 1963. (Classified)
4. Hanford Atomic Products Operation, Reactor and Fuels Laboratory Monthly Report, March 1963, USAEC Report HW-77046A, Apr. 15, 1963. (Classified)
5. Raytheon Co., High Temperature Materials Development, Progress Report No. 29, May 1962, Report AD-281238, June 15, 1962.
6. R. F. Bunshah, Future Trends in Beryllium Metallurgy Research, USAEC Report UCRL-7289, University of California, Lawrence Radiation Laboratory, Mar. 29, 1963.
7. J. P. Denny and W. H. Santschi, Melting and Casting Beryllium, *Metal Progr.*, 84(1): 111-113, 126, 128, 130, 132 (July 1963).
8. L. A. Hughes and H. J. Garber, Feasibility of Producing Spherical Beryllium Particles, USAEC Report NUMEC-P-49, Nuclear Materials & Equipment Corp., 1960.
9. G. Boisde, M. Broc, G. Chauvin, H. Coriou, L. Hardy, and P. Jarny, Production of High-Purity Beryllium by Electrorefining in a Fused Salt Bath (in French), *Bull. Inform. Sci. Tech. (Paris)*, No. 62: 29-38 (June 1962).
10. Nuclear Metals, Inc., Beryllium Research and Development Program, Report ASD-TDR-62-509 (Vol. II), April 1963.
11. Western Gear Corporation, Report to Refractory Composites Working Group, paper presented at the 7th Meeting of NASA-ASD Refractory Composites Working Group, Lockheed Missiles and Space Company, Palo Alto, California, Mar. 12–14, 1963.
12. E. M. Grala, R. G. O'Rourke, G. L. Marsh, and L. S. Busch, Rolling Improved Beryllium Sheet. Phase III. Interim Engineering Progress Report, September 1, 1962–December 31, 1962, Report NP-12802 [IR-7-753 (III)], Brush Beryllium Co.
13. A. Moore and C. I. Bort, Metallurgical Process for Working Beryllium, British Patent 919,423, Feb. 27, 1963.
14. V. Nerses and J. M. Siergiej, Phase I. Final Report. Ribbed Beryllium Tubing Extrusion Program, USAEC Report NMI-4950, Nuclear Metals, Inc., May 17, 1961.
15. J. P. Papacosta, D. M. Murdock, and R. W. Crews, Brazing Thin Beryllium Windows, *Rev. Sci. Instr.*, 33:1289-1290 (November 1962).
16. R. G. Gilliland and G. M. Slaughter, Fusion Welding of End Caps in Beryllium Tubes, *Welding J. (N. Y.)*, 42: 29-36 (January 1963).

17. R. G. Gilliland, Investigation of the Wettability of Various Pure Metals and Alloys on Beryllium, USAEC Report ORNL-3438, Oak Ridge National Laboratory, June 13, 1963.
18. J. P. Pemsler, R. W. Anderson, and E. J. Rapperport, Solubility and Diffusion of Gases in Beryllium, Report ASD-TDR-62-1018, Nuclear Metals, Inc., February 1963.
19. V. D. Scott, Electron Microscope Studies of Beryllium, British Report AWRE-O-59/62, October 1962.
20. P. M. Arzhanyi, R. M. Volkova, and D. A. Prokoshkin, Thermodiffusion in the Tungsten-Beryllium System (in Russian), *Izv. Akad. Nauk SSSR, Otd. Tekhn. Nauk Met. i Toplivo*, No. 6: 162-166 (November–December 1962).
21. W. Bonfield and C. H. Li, Dislocation Configurations and the Microstrain of Polycrystalline Beryllium (in English), *Acta Met.*, 2(6): 585-590 (June 1963).
22. A. G. Gross, Jr., and R. G. O'Rourke, Development of Fine Diameter High-Purity Wire from Zone-Refined Beryllium, Final Report, Report AD-297178, Brush Beryllium Co., December 1962.
23. M. Weisz and Y. Adda, Brittleness of Beryllium (in French), *Bull. Inform. Sci. Tech. (Paris)*, No. 62: 5-15 (June 1962).
24. Nuclear Metals, Inc., Fundamental and Applied Research and Development in Metallurgy. Progress Report to USAEC for January 1963, USAEC Report NMI-2114, Apr. 12, 1963.
25. F. Morrow and A. Moore, A Comparison of the Effects of Machining and Grinding on the Tensile Properties of Beryllium, British Report AWRE-O-63/62, November 1962.
26. D. B. King, Design Allowables for Beryllium, Brush Beryllium Co., Nov. 15, 1962.
27. J. A. Keller, J. W. Natwick, and F. J. Majeske, Manufacturing Research Investigation, Chemical Conversion Coating for Beryllium, Report AD-292351, Lockheed Aircraft Corp., Feb. 6, 1961.
28. A. L. Feild, Jr., Study of Beryllium Burnup and Dispersion for Re-entering Nuclear Auxiliary Power Systems, Report AFSWC-TDR-62-119 (WANL - TNR - 064, AD - 294404), Westinghouse Electric Corp., Astronuclear Laboratory, December 1962.
29. D. S. Kneppel, Beryllium Corrosion, Quarterly Report to United States Atomic Energy Commission for the Period Sept. 25, 1962 to Dec. 31, 1962, Report NMI-1908, Nuclear Metals, Inc., Jan. 23, 1963.
30. J. E. Palmer, B. R. Borton, D. A. Triner, and P. J. Phennah, United Kingdom Atomic Energy Authority, May 1962. (Unpublished)
31. J. E. Palmer and P. J. Phennah, United Kingdom Atomic Energy Authority, May 1962. (Unpublished)
32. V. Levy, Behavior of Helium in Beryllium (in French), *Bull. Inform. Sci. Tech. (Paris)*, No. 62: 56-59 (June 1962).
33. University of California, Lawrence Radiation Laboratory, Current Beryllium Literature: A Selected Bibliography, January 1961–December 1962, USAEC Report UCRL-5705 (Suppl. 2), January 1963.
34. F. J. P. Clarke, A Model for the Strength of Irradiated Beryllium Oxide, British Report AERE-R-4275, February 1963.
35. General Electric Company, Flight Propulsion Laboratory Department, High-Temperature Materials and Reactor Component Development Programs. Volume I. Materials. Second Annual Report, USAEC Report GEMP-177A, Feb. 28, 1963.
36. J. Motz, Concerning the System Zirconium-Hydrogen, *Z. Metallk.*, 53: 770-774 (December 1962).
37. H. Rosenberg (Ed.), SNAP-8 Reactor Preliminary Design Summary, USAEC Report NAA-SR-6207, Atomics International, June 15, 1961. (Classified)
38. R. L. Beck, Zirconium-Hydrogen System, *Trans. Am. Soc. Metals*, 55: 542-555 (September 1962).
39. U. Merten, Production of Zirconium Hydride, U. S. Patent 3,070,526 (to General Dynamics Corp.), Dec. 25, 1962.
40. H. H. Krause, H. E. Bigony, and J. R. Doig, Jr, Phase Studies in the Zirconium-Hydrogen-Uranium System, *Advan. Chem. Ser.*, No. 39: 131-143 (1963).
41. H. E. Bigony, J. R. Doig, Jr., and H. H. Krause, Jr., The Reaction of Hydrogen with Zirconium–1 and –25 wt.% Uranium Alloys, USAEC Report BMI-1359, Battelle Memorial Institute, July 6, 1959.
42. V. Y. Labaton, E. V. Garner, and E. Whitehead, Phase and Equilibrium Pressure Studies of the Zirconium-Titanium-Hydrogen System, *J. Inorg. Nucl. Chem.*, 24: 1197-1204 (1962).
43. G. S. Upadhyaya and A. D. McQuillan, Crystal Structure of Saturated Mixed Hydrides of Titanium and Niobium, *Trans. AIME*, 224: 1290-1291 (December 1962).

Section

III

Reactor Materials

# Nuclear Poisons

## Metallic Poison Materials

The recently published American Society for Metals monograph,[1] "Fabrication of Control Rods for Nuclear Reactors," contains a complete discussion on the properties of control-rod materials and the techniques of control-rod fabrication from these materials.

The effect of cold work and annealing on the tensile properties of hafnium has been determined at Bettis.[2] Also the effect of heat-treatment on hardness has been determined.[3] Determinations of hardness conversions for hafnium permit the comparison of $R_A$, $R_B$, $R_{15N}$, $R_{15T}$, $R_{30T}$, and DPH hardness values.[4]

The thermal expansion of various zirconium-hafnium alloys (1.1 to 18% hafnium) was evaluated.[5] It was found that the addition of hafnium increased the temperature of the alpha-to-beta transformation in zirconium and consequently caused a shift in abrupt change in the thermal expansion which takes place during transformation. Alloys with 7.6 and 18% hafnium retain a linear temperature dependence of thermal expansion up to 900°C.

Results on the development of the following phase diagrams continue to be reported: hafnium-HfC,[6] molybdenum-rhenium-hafnium,[7] rhenium-hafnium,[8] and iron-carbon-hafnium.[9]

A final report has been issued by Allis-Chalmers Mfg. Co. on boron–stainless-steel control rods for the Pathfinder reactor.[10] The report gives the fabrication and design details of these control rods, along with previous irradiation results of 2.0 wt.% boron in stainless steel. The phase relations of dysprosium, erbium, gadolinium, and samarium-rich alloys of selected non-rare-earth metals have been summarized in the form of diagrams.[11] Hot-water testing of dysprosium, gadolinium, and their alloys indicated that aluminum additions increased the corrosion resistance of the rare-earth metal at temperatures up to 350°F. The solid-state compatibility of boron carbides with commercial copper, types 304 and 430 stainless steel, and AISI 4130 steel was investigated.[12] Diffusion couples were run at 750, 950, 1100, and 1300°F for periods of 500, 1,000, 5,000, and 10,000 hr. Results of the study showed that commercial copper and type 430 stainless steel were compatible with $B_4C$ under the most stringent conditions. Type 304 stainless steel was compatible for 10,000 hr up to 1100°F. A considerable reaction band was formed between $B_4C$ and AISI 4130 steel at temperatures above 950°F.

The metal-boron systems, including borides of the alkali and alkaline-earth metals, borides of rare-earth metals, and actinides and borides of the transition metals of groups IV, V, VI, VII, and VIII, are discussed in detail.[13] The thermal, mechanical, magnetic, electrical, and bonding properties of borides are also presented. The equilibria of high melting systems such as uranium-boron-carbon, thorium-boron-carbon, molybdenum-boron-carbon, thorium-uranium-boron, uranium-titanium-boron, and uranium-zirconium-boron were determined by metallography and X-ray diffraction techniques.[14]

(M. Kangilaski)

## Dispersion Control Materials

The resistance of hydrogen-sintered urania–rare-earth oxide compacts to corrosion by high-temperature high-pressure water was

studied, and the results are discussed in a recent Argonne report.[15] The compacts had been sintered at temperatures up to 1700°C for 4 hr and were exposed to 360°C water at a pressure of 2750 psi. Test times of 15, 69, and 138 hr in deoxygenated distilled water and 138 hr in oxygenated distilled water were employed in these tests. The results of these tests were discussed qualitatively for each of the rare-earth–urania samples with due regard to corrosion products observed and weight changes noted. The additions of the rare-earth oxides were found to improve the corrosion resistance of the pure urania for similar environments. Little damage was noted for the rare-earth-containing specimens after exposures of 138 hr in deoxygenated water. The greatest damage to all the specimens was noted for the 138-hr exposure to oxygenated water.

A recent Russian article[16] describes studies in which the physical properties of hafnium carbide were determined. The carbide was hot pressed from a mixture of prealloyed hafnium carbide powder (6.3 wt.% carbon) and 0.02 wt.% carbon powder. Temperatures from 2900 to 3000°C and pressures of 180 kg/mm$^2$ (256,000 psi) were used. The generated data were compared with those for titanium and zirconium carbides.

The fabrication of thin-walled cylinders of $Gd_2O_3$-$Al_2O_3$ mixtures was discussed in a recent unpublished report by Oak Ridge.[17] This mixture is of interest for control-rod elements of the Molten-Salt Reactor Experiment. It was found necessary to prereact the powders to produce $GdAlO_3$ prior to the sintering operation to prevent distortion in the elements. A 20 wt.% $Al_2O_3$ content was found to result in the least distortion.

The effects of high boron burnups on $B_4C$ and $ZrB_2$ dispersions in $Al_2O_3$ and Zircaloy-2 have been studied at Battelle and the results reported.[18] Various types of dispersions of $B_4C$ in $Al_2O_3$ and Zircaloy-2 and $ZrB_2$ in Zircaloy-2 were irradiated at temperatures of about 400 to 500°F to $B^{10}$ burnups of 81 to 96%. The irradiated $Al_2O_3$ matrix pellets increased in diameter from 1.5 to 3.3% and released from 1.3 to 2.6% of the helium formed. The irradiated Zircaloy-2 matrix pellets were unchanged except that boride particles at the pellet surfaces were swollen. Pellets containing $B_4C$ exhibited little change in diameter, whereas those containing $ZrB_2$ exhibited up to 0.3% increase in diameter. (E. G. Smith, Jr.)

## References


1. W. E. Ray, Fabrication of Control Rods for Nuclear Reactors, ASM Monograph, 1963.
2. J. G. Goodwin, Hardness Conversion Relationships for Hafnium, USAEC Report WAPD-T-1433, Westinghouse Electric Corp., Bettis Atomic Power Laboratory, Mar. 28, 1962.
3. J. G. Goodwin, The Tensile Properties of Cold-Rolled and Annealed Hafnium, USAEC Report WAPD-T-1431, Westinghouse Electric Corp., Bettis Atomic Power Laboratory, May 5, 1962.
4. J. G. Goodwin, The Annealing of Iodine Hafnium, USAEC Report WAPD-T-1427, Westinghouse Electric Corp., Bettis Atomic Power Laboratory, Mar. 16, 1962.
5. K. S. Pridantreva, Thermal Expansion of Zirconium-Hafnium Alloys, *Sb. Tr. Tsentr. Nauchn-Issled. Inst. Chernoi. Met.*, No. 25: 298-302(1962).
6. R. C. Avarbe, A. I. Avgustinik, Yu. N. Vil'k, [Yu. D. Kondrashov, S. S. Nikol'skii], Yu. A. Omel'chenko, and S. S. Ordan'yan, Phase Diagram of the Hf-HfC System, USAEC Translation AEC-tr-5645 [translated from *Zh. Prikl. Khim.*, 35: 1976-1980 (1962)].
7. A. Taylor et al., The Ternary Alloy System, Molybdenum-Rhenium-Hafnium, *Am. Soc. Metals, Trans. Quart.*, 56: 49-67 (March 1963).
8. A. Taylor, The Constitution Diagram of the Rhenium-Hafnium System, *J. Less-Common Metals*, 5: 26-40 (February 1963).
9. V. N. Sevechnikov, Constitution Diagram of Fe-C-Hf System (in Russian), *Sb. Nauchn. Tr. Inst. Metallofiz. Akad. Nauk Ukr. SSR*, No. 16: 124-127 (1962).
10. D. A. Patterson, D. A. Nehrig, R. H. Klumb, and T. E. Peterson, Pathfinder Atomic Power Plant. Boron Stainless Steel Rods for Pathfinder Reactor. Final Summary Report, USAEC Report ACNP-63001, Allis-Chalmers Mfg. Co., Feb. 15, 1963.
11. U. S. Bureau of Mines, Quarterly Metallurgical Progress Report No. 18 for the Period January 1 to March 31, 1963, USAEC Report USBM-U-1031, March 1963.
12. R. D. Hahn, Compatibility of Boron Carbide with Potential AOMR Control Rod Cladding Materials, USAEC Report NAA-SR-Memo-8055, Atomics International, Jan. 31, 1963.
13. B. Post, Refractory Binary Borides, Report NP-12652, Brooklyn Polytechnic Institute, 1962.
14. H. Nowotny, Advanced Experiments on Metal–Silicon–Boron and Metal–Carbon–Boron Systems, Report AD-278041L, Vienna Universität, June 30, 1962.

15. Argonne National Laboratory, Reactor Development Program Progress Report, March 1963, USAEC Report ANL-6705, Apr. 15, 1963.
16. V. H. Paderno, Physical Properties of Metal-Ceramic Specimens of Hafnium Carbide, *Izv. Akad. Nauk SSSR, Otd. Tekhn. Nauk Met. i Toplivo*, No. 6: 176-178 (November-December 1962).
17. Oak Ridge National Laboratory, June 11, 1963. (Unpublished)
18. R. J. Burian, E. O. Fromm, and J. E. Gates, Effect of High Boron Burnups on $B_4C$ and $ZrB_2$ Dispersions in $Al_2O_3$ and Zircaloy-2, USAEC Report BMI-1627, Battelle Memorial Institute, Apr. 24, 1963.

Section

IV

Reactor Materials

# Cladding and Structural Materials

## Corrosion

### Zirconium Corrosion

A recent report from Bettis[1] presents a historical review of the development of Zircaloy-1, Zircaloy-2, Zircaloy-3, and Zircaloy-4. The report also discusses the corrosion properties of Zircaloy-2 and Zircaloy-4 in high-temperature water and steam, including hydrogen absorption during corrosion and the effects of composition, heat-treatment, and water chemistry on oxide film formation.

Argonne[2] is attempting to determine the underlying reasons for lower hydrogen absorption by zirconium-nickel-iron and zirconium-copper-iron alloys in 650°C, 600-psi steam than in 540°C, 600-psi steam. In specimens exposed in 540°C steam to about 1000-ppm hydrogen uptake and then subsequently exposed to 650°C steam, the hydrogen content increased slightly, corresponding to the amount of new hydrogen produced by the additional corrosion at 650°C. This suggests that the alloy hydrogen content was more directly related to the corrosion process than to hydrogen equilibrium conditions existing at the conditions of exposure. Hanford[3] has found that Zircaloy-2 samples prefilmed in 500°C oxygen hydride more rapidly in 375 to 425°C helium contaminated with 3% $H_2$, 2% CO, and 0.05% $H_2O$ than do samples prefilmed in 400°C, 1500-psi steam. This has been attributed to the thicker oxide film (at 500°C) acting as a semipermeable membrane in which the light $H_2$ molecule diffuses more readily than the heavier $H_2O$ molecule. Thus hydriding of the thicker film occurs as the result of depletion of oxidant ($H_2O$) at the metal surface.

Hanford[4] has also studied the corrosion behavior of Zircaloy-2 and Zircaloy-4 in 400°C, 1500-psi $D_2O$ steam and found no isotope effect on corrosion, although deuterium absorption rates in the alloys were somewhat lower than hydrogen absorption rates in $H_2O$. This indicated to the Hanford scientists that hydrogen and deuterium diffuse through the $ZrO_2$ lattice as entities rather than as $OH^-$ or $OD^-$ ions. Hydroxyl-ion diffusion would be expected to result in little or no isotope effect because of the small percentage weight-and-size change caused by substituting deuterium for hydrogen.

In-pile and Van de Graaff electron-irradiation studies conducted at Oak Ridge[5] on the corrosion of Zircaloy-2 in oxygenated high-temperature solutions of $UO_2SO_4$, dilute acids, or water have shown that fission fragments and fast neutrons accelerate corrosion in these environments, but beta and gamma irradiation do not. Experiments are under way to determine whether the corrosion acceleration from radiation is due to increased defects in the oxide film or to increased reactivity of the metal. Capacitance and weight change of the oxide will be followed on specimens that are irradiated and then exposed to a steam-oxygen mixture at 300°C. These will be compared with similar properties for oxide formed on unirradiated specimens.

Electron-microprobe analyses conducted at Savannah River[6,7] on Zircaloy-2 prior to, and after, corrosion in high-temperature water have shown the following:

1. Tin is uniformly distributed in the metal and in the oxide.
2. Iron, nickel, and chromium appear in the metal as discrete metallic particles—nickel almost always coincident with iron, and chromium sometimes, but not always, occurs at points of high iron content.
3. Iron and nickel are more uniformly distributed in the oxide than in the metal.
4. Chromium occurs in the oxide as local concentrations.

5. There is a qualitative relation between the amount of the alloying element in the oxide film and its concentration in the adjacent metal.

Approximately 1600 marks were found and measured.[8] The maximum number of marks found in a single tube was 78. The maximum penetration, 26 mils, occurred in about two months of reactor operating time. Eleven percent of the tubes (9 tubes) were found to have marks deeper than 10 mils; 14% (12 tubes) had marks with a depth from 6 to 10 mils; and 75% (64 tubes) had marks with a maximum depth of 6 mils.

Recent work at Hanford[9] has provided additional evidence of severe crevice corrosion of Zircaloy-2 under heat-transfer conditions in high-temperature water containing LiOH for *p*H adjustment. A maximum penetration of 3 mils was observed beneath stainless-steel supports in an electrically heated Zircaloy-2 sample exposed 146 days to *p*H 10 (LiOH), 315°C water at a heat flux of 380,000 Btu/(hr)(sq ft). On the other hand, Russian scientists[10] have found that heat fluxes in the range of 100,000 to 550,000 Btu/(hr)(sq ft) had no effect on the corrosion of zirconium–0.95 wt.% niobium alloy in aerated water at 275°C even under boiling conditions.

(W. E. Berry)

## Aluminum Corrosion

Experiments conducted for 5300 to 6800 hr at Oak Ridge[5] in flowing *p*H 5 ($HNO_3$) water at 100°C have revealed pitting of 6061-T4 aluminum of up to 35 mils when coupled to type 304 stainless steel, of 17 mils when coupled to hardened type 420 stainless steel, and of 4 mils when coupled to itself. In preliminary tests either coating the aluminum with a chromium deposit or coating the stainless steel with aluminum has shown promise of avoiding pitting in the stainless-to-aluminum crevice region.

Hanford[3] is using rotating disks (4150 rpm) to study the effect of velocity on the aqueous corrosion of aluminum. Erosion in the form of "plateaus and valleys" occurred in a 0.25-in.-wide band at the periphery of a 4-in. disk rotated in tap water at 90 to 95°C. Little or no erosion was observed on 4-in. disks rotated in tap water at 80°C or in reactor process water at 90 to 92°C.

Ruther and Draley[11] have examined the corrosion behavior of aluminum alloys in research reactors in light of proposed corrosion mechanisms and found the "colloidal-deposit theory" applicable in more instances than the "aluminum-oxide-solubility theory." The latter assumes that the corrosion rate is affected by the solubility of the oxide in the water coolant, whereas the former assumes that the corrosion rate is influenced by colloidal particles depositing on the aluminum surface but not necessarily restricted to particles of aluminum oxide.

Hanford[9] has reported lower corrosion rates for in-reactor aluminum coupons (1.0 mil/month) than for out-of-flux coupons (maximum, 2.7 mils/month). Conditions were 109 days' exposure to *p*H 7.9 water at velocities of up to 25 ft/sec, of which 46 days were at 550°F with the remainder at low temperatures. Iron oxide was deposited on the in-flux coupons and was believed to have protected the aluminum oxide from dissolution by the water, thus reducing the corrosion rate. (W. E. Berry)

## Stainless-Steel Corrosion

In contrast to previous results, recent experiments at Argonne[12] have indicated little or no effect of oxygen (0.05 and 30 ppm) on the corrosion behavior of types 304 and 406 stainless steels in 650°C, 600-psig steam flowing at 100, 200, and 300 ft/sec. Corrosion rates after exposure for five weeks to the low-oxygen steam were less than 0.1 mil/year for the type 406 stainless steel and 3 to 4 mils/year for the type 304 stainless steel. The latter also exhibited pits 3 mils deep.

In connection with the nuclear superheat program, General Electric[13] has found that high-nickel alloys withstood a 14-day cyclic run under out-of-reactor superheat conditions, whereas type 304 stainless steel failed in 4 days and type 348 stainless steel failed in 14 days. Tests of stressed specimens exposed at 1150°F in steam with salt deposits revealed Incoloy, Hastelloy X, and Nionel to be virtually unattacked after a 1500-hr exposure, whereas Hastelloy N, Inconel, and type 304 stainless steel exhibited severe attack after 60-, 260-, and 1500-hr exposures, respectively.

A recent Euratom[14] report has summarized a technique for obtaining quantitative measurements of the corrosion taking place on stainless steels in high-temperature water and steam when conventional descaling techniques do not work. The method employs hydrogen at 800°C to reduce the metal oxides. The method is not effective if the specimens are allowed to cool

(from the operating temperature) in the aqueous media and hydroxides are formed on the metal surface. (W. E. Berry)

## Corrosion of Iron- and Nickel-Base Alloys

*Superheated Steam.* Vallecitos[15] is conducting corrosion experiments with nickel-base alloys in superheated steam under heat-transfer conditions. Results given in Table IV-1 show Inconel to have superior corrosion resistance.

Table IV-1 CORROSION IN SUPERHEATED STEAM[15]

| Alloy | Weight loss, mg/dm$^2$ | | | |
|---|---|---|---|---|
| | With heat transfer, metal at 1100 to 1300°F, weight loss at about 1000 hr | Loss to system | With no heat transfer, 1050°F steam | |
| | | | 1000 hr | 5000 hr |
| Type 304 S.S. | 284 | 62 | 227 | 372 |
| Incoloy | 165 | 31 | 108 | 140 |
| Hastelloy X | 151 | 74 | 94 | 134 |
| Inconel | 97 | 34 | 30 | 46 |

It is to be noted that about one-third of the Inconel corrosion products went into the system, whereas only one-fifth was observed for the Incoloy. The net effect is to have less nickel in the system for Incoloy. This results in less activity from the $Co^{58}$ formed by nuclear radiation of the nickel in the crud and less residual $Co^{60}$.

During exposure an alloy layer forms on the surfaces of the nickel-base materials. For Inconel, it is thinner at 1300°F than at 1100°F. The reverse is the case for the other two alloys.

A probe study was made of Incoloy after exposure at 1300°F for 905 hr. In the 9-$\mu$ alloy layer, the chromium at the surface was depleted to about one-half. Iron and nickel showed corresponding increases. Inconel at 1100°F, after 1000 hr, showed a 25-$\mu$ alloy layer depleted in both iron and chromium. For Hastelloy X, the layer was 32 $\mu$ thick. The chromium decreased from around 20 to 10% at the surface.

Rolled A-nickel and TD nickel are being studied by Argonne[12] in 650°C (1200°F), 600-psi oxygenated steam at rates of 100, 200, and 300 ft/sec. In a 40-day test, A-nickel showed a rapid gain in weight and excessive intergranular corrosion. Oxide developed on the inside surface of a large void. For TD nickel, no intergranular attack developed. There was a thin homogeneous film at the surface of the specimen and sound metal below. It is postulated that the 2% thoria in TD nickel (*a*) physically modifies the film or (*b*) increases its conductivity.

A comparison of rates of attack in steam with 0.05 and 30 ppm oxygen showed little difference.

In superheated steam at 650°C (1200°F) containing 30 ppm oxygen, Argonne[16] observed corrosion attack of 0.05 to 0.15 mil after 42 days for a series of alloys. INCO-625 and René 41 are considered promising, whereas type 405 stainless steel (12 chromium, 2 aluminum) and type 410 modified stainless steel (12 chromium, 0.5 titanium, 0.5 silicon) were not.

Under conditions of partial hot spot in steam at 550°C (1020°F), Hanford[17] found the most resistant alloys to be type 446 stainless steel, Hastelloy X, Incoloy, Inconel X, and PDRL-102. Small additions of oxygen did not alter corrosion significantly.

*Aqueous.* After 83 days in degassed 360°F water, Argonne[16] reports rates of 0.354 mg/cm$^2$ for barstock samples of TD nickel vs. 0.299 mg/cm$^2$ for commercially pure nickel. The TD nickel shows small protuberances not seen on the nickel. At the end of 50 days, Argonne[2] reports TD sheet superior to A-nickel sheet.

Hanford[9] exposed sensitized type 304 stainless steel to *p*H 10 water ($NH_4OH$) at 290°C (550°F). A penetration rate of 0.01 mil/year was observed, compared to 0.12 mil/year for steel.

In the Vallecitos Boiling-Water Reactor (VBWR),[15] high-nickel alloys are performing well. Intergranular cracking has been observed on type 300 series stainless steels. However, according to Vallecitos the test cycle does not precisely duplicate reactor systems.

*Gaseous Corrosion.* In connection with the Mobile Low-Power Plant No. 1 (ML-1), Aerojet-

General[18] has exposed seven nickel-base alloys and one austenitic stainless steel to 99.5 vol.% nitrogen and 0.5 vol.% oxygen and to air for up to 10,000 hr at 1750°F to explore their use as fuel cladding. The alloys under study include Hastelloys X and R-235; Inconels 600, 702, and 604; G-157; Nichrome V; vanadium-niobium; and AISI 310. Solid-solution strengthened nickel-base alloys were, in general, best. It was found that precipitation-hardened nickel-base alloys showed heavy oxidation and nitriding.

Hastelloy X had excellent oxidation and nitriding resistance at 1750°F and is recommended for fuel-element cladding in the ML-1. It has an adherent oxide scale, is resistant to intergranular oxidation, to nitriding, and to oxide-scale spallation. The oxide is a spinel of the $Cr_2O_3$ type.

Hanford[9] studied Hastelloy C at 1000°C, exposed at oxygen pressures of 1 atm and of 5 mm Hg. Initial weight gain was found to be pressure dependent, and, after 10 hr, the weight gain of a 1-atm exposure is twice that of the 5-mm-Hg exposure. A constant difference was observed after this point.

Experiments with Hastelloy C at 3-mm-Hg oxygen pressure showed slight weight loss, possibly due to molybdenum and tungsten volatile oxides.

General Atomic[19] is conducting a fundamental study of 99.999% pure polycrystalline copper at 100, 150, 200, 250, and 300°C in oxygen at a pressure of 50 mm. Transitions from one growth rate to the next corresponded to film thickness at each temperature. For the thickness-dependent parabolic growth-rate region, gamma radiation was without effect. In the time-dependent logarithmic rate region, oxidation was 12% higher with gamma radiation. Preirradiation had no effect on oxidation at 200°C.

A critical review of recent literature on gas-metal reactions for iron- and nickel-base alloys has been prepared by Hanford.[20] Small additions of elements with strong oxygen affinity are found to increase the rate of internal oxidation. Resistant alloys dependent upon the presence of aluminum or chromium may not hold up well as thin sheets because of the depletion of these elements. (F. W. Fink)

## Corrosion of Uncoated Refractory Metals

A powder-metallurgy molybdenum–17 wt.% $Gd_2O_3$ alloy was oxidized in static air at 1800°F in recent Bureau of Mines studies.[21] The material showed about 10 times the oxidation resistance (surface recession of 0.1 to 0.2 in./day) of unalloyed molybdenum but could hardly be called oxidation resistant.

The deoxidation of niobium containing 0.5 wt.% oxygen by calcium and magnesium was studied by the Russians.[22] In the presence (blended, briquetted powders) of 300% excess sodium or magnesium, treatment at 1830°F for 6 hr reduced the dissolved oxygen content of niobium to 0.1 to 0.2%. As a side issue, free energies of formation of oxides of niobium at 1830°F were calculated from data as follows: NbO, 167.7 kcal/mole $O_2$; $NbO_2$, 135.8 kcal/mole $O_2$; $Nb_2O_5$, 128.2 kcal/mole $O_2$. These agree well with published values.

Numerous experimental niobium alloys are being tested for resistance to oxidation in 1500 psi, 1000°F steam in studies at Battelle.[23] Alloys containing from 13 to 16 wt.% titanium, 8 to 13 wt.% vanadium, and 6 to 9 wt.% chromium exhibited outstanding oxidation resistance for 133 days (tests are continuing). Weight gains for this period of time are on the order of 1.5 to 2.0 mg/cm$^2$. Good oxidation resistance of cold-rolled (fibered) structures of these alloys contrasted consistently with relatively poor oxidation resistance (nonadherent oxides) of annealed (recrystallized) structures.

## Corrosion by Liquid Metals and Fused Salts

The mechanisms of interaction of structural metals with molten metals have been the subject of numerous investigations and a number of review papers over the past 15 years. The most recent of these review papers is a well-organized and well-documented summary of corrosion mechanisms in refractory metal–alkali metal systems[24] compiled by DiStefano and Hoffman of Oak Ridge and presented at the Oslo, Norway, Advisory Group for Aeronautical Research and Development Conference on Refractory Metals in June 1963. A brief but lucid description is given of various types of corrosion by liquid metals, followed by discussions and examples of interactions encountered in refractory metal–alkali metal systems. Practically all the known solubility and compatibility data are summarized in the course of this presentation. The need is emphasized for more work on solubility, analytical techniques, and temperature-gradient mass transfer.

Not included in the Oak Ridge review[24] are the recent significant findings by Rocketdyne[25] on corrosion by cesium. The following conclusions were drawn from 30-day, 1600°F, static, isothermal tests on cesium-containing capsules made of the various test materials:

1. Annealed type 310 stainless steel was not dissolved, although carbide was leached out, a white phase appeared intergranularly, and the container surface was softened slightly.
2. Hot-rolled Inconel X was not dissolved, although the exposure resulted in extensive decarburization, leaching of precipitate within grains, and severe overaging and surface weakening.
3. Recrystallized zirconium showed no chemical attack or dissolution, but this material is not suitable for use at 1600°F because of the phase transformation that occurs near that temperature.
4. Recrystallized hafnium was neither dissolved nor attacked, but its strong oxygen-gettering ability resulted in severe surface embrittlement and the formation of a reaction layer.
5. Recrystallized niobium, niobium–1 wt.% zirconium, molybdenum, tantalum, and tungsten all have adequate resistance to attack by stagnant cesium liquid or vapor at 1600°F, although the liquid-exposed surfaces of the more reactive metals became cloudy.

No material was found to be satisfactory for long-time use under boiling, splashing, and refluxing cesium at 1800 and 2500°F. Molybdenum was clearly the worst, showing extreme general dissolution and some grain-boundary attack. The niobium–1 wt.% zirconium alloy suffered severe intergranular attack in 720 hr at 1800°F but not in 55 hr at 2500°F. In fact, this alloy was the best of the metals tested at 2500°F.

Workers at General Electric[26] are investigating mass transfer by sodium of the following steels in the temperature range 600 to 1300°F: type 316 stainless steel (316 S.S.), 2¼ wt.% chromium–1 wt.% molybdenum (2¼ Cr–1 Mo), and 5 wt.% chromium–0.5 wt.% molybdenum–0.5 wt.% titanium (5 Cr–0.5 Mo–0.5 Ti). General findings from cold-trapped polythermal pumping loop experiments are discussed as follows:

316 S.S. — This alloy was approximately neutral to carbon transport in a monometallic system but carburized somewhat in a bimetallic 316 S.S.–2¼ Cr–1 Mo system. An austenitic-to-ferritic transformation was observed at certain hot surfaces.

2¼ Cr–1 Mo — This material decarburized in both nonmetallic and bimetallic 316 S.S.–2¼ Cr–1 Mo systems with a significant loss of tensile strength. This effect was not observed with two special carbide stabilized alloys.

5 Cr–0.5 Mo–0.5 Ti — This alloy was approximately neutral to carbon transport, both in a nonmetallic and in a bimetallic 316 S.S.–5 Cr–0.5 Mo–0.5 Ti system. Hot-zone penetration accompanied by chromium depletion was about 1 mil in 2800 hr.

Argonne researchers[12] exposed a sample of niobium–0.5 wt.% molybdenum for 504 hr to flowing (2 ft/sec) sodium containing 1 to 5 ppm oxygen at 650°C. The oxygen content of the sample increased from about 200 ppm before exposure to about 275 ppm after exposure, with no loss in room-temperature ductility. In contrast, a niobium–4.33 wt.% zirconium sample was completely embrittled and increased in oxygen content from 70 to 1100 ppm during the same test.

The solubility of niobium in sodium in the range 1846 to 2518°F, as measured by a radiochemical technique at the Naval Research Laboratory,[27] is shown below.

| Temp., °F | Solubility, ppm niobium |
|---|---|
| 1846 | 7.4 |
| 2185 | 35.0 |
| 2518 | 243.0 |

Delving into the mechanism of niobium attack by lithium, workers at Oak Ridge[28] found that both grain size and temperature are important. At 400°C, the depth of attack increased with increasing grain size and the mode changed from primarily intergranular to transcrystalline. At 1000°C, penetration was along grain boundaries for all grain sizes. Zirconium in niobium alters its corrosion behavior, providing the oxygen in the alloy is associated with the zirconium. This was demonstrated by tests in 500°C lithium, in which 5 to 20 mils of attack occurred in specimens heat-treated for less than 5 hr at 1000°C following contamination with oxygen, whereas no attack was observed in specimens heat-treated for 8 hr or longer.

According to Argonne workers,[16] the attack of crystal-bar titanium by mercury at 538°C is

inhibited by additions of either nickel or aluminum but is accelerated when both aluminum (50 ppm) and nickel (750 ppm) are added.

Mercury thermal-convection loops of carbon steel, run at Brookhaven[29] for almost a year with $T_{max}$ = 1000°F and $\Delta T$ = 400°F, showed a corrosion penetration of no more than 1 mil in the hot zone when no titanium or zirconium inhibitors were added. This is an order of magnitude lower than that found by earlier investigators. The explanation suggested by Brookhaven is that the loop might have been "self-inhibited," i.e., the iron crystallites precipitated in the cold zone do not adhere to the walls but are carried into the hot zone where, because of their small size and greater specific area, they dissolve at a faster rate than the bulk wall material. Similarly, low corrosion effects were found in boiling mercury loops of carbon steel, 2¼ wt.% chromium–1 wt.% molybdenum steel, and Haynes 25 alloy operated at superheat temperatures to 1300°F for times up to 10,080 hr.

The solubility of iron in mercury over the temperature range 450 to 700°C has been measured by workers at Brookhaven[29] and found to be in general agreement with results from other sources. For this temperature range, the solubility can be approximated by the equation log (ppm iron) = 2.80 – (2700/$T$, °K).

Molten tin at 800°C was found[30] by Westinghouse researchers to attack molybdenum, tantalum, niobium, and tungsten in evacuated vibrated capsules with a temperature drop of about 5°C from top to bottom. At 630°C, niobium showed no visible corrosion but molybdenum and tantalum were still attacked. Tungsten was not tested at the lower temperature.

Studies at Oak Ridge[31] of the compatibility of molten LiF-$BeF_2$-$ZrF_4$-$UF_4$-$ThF_4$ fuels with graphite and INOR-8 under irradiation have revealed a radiolytic oxidation of graphite to $CF_4$. Although a corresponding reduction of $UF_4$ to $UF_3$ might be expected, this has been opposed by the oxidizing effects of nuclear reactions. Indeed, experiments suggest that the approximate balance of these oxidizing and reducing effects should help promote fuel stability and low corrosion in the Molten-Salt Reactor Experiment (MSRE). This has been borne out[5] by the absence of any noticeable deleterious effects on the graphite and INOR-8, which had been irradiated in contact with MSRE fuel.

To make the rapidly expanding volume of data in the field of high-temperature liquid metals available as promptly as possible, the U. S. Atomic Energy Commission's Division of Reactor Development has commissioned Brookhaven to prepare bimonthly reviews[32,33] of unclassified AEC-, NASA-, and Air Force-sponsored work in this field. The first of these reviews appeared in February 1963. They cover all phases of liquid-metal technology, including materials development, heat transfer, fluid flow, component development, physical properties, and power systems, as well as corrosion. They may be purchased from the Office of Technical Services, U. S. Department of Commerce, Washington, D. C. 20545.

(J. H. Stang and E. M. Simons)

# Radiation Effects in Nonfuel Materials

## Defects: Structure and Properties

*Metals.* In studies of the transmission of 75-kev protons through thin crystals of gold, it was found[34] that penetration was greatly enhanced when ions were incident along ⟨110⟩ directions. In other experiments the reflection of 50-kev $H^+$, $He^+$, $Ne^+$, and $Xe^+$ ions from the (110) surface of a copper crystal was found to diminish sharply whenever incidence occurred along low-index directions or parallel to low-index planes. These experiments suggest that ion trajectories follow open channels in the crystal lattice. Two types of channels exist in the face-centered cubic lattice; those formed between adjacent close-packed planes of atoms (in the case of these experiments between {111} or {100} planes) and those between rows of atoms in particular directions (between ⟨110⟩ or ⟨100⟩ from the evidence reported here). Piercy et al.[35] have shown that channeling of 40-kev $Kr^{85}$ ions in aluminum increases with direction in the order ⟨111⟩, ⟨211⟩, ⟨100⟩, ⟨110⟩.

Nelson[36] has extended his work on focusing collision to include observations in tungsten and molybdenum. The bombarding ion was $A^+$, and the atoms were ejected preferentially in the ⟨111⟩, ⟨100⟩, and ⟨110⟩ crystallographic directions because of collision sequences in these directions. Some calculations of focusing energies and ranges are found to be consistent with these results. Additional structure is explained by channeling of recoil atoms between the {110} planes.

Recovery occurred in neutron-irradiated (doses up to $4 \times 10^{19}$ nvt at 40°C) molybdenum at 160°C and in niobium at 120°C.[37] The associated enthalpies were $1.25 \pm 0.08$ ev and $1.22 \pm 0.02$ ev, respectively. For both metals, magnitude of the recovery stage was a maximum at a dose of about $3 \times 10^{19}$ nvt. These recoveries are explained in terms of lattice vacancies diffusing either to interstitial impurities, where they are trapped, or to defect clusters created by the irradiation, where they are annihilated. In lightly irradiated specimens, trapping by interstitial impurities is believed to be the dominant mechanism, but annihilation at clusters probably becomes more important as the neutron dose increases.

*Defects in Metal Alloys.* Magnetic studies of iron-nickel (50–50) during neutron irradiation have shown[38] a new order-disorder transition of the type AuCu, for which the critical temperature is 320°C. The tetragonal axis develops in the direction of the field for crystallites whose [1 0 0] axes are approximately parallel to the field. A study on the single crystal shows that this tetragonal axis is the only axis of easy magnetization in the ordered structure.

Damage produced in metals by neutron irradiation[39] can be expressed by equations that take into account neutron flux, dose, and energy spectrum, as well as the temperature of irradiation. For mild steel, the change in ductile-to-brittle transition temperature and the yield stress depend on the square root of the irradiation damage. The temperature dependence of the damage in mild steel can be accounted for by a second-order annealing process with an average activation energy of 1.84 ev between 140 and 325°C.

*Defects in Other Materials.* Brookhaven[29] has reported data indicating that the property changes resulting from thermal annealing of neutron-irradiated graphite are due to reactions of many different interstitial complexes. These complexes form by clustering reactions during the thermal anneals. The data have been accumulated from samples periodically irradiated and annealed. The report gives a partial survey of the experiments, which suggest the existence of consecutive and steady-state reactions between interstitial complexes. Kinetic equations for the consecutive reactions are described and compared with the results of the experiments.

Kelly et al.[40] at Culcheth have observed contraction in graphite, both parallel and perpendicular to extrusion direction after doses of $6.26 \times 10^{20}$ nvt at 450°C. They point out that Hanford explained similar contractions in terms of radiation-induced graphitization. However, dimensional changes at lower temperatures can be explained as changes in the graphite crystals alone, and so the Culcheth group is proposing this as an alternative theory. They discuss property changes and their thermal annealing in terms of the two theories.

## Theories of Radiation Effects

Atom displacement production by primary knock-on atoms with energies greater than the ionization threshold is found to be enhanced, in specimens of finite geometry, relative to the displacements in a semi-infinite system.[41,42] The atom displacements are shown to depend also on the angular distribution of neutrons incident on the material and the angular dependence of scattering within the medium. Hence these effects must be considered when relating data obtained from small test specimens to those for larger engineering structures. Besco and Beeler,[42,43] in addition, have extended their computer calculations of displacement cascades to include 10-kev ion bombardment of an iron lattice. Erginsoy[44] has also presented computer calculations of cascades in alpha iron, whereas Hauser and Balarin[45] have commented on cascade calculations by critically evaluating the assumptions and limitations involved. Comparisons are shown for copper.

Bennemann[46,47] has extended his calculations to include determinations of lattice distortion[48] when taking into account the coupling between lattice and electrons.

## Surveys on Radiation-Induced Defects

Sosin[49] has issued a review of radiation-effects theory. The review starts with the nature of the original collision and proceeds through all stages of the various displacement processes: primary displacements, secondary displacements and cascades, thermal and displacement spikes, and focusing. Eighty-eight references are listed.

Bichsel[50] has prepared an extensive report and bibliography on the passage of charged particles through matter.

Radiation and anneal effects of point defects in metals, covalent solids, and ionic solids have been reviewed by Friedel.[51] The proceedings of

the September 1962 International Conference on Crystal Lattice Defects, held at Kyoto, have been published.[52] Other summaries of the behavior of crystal defects under irradiation have also appeared.[53,54]

## Effect of Irradiation on Mechanical Properties

The radiation-induced mechanical-property changes in structural metals and alloys continue to be the subject of a number of investigations. The extent of these property changes is usually measured as a function of the total fast flux experienced by the material. Iron-base alloys used as pressure-vessel materials have received considerable research in this area. For example, Brookhaven National Laboratory[29] is concerned with the damage occurring in pure iron and iron alloys in a study dealing with changes of mechanical properties. This is a continuing investigation in which the effect on mechanical properties of such variables as alloy additions, grain size, cold work, irradiation exposure, irradiation temperature, and testing temperature are of interest. To date, materials under study include pure iron and some of the carbon and low-alloy steels. The data indicate that, for pure iron at exposures between $8 \times 10^{17}$ and $2 \times 10^{18}$ neutrons/cm$^2$, a transition of types of fracture occurs. Also, embrittlement was observed when the exposure was increased to $2 \times 10^{18}$ neutrons/cm$^2$. The property changes after a $2 \times 10^{18}$ neutrons/cm$^2$ exposure are reported. Workers at Oak Ridge[55] also have been investigating effects of irradiation on pressure-vessel materials. They have been considering the changes resulting from irradiation in ASTM A-212B steel, a pressure-vessel steel used in the Stationary Medium-Power Plant No. 1 at Fort Belvoir, Va. An irradiation surveillance program has been conducted using the change in impact properties as a measure of irradiation effects. The materials have been tested after a total exposure of about $2.5 \times 10^{18}$ neutrons/cm$^2$ on the basis of sulfur dosimetry. Extrapolations of the results have been made to predict a 20-year accumulated effect. It was found that the brittle-to-ductile transition temperature for this particular steel in a midsection of the pressure vessel will have increased about 229°F.

The effects of irradiation on some of the stainless steels exposed in a superheated steam and neutron-radiation environment have been summarized.[13] Some of the stainless steels that have been investigated include types 347, 316, and 406. The results for one group of specimens irradiated at approximately 650°C were compared with those for control specimens heated for 500 hr at 650°C. The total integrated neutron flux for the irradiated specimens was approximately $2.5 \times 10^{20}$ thermal neutrons/cm$^2$. The effects of irradiation should indicate minor property changes resulting from the irradiation. There was a reduction in strength and elongation. A somewhat similar effect was noted for the tests made at 700°C. It was noted that the radiation-induced changes were more severe at the higher test temperature. Similar irradiations made on AISI 406 and RA-330 along with some additional samples on types 316 and 347 stainless irradiated at 700°C showed some small changes when tested at room temperature, the main change occurring in the yield strength. However, when these specimens were tested at 1100°F, the changes in yield strengths were within ±4% of those for the preirradiated control. The unirradiated controls had not received a similar heat-treatment simulating in-reactor temperatures for this series of tests. The conclusions drawn from a high-temperature irradiation program on A-286 stainless steel, Hastelloy X, and René 41 are summarized in a recent General Electric report.[42,43] A major conclusion was that the precipitation-hardening materials showed some reduction in short-time stress-rupture properties as a result of irradiation at elevated temperatures.

A program being conducted at Oak Ridge[28] deals with irradiation tests on stainless steels. A typical composition of materials under study is 20 wt.% chromium, 25 wt.% nickel, 1 wt.% niobium, balance iron. These materials were compared in out-of-pile stress-rupture tests in an atmosphere of carbon dioxide and 5% carbon monoxide at 750°C. In-pile rupture tests were also conducted at 750°C. The effects of irradiation were not as noticeable at 750°C as they were at 100°C lower. Also, strain at fracture for tests at 650°C was lower by 30 to 50% than that for corresponding out-of-pile tests, and it was noted that a number of the in-pile specimens failed in or near the end-weld closures, which indicates perhaps an irradiation-induced weakening or an embrittlement of the welds.

Chalk River,[56] in cooperation with Oak Ridge, has conducted a study on the effects of irradia-

tion in beryllium. Several types of beryllium and several different heat-treating conditions were investigated. In summary, the results show that the mechanical properties of beryllium irradiated at about $1.5 \times 10^{19}$ neutrons/cm$^2$ (>1 Mev) at 200 to 300°C undergo no great change in the test-temperature range of 200 to 500°C. However, a significant loss of ductility is noted in the same material when irradiated at $1 \times 10^{21}$ neutrons/cm$^2$ under similar temperature conditions. If the test temperatures are less than 200°C after irradiation at $1 \times 10^{21}$ neutrons/cm$^2$, there is no apparent ductility in beryllium. Other lots of beryllium show slightly different results after irradiation under similar conditions. (F. R. Shober)

# Selected Mechanical Properties of Structural and Cladding Materials

## Refractory Metals

The mechanical properties of niobium-hydrogen alloys, as a function of hydrogen content, temperature, and strain rate, were investigated at the University of Oklahoma.[57] Hydrogen embrittles niobium even at concentrations below the limits of solubility. The concentration of hydrogen necessary to effect a given degree of embrittlement increases with increasing temperature in a roughly exponential manner. When not masked by a high ductile-brittle transition temperature caused by other factors (e.g., grain structure or other embrittling impurities), a restoration of ductility is observed at low temperatures. The ductility minimum occurs at about −78°C, which appears to be the temperature of hydrogen strain aging during the tensile test. The embrittlement associated with the presence of hydrogen can be removed by vacuum dehydrogenation. Hydrogen solubility in niobium increases with increasing temperature. The hydrogen concentration necessary to cause embrittlement varies with temperature in a manner similar to that of the solubility. At hydrogen contents above the limit of solubility, a second phase forms which results in a volume expansion of 10%. This expanded second phase constitutes prestressed Griffith cracks on (1 0 0) planes and is the evident cause of embrittlement. At concentrations below the limit of solubility, hydrogen is believed to segregate at microcrack vertices during plastic straining. The repulsive forces consequent to the segregation increase the stress concentration at the crack vertices. The applied stress required for fracture is thus lowered. It was found that the fracture stress of niobium decreases with increasing hydrogen content most rapidly at the strain-aging temperature.

Experimental vanadium-niobium-base alloys were fabricated at Armour[58] to sheet from 200-g arc-melted ingots. The composition vanadium–60 wt.% niobium–1 wt.% zirconium–0.075 wt.% carbon had ultimate tensile-strength values of 97,000, 77,000, and 20,000 psi at 1800, 2000, and 2400°F, respectively. On a density-corrected basis, this material, up to 2000°F, gave the highest strengths of all materials studied under this and the preceding programs. The vanadium–40 wt.% niobium–30 wt.% tantalum–1 wt.% hafnium alloy had higher strength (25,400 psi) at 2400°F but lacked the high room-temperature ductility of the vanadium-niobium-zirconium-carbon material.

The influence of oxygen on the yield strength of two binary alloys of niobium containing 4.7 at.% molybdenum and 5.3 at.% tantalum is reported by British investigators.[59] The alloys were prepared by arc-melting the raw materials in argon using a nonconsumable niobium electrode. An anodizing technique was used to produce a controlled increase in the oxygen content of the recrystallized alloys. Specimens were strained at a rate of $9.2 \times 10^{-5}$ per second at room temperature and $8.3 \times 10^{-5}$ per second at −196°C. Well-defined yield points were produced in specimens from each alloy in tests at room temperature. In tests at −196°C, yield points of the type produced at room temperature were found in only two cases. An increase in oxygen content from 0.01 to 0.1 wt.% increased the yield strength approximately $25 \times 10^3$ psi. The increase in strength resulting from a decrease in temperature was greater in the case of the two alloys than for the unalloyed material.

Cooper and Srp[60] present a brief review of the significant properties of the refractory metals that make them potentially useful materials. Also, the applications for which the materials appear suited and the problems that hinder their development, such as their notoriously poor oxidation resistance and their ductile-brittle transition behavior, are discussed.

A study was conducted at Union Carbide[61] to determine the effect of oxygen on the mechanical properties of niobium. Niobium specimens with grain sizes ranging from 0.1 to 2 mm and with dissolved oxygen contents ranging from 500 to 600 ppm were shown to twin at −196°C after yielding in compression. Twinning did not occur at −196°C in specimens contaminated with oxygen or in any specimens at −75°C or higher. The effect of grain size on the yield strength, either with or without twinning, increased with oxygen content. Larger grained specimens yield at lower stresses than do finer grained specimens. At elevated temperatures the greatest influence of oxygen on tensile properties was between 300 and 400°C, the range where it is believed to cause strain aging. Any effect was lost above about 700°C.

In a book written by Savitskii,[62] an experimental and systematic examination is presented of the influence of temperature on the mechanical properties of typical metallic systems in relation to the crystalline structure and the chemical interactions of the components. A basis is given for choosing the most favorable temperature conditions for hot working. Experimental data are presented for 20 metals, 15 metallic compounds, 16 binary systems, and 2 ternary systems, and conclusions are given in a final chapter for each group of metals studied.

(J. A. DeMastry)

# Selected Metallurgical Aspects of Cladding and Structural Materials

## Aluminum

The effects of plastic deformation on the superconducting transition temperature, $T_c$, and on the residual electrical resistivity of pure aluminum were determined by investigators at Rutgers University.[63] Specimens were filed, cold rolled 97%, fatigued, and deformed in uniaxial tension at room temperature. In all cases where a change in $T_c$ was observable, the transition point decreased. The rate of decrease with resistivity and the change in $T_c$ of a quenched specimen subsequently aged at room temperature were consistent with other observations. Isochronal annealing of the rolled specimens showed that $T_c$ and $\rho$ could be restored to the values for undeformed specimens.

## Titanium

Russian workers[64] have shown that, at room temperature, one-phase fields occupy a very small area of the concentration triangle in the titanium-boron-chromium system. This is in the small regions of solutions in a base of titanium, chromium, boron, and binary and possibly ternary chemical compounds, as well as the continuous series of solid solutions in the base of diborides of titanium and chromium. It is probable that there are three-phase fields of titanium-TiB-$TiCr_2$, such as a chromium intermetallic compound of titanium with chromium boride.

## Refractory Metals

A two-band model of superconductivity was investigated by workers at Tokyo University.[65] One band was treated in line with Bardeed-Cooper-Schrieffer, the cut of the interaction outside $\hbar\omega$ of the Fermi energy. In the other band the interaction was assumed to be repulsive. The superconducting transition temperature was always raised over that of the single attractive band when an interaction between the bands was introduced. The increase of the temperature was shown to be large when the density of states of the repulsive band at the Fermi surface was large. The isotope effect vanished when the interband interaction was large. This model can account for the superconducting properties of the $V_3M$ series and $Nb_3Sn$. It can be argued that superconducting nontransition metals belong to single-band superconductors, whereas the superconductivity of transition metals is largely due to their overlapping bands, especially in lanthanum.

A proposed constitutional diagram was developed at Iowa State University[66] from equilibrium data obtained for the niobium-tin binary-alloy system. The equilibrium solubility of niobium in liquid tin varied from approximately 250 to 2000 ppm at 580 and 1000°C, respectively. The equilibrium solubility of tin in niobium varied from approximately 2.5 to 3 wt.% tin at 550 and 1000°C. Two previously unreported intermetallic compounds, $Nb_2Sn_3$ and $Nb_3Sn_2$, in addition to $Nb_3Sn$ were found in the system. $Nb_3Sn$ decomposed peritectically into niobium and liquid tin at 2125 ± 25°C. $Nb_3Sn_2$ decomposed into

$Nb_3Sn$ and liquid tin at 915 ± 5°C. $Nb_2Sn_3$, the assumed but unverified composition for the most tin-rich compound, decomposed into $Nb_3Sn_2$ at 820 ± 3°C. $Nb_2Sn_3$ has a $D_{2h}^{24}$–$Fddd$ structure with lattice parameters of 5.72 ± 0.04, 10.03 ± 0.06, and 19.06 ± 0.06 A. $Nb_3Sn_2$ has a body-centered orthorhombic crystal structure with lattice parameters of 5.637 ± 0.001, 9.204 ± 0.003, and 16.667 ± 0.003 A. The number of possible space groups for $Nb_3Sn_2$ was reduced to four, $D_2^8$–$I222$, $D_2^9$–$2_i2_i2_i$, $D_{2h}^{25}$–$Immm$, and $C_{2v}^{20}$–$Imm$. The intermetallic compounds $Nb_3Sn$ and $Nb_3Al$ were found to be completely miscible in the solid state. All their alloys were simple cubic ($Cr_3O$ type). Their lattice constants followed Vegard's rule except in the vicinity of mole ratios of 1:3 and 3:1. At these mole ratios, the lattice constants deviated to values larger than predicted by Vegard's rule. Alloying $Nb_3Sn$ with $Nb_3Al$ appears to raise the zero field superconducting transformation temperature of $Nb_3Sn$ slightly.

Hall coefficient measurements were made on cold-rolled niobium–25 wt.% zirconium in the zero-resistance mixed state at 4.2°K and in the normal state at 4.2, 77, and 317°K at the Naval Research Laboratory.[67] At sample current densities from $2 \times 10^3$ to $1 \times 10^4$ amp/cm$^2$ in fields of 1 and 9 gauss, no Hall voltage for the superconducting sample could be observed with equipment capable of detecting voltages as small as $10^{-9}$ volt. An upper limit of the superconducting Hall coefficient was calculated to be $10^{-15}$ m$^3$/amp-sec. The values of the Hall coefficient for niobium–25 wt.% zirconium in the normal state are $1.14 \times 10^{-10}$, $1.05 \times 10^{-10}$, and $0.84 \times 10^{-10}$ m$^3$/amp-sec at 4.2, 77, and 317°K, respectively.

The thermal expansion, heat capacity, thermal conductivity, total normal emittance, electrical resistivity, and thermoelectric voltage were investigated at Southern Research Institute[68] for 26 refractory materials, including the borides, carbides, nitrides, oxides, ATJ graphite, tungsten, and alloys of molybdenum and niobium. The temperature range was from 500 to 5000°F. In addition to these thermophysical properties, the density, chemical analysis before and after temperature exposure, and microscopic pictures before and after temperature exposure are included to define the materials and assist in the analysis of the data.

Russian investigators[69] utilized metallographic and X-ray structural analysis methods and measurements of the hardness and microhardness of phases to study the structure of tungsten-niobium-silicon alloys. A phase diagram was constructed of the pseudobinary section of $WSi_2 + NbSi_2$ in the form of a diagram with a eutectic of $WSi_2 + NbSi_2$, a solid solution containing 60 at.% $WSi_2$ and melting at 1860°C. The triangulation of the ternary system tungsten-niobium-silicon is indicated, and its phase diagram was constructed. Four regions of ternary solid solutions were found and approximately outlined in the ternary system on the basis of the compounds $NbSi_2$, $Nb_4Si$, and tungsten-niobium. Alloys of the $WSi_2$-$NbSi_2$ systems are not refractory. When heated in air to 1100 to 1200°C, they become coated with a loose film of oxides, which does not prevent the further oxidation of the alloy surface.

A study by Russian investigators[70] of the lattice constants of the solid solutions of niobium and titanium in chromium by X-ray diffraction methods indicates that the alloys undergo a complete decomposition. Examination of the microstructure and of the hardness changes in terms of the composition revealed that the boundary between the one- and two-phase regions in the chromium-niobium and the chromium-titanium systems lies between 2 and 3 at.% niobium and 5 and 7 at.% titanium, respectively. Changes in the lattice constants showed that the chromium-niobium alloys decompose slowly but noticeably at 820 to 850°C; the value of the constant ultimately reaches, or approaches within experimental error, that of pure chromium. Similar observations were made with the chromium-titanium solid solutions. The niobium alloys decompose gradually, whereas the titanium alloys undergo a two-phase decomposition. It was also found that the solubility of titanium in chromium at 1200°C does not exceed 0.3 to 0.6 at.%; niobium possesses approximately the same solubility at 1000°C or at even lower temperatures.

## Zirconium

Characteristics of the omega transformation in the zirconium-niobium system were studied by single-crystal X-ray diffraction techniques at Case Institute of Technology.[71] Two distinct mechanisms for establishing a metastable equilibrium between beta and omega were studied. The first mechanism involved the diffusionless transformation of beta to omega on cooling from the beta field. This reaction was found to be continuously reversible, with little or no hys-

teresis over a broad temperature range. The Lorentz expression for the shape of a pressure-broadened line was found to fit the true line shape quite well if the power, $n$, of the distance from the line center was allowed to vary. For lines whose width at one-half their maximum percent absorption was less than 2.2 $cm^{-1}$, $n$ was found to be equal to 2. The value of $n$ decreased for lines wider than the above to as low as 1.79, and the average value was 1.85. In the range of pressures studied (1 cm to 5 atm pressure), $n$ was measurably dependent on pressure. Within experimental error, $n$ was constant from the line center to at least 10 $cm^{-1}$ from the line center for a particular line.

An investigation made of the copper-zirconium system for the purpose of accurately establishing the solidus and solvus curves and the eutectic temperature in copper-rich alloys is reported.[72] Metallographic and electrical-resistivity measurements were used as the primary methods for the investigation; however, some thermal-analysis studies were also performed. From breaks in the electrical resistivity-vs.-concentration curves for the alloys, the limits of zirconium solubility in copper at the various temperatures were ascertained. The maximum solubility of zirconium in copper was found to be 0.24 wt.%. The apparent molar heat of solution of zirconium in copper was calculated to be 28,900 cal/mole.

The constitution diagram of $ZrCr_2$-$ZrFe_2$, as reported by the Russians,[73] indicates two separated solubility regions in alloys with 51% chromium, 4% iron to 41% chromium, 14% iron at 1635°C and with 33% chromium, 20% iron to 5% chromium, 50% iron at 1625°C. The observed two peritectic regions join at the liquidus-solidus point at 1600°C with 38% chromium, 16% iron, and 46% zirconium. The $ZrCr_2$-$ZrFe_2$ section is quasi-binary.

The constitutional diagram of iron-zirconium alloys was studied by Russian workers.[74] X-ray diffraction, microstructural, thermal, and durometric analyses of 21 specimens of electrolytic iron and iodide zirconium showed two peaks for alloys with 30% zirconium at 1320 and 1325°C (eutectic melting and liquidus point). Another peak was found for alloys with more than 30% zirconium at 1480°C. Microstructure studies revealed a two-phase region for 30 to 34% zirconium and a two-phase region for alloys with more than 34% zirconium; both phases had identical microhardness corresponding to the intermetallic $\epsilon'$. A new intermediate $\epsilon'$ phase was studied, and changes in the 35 to 50% zirconium $\eta$-phase lattice parameters were analyzed.

### Miscellaneous

A compilation of data on thermal radiative properties[75] includes a discussion of the fundamental properties and methods for measuring them. Thermal radiative data (emittance, reflectance, and absorptance) are included for the following materials: titanium and its alloys; stainless steels; iron, nickel, and cobalt superalloys; the refractory metals (chromium, niobium, molybdenum, tantalum, and tungsten) and their alloys; coated materials for elevated-temperature service; and ceramics and graphite.

The original graphical method proposed by Darken and Gurry for predicting the elements that are soluble in a given element was slightly modified by Los Alamos workers[76] and was then used to predict terminal solubilities in 1455 known binary combinations. The modified Darken and Gurry method had a reliability of 61.7% in predicting extensive solid solubility (>5 at.%), 84.8% in predicting limited solid solubility (<5 at.%), and an overall reliability of 76.6%. The Hume-Rothery size-effect criterion was 50.1% reliable in predicting extensive solid solubility, only slightly better than a purely random choice, and 90.3% reliable for predicting limited solid solubility, an overall reliability of 67.6%. (J. A. DeMastry)

## Diffusion Studies

Self-diffusion and diffusion of rhenium tracer in single-crystal tungsten over the temperature range 2660 to 3230°C have been measured at Los Alamos[77] using the direct sectioning technique. The temperature dependence of the diffusion coefficients in the two systems is represented by the equations:

$$D(W) = (42.8 \pm 4.8) \exp -(153{,}100 \pm 600)/RT \quad cm^2/sec$$

$$D(Re) = (275 \pm 110) \exp -(162{,}800 \pm 2500)/RT \quad cm^2/sec$$

The author proposes that the results are consistent with a ring mechanism as the fundamental step in tungsten self-diffusion.

A graphical method of interest has been described for separating the effects of grain boundary and lattice diffusion in polycrystalline materials. The method was developed and tested at Oak Ridge,[78] and a study of the diffusion of $Nb^{95}$ in $UO_2$ is presented as an example.

(D. C. Carmichael)

## Ceramic Technology

The basic research program in ceramics at Massachusetts Institute of Technology[79] is continuing. The recent study topics are sample preparation (powder compaction), kinetic processes and microstructure development, relation of properties to crystal structure and microstructure, and the structure and properties of noncrystalline solids. The work on kinetic processes indicates that there is a substantial influence of grain boundaries in oxide systems on the diffusion-controlled processes, which include sintering and creep deformation. Studies of the kinetics of hot pressing of aluminum oxide show that the contribution of plastic flow to densification is small and that final-stage densification is enhanced by diffusion under the influence of stress. In the dissolution of refractory materials in liquid slags, diffusion through the boundary layer is rate controlling. Studies of the effects of unusual convection on dissolution are in progress. In investigations of deformation behavior, it was found that creep deformation in polycrystalline $Al_2O_3$ occurs by a diffusional transport of material, with the aluminum-ion diffusion controlling the rate. At high temperatures, enhanced rates are caused by stress redistribution following boundary separation with deformation by a diffusional mechanism. Work is under way to examine the transition from diffusion-controlled creep to dislocation-movement-controlled creep at higher temperatures. In studies of noncrystalline oxides, films, as well as the solubility limits of components for which the solid solubility is limited, are being studied.

In studies at Du Pont,[80] a ternary composition diagram of the system tungsten-yttrium-oxygen has been developed. $WO_3$ and $YO_3$ react to form five compounds.

The effects of additives and sintering atmosphere on the sintering of refractory oxides have been covered in a literature survey published by Blackman.[81]

Pennsylvania State University investigators[82] have studied high-temperature-materials phenomena. Highly sensitive equipment for measuring dielectric loss has been designed and constructed for studies on high-permittivity-relaxation materials. A computer program yields exact values of the partial oxygen pressure generated for a certain ratio of mixed gases at a certain temperature, which is very useful in metal-oxygen work. They have shown that infrared spectra may be used to determine the coordination of the metal ion in simple oxide structures.

(D. J. Bowers)

## References


1. S. Kass, The Development of the Zircaloys, USAEC Report WAPD-T-1549, Westinghouse Electric Corp., Bettis Atomic Power Laboratory, October 1962.
2. Argonne National Laboratory, Reactor Development Program Progress Report, March 1963, USAEC Report ANL-6705, Apr. 15, 1963.
3. Hanford Atomic Products Operation, Reactor and Fuels Laboratory Monthly Report, March 1963, USAEC Report HW-77064A, Apr. 15, 1963. (Classified)
4. R. L. Dillon, Hanford Atomic Products Operation, Mar. 4, 1963. (Unpublished)
5. Oak Ridge National Laboratory, Reactor Chemistry Division Annual Progress Report for Period Ending January 31, 1963, USAEC Report ORNL-3417, May 1, 1963.
6. R. R. Hood and L. Isakoff (Comps.), Heavy Water Moderated Power Reactors Progress Report, January 1963, USAEC Report DP-825, E. I. du Pont de Nemours & Company, Inc., February 1963.
7. E. I. du Pont de Nemours & Company, Inc., Application of the Electron Microprobe to the Study of Zircaloy Corrosion Films. Quarterly Progress Report, October–December 1962, USAEC Report DPST-62-71-4, February 1963.
8. D. R. Doman and P. J. Pankaskie, In-Reactor Monitoring of Zircaloy-2 PRTR Pressure Tubes, Part II. May and June 1962, USAEC Report HW-74731, Hanford Atomic Products Operation, August 1962.
9. F. W. Albaugh, Reactor and Fuels Laboratory Monthly Report, April 1963, USAEC Report HW-77397A, Hanford Atomic Products Operation, May 15, 1963. (Classified)
10. N. G. Rassokhin and V. N. Mel'nikov, The Stability of Zirconium Alloys in a Circulating Aqueous Medium, USAEC Translation AEC-tr-5414 [translated from *Teploenerg.*, 2: 60-62 (1962)].
11. Oak Ridge National Laboratory, Research Reac-

tor Fuel Element Conference, September 17–19, 1962, Mountain View Hotel Auditorium, Gatlinburg, Tennessee, USAEC Report TID-7642.

12. Argonne National Laboratory, Reactor Development Program Progress Report, April 1963, USAEC Report ANL-6717, May 15, 1963.
13. Proceedings of the Nuclear Superheat Meeting, No. 7, Sept. 12–14, 1962, Sioux Falls, South Dakota, USAEC Report TID-7658, Oct. 30, 1962.
14. Société d'Études de Recherches et d'Applications pour l'Industrie, Studies of Steel Corrosion in High Temperature Water and Steam, USAEC Report EURAEC-552, Jan. 30, 1963.
15. W. L. Pearl and G. G. Gaul, General and Stress Corrosion of High Nickel Alloys in Simulated Superheat Reactor Environment, USAEC Report GEAP-4165A, General Electric Company, Vallecitos Atomic Laboratory, March 1963.
16. Argonne National Laboratory, Reactor Development Program Progress Report, May 1963, USAEC Report ANL-6739, June 15, 1963.
17. M. M. Hendrickson and J. K. Green (Eds.), Research and Development Programs Executed for the Division of Reactor Development, Quarterly Progress Report for October–December 1962, USAEC Report HW-76559, Hanford Atomic Products Operation, January 1963.
18. J. S. Brunhouse and G. W. Titus, Army Gas-Cooled Reactor Systems Program, Evaluation of Long-Term Gas Corrosion of Heat-Resistant Alloys for Use as Gas-Cooled Reactor Fuel Cladding, USAEC Report IDO-28605, Aerojet-General Nucleonics, April 1963.
19. J. Tobin, A Study of Copper Oxidation and Some Irradiation Effects, Final Report, USAEC Report GA-3349, General Atomic Division, General Dynamics Corp., Feb. 6, 1963.
20. D. A. Jones, Gas-Metal Reactions with Iron- and Nickel-Base Heat Resistant Alloys. An Interpretative Literature Survey, USAEC Report HW-76952, Hanford Atomic Products Operation, March 1963.
21. Bureau of Mines, Metallurgical Quarterly Progress Report No. 17 for the Period October 1–December 31, 1962, USAEC Report USBM-U-1001.
22. G. A. Meerson and T. Segorceanu, The Affinity of Niobium to Oxygen, *At. Energ. (USSR)*, pp. 597-599 (December 1962).
23. J. A. DeMastry, A. A. Bauer, and F. A. Rough, Development of Niobium-Base Alloys for Use in a Nuclear Superheater, USAEC Report BMI-X-10040 (EURAEC-626), Battelle Memorial Institute, Apr. 1, 1963.
24. J. R. DiStefano and E. E. Hoffman, Corrosion Mechanisms in Refractory Metal-Alkali Metal Systems, USAEC Report ORNL-3424, Oak Ridge National Laboratory, Sept. 16, 1963.
25. Rocketdyne Division of North American Aviation, Inc., Effects of Liquid and Vapor Cesium on Container Metals, Report ASD-TDR-62-965, Oct. 31, 1962.
26. F. J. Hetzler and R. S. Young, Sodium Mass Transfer. II. Screening Test Data and Analysis. Volume 2. Metallurgy, USAEC Report GEAP-3726, General Electric Company, Atomic Power Equipment Department, June 1962.
27. T. A. Kovacina, C. T. Ewing, J. P. Stone, and R. R. Miller, High Temperature Properties of Sodium and Potassium. Progress Report No. 8, July 1 to September 30, 1962, Report NRL-5904, Naval Research Laboratory, Dec. 17, 1962.
28. Oak Ridge National Laboratory, March 1963. (Unpublished)
29. J. H. Reynolds (Ed.), Nuclear Engineering Department Progress Report, May 1–August 31, 1962, USAEC Report BNL-759, Brookhaven National Laboratory.
30. J. R. Lance and G. A. Kemeny, Corrosion of Refractory Metals by Liquid Tin, *Am. Soc. Metals. Trans. Quart.*, 56: 204-205 (March 1963).
31. Oak Ridge National Laboratory, Third Conference on Nuclear Reactor Chemistry, Gatlinburg, Tennessee, October 9 through 11, 1962, USAEC Report TID-7641.
32. O. E. Dwyer (Ed.), High-Temperature Liquid-Metal Technology Review. A Bimonthly Technical Progress Review. Vol. 1, No. 1, USAEC Report BNL-788, Brookhaven National Laboratory, February 1963.
33. O. E. Dwyer (Ed.), High-Temperature Liquid-Metal Technology Review. A Bimonthly Technical Progress Review. Vol. 1, No. 2, USAEC Report BNL-801, Brookhaven National Laboratory, April 1963.
34. R. S. Nelson and M. W. Thompson, The Penetration of Energetic Ions Through the Open Channels in a Crystal Lattice, British Report AERE-R-4262. February 1963.
35. G. R. Piercy, F. Brown, J. A. Davies, and M. McCargo, Experimental Evidence for the Increase of Heavy Ion Ranges by Channeling in Crystalline Structure, *Phys. Rev. Letters*, 10: 399-400 (May 1, 1963).
36. R. S. Nelson, Focused Collision Sequences in Tungsten and Molybdenum, *Phil. Mag.*, (8) 8: 693-705 (April 1963).
37. D. E. Peacock and A. A. Johnson, Stage III Recovery in Neutron-Irradiated Molybdenum and Niobium, *Phil. Mag.*, (8) 8: 563-576 (April 1963).
38. J. Pauleve, D. Dautreppe, J. Laugier, and L. Neel, A New Order-Disorder Transition in Fe-Ni (50-50), *J. Phys. Radium*, 23: 841-843 (October 1962).
39. R. F. Hanstock, United Kingdom Atomic Energy Authority, July 17, 1962. (Unpublished)
40. B. T. Kelly, D. Jones, and A. James, Irradiation Damage to Pile Grade Graphite at 450°C, *J. Nucl. Mater.*, 7: 279-291 (1962).
41. General Electric Company, Flight Propulsion

Laboratory Department, High-Temperature Materials Program Progress Report No. 19, Part A, USAEC Report GEMP-19A, Jan. 25, 1963.

42. General Electric Company, Flight Propulsion Laboratory Department, High-Temperature Materials and Reactor Component Development Programs. Volume I. Materials, Second Annual Report, USAEC Report GEMP-177A, Feb. 28, 1963.
43. General Electric Company, Flight Propulsion Laboratory Department, High-Temperature Materials Program. Progress Report No. 21, Part A, Jan. 1, 1963, to Feb. 15, 1963, USAEC Report GEMP-21A, Apr. 23, 1963.
44. C. Erginsoy, Dynamics of Low-Energy Radiation Damage Processes in a Body-Centered Cubic Lattice Simulating Alpha-Iron, USAEC Report BNL-6842, Brookhaven National Laboratory, 1962.
45. O. Hauser and M. Balarin, Remarks on the Cascade Theory for the Calculation of the Number of Radiation Defects in Solids, *Phys. Status Solidi*, 2: 1471-1478 (1962).
46. K. H. Bennemann, General Method for Determining Lattice Point Defect Configurations, Including Their Dependence on Electron Redistribution, *Phys. Rev.*, 130: 1756-1762 (June 1, 1963).
47. K. H. Bennemann, General Treatment of the Conduction Electron Redistribution Due to Point Defect Complex and Lattice Distortion in Noble Metals, *Phys. Rev.*, 130: 1763-1777 (June 1, 1963).
48. K. H. Bennemann, Lattice Point Defect Configurations, Including Their Dependence on Electron Redistribution, USAEC Report TID-16340, University of Illinois, July 1962.
49. A. Sosin, Mechanisms of Atomic Displacements Induced by Radiation, USAEC Report TID-17964, Atomics International, 1962.
50. H. Bichsel, Passage of Charged Particles Through Matter, Technical Report No. 2, USAEC Report TID-18436, University of Southern California, Jan. 6, 1961.
51. J. Friedel, Point Defects and Irradiation, *Low-Temperature Physics*, pp. 549-628, Gordon & Breach Science Publishers, 1962.
52. Proceedings of the International Conference on Crystal Lattice Defects, Kyoto, September 7–12, 1962, *J. Phys. Soc. Japan*, 18 (Suppl. 2): (March 1963).
53. Problems in Metal Physics, *Sb. Nauchn. Tr. Inst. Metallofiz., Akad. Nauk Ukr. SSR*, No. 16: 1-232 (1962).
54. A. Degeilh and R. Simon, Faults Created in Solids by Bombardment with Charged Particles, *Ind. At.*, 6: 57-62 (1962); 7: 81-85 (1963).
55. Oak Ridge National Laboratory, Army Reactor Program Annual Progress Report for Period Ending October 31, 1962, USAEC Report ORNL-3386, Apr. 10, 1963.
56. Unpublished progress report from Chalk River Nuclear Laboratories, Chalk River, Canada.
57. T. W. Wood, The Effect of Hydrogen on the Mechanical Properties of Columbium, Thesis, University of Oklahoma, 1963.
58. F. C. Holtz, Pilot Evaluation of Vanadium Alloys, Report ARF-B231-8, Illinois Institute of Technology, Armour Research Foundation, Feb. 11, 1963.
59. J. D. W. Rawson and B. B. Argent, The Influence of Oxygen on the Yield Strength of Two Zone-Melted Niobium Alloys, *J. Inst. Metals*, 91: 223-224 (February 1963).
60. T. D. Cooper and O. O. Srp, Refractory Metals and Their Protection, *Aerospace Eng.*, 22(1): 46-55 (January 1963).
61. W. F. Sheely, Mechanical Properties of Niobium-Oxygen Alloys, *J. Less-Common Metals*, 4: 487-495 (December 1962).
62. E. M. Savitskii, *The Influence of Temperature on the Mechanical Properties of Metals and Alloys*, 1961.
63. W. C. H. Joiner, Superconducting Properties of Plastically Deformed Aluminum, Thesis, Rutgers University, 1962.
64. T. F. Fedorov et al., Some Data on the Ternary System Titanium-Boron-Chromium, *Poroshkovaya Met., Akad. Nauk Ukr. SSR*, 2(6): 42-49 (1962).
65. J. Kondo, Superconductivity in Transition Metals, *Progr. Theoret. Phys. (Kyoto)*, 29: 1-9 (January 1963).
66. T. G. Ellis, Niobium-Tin-Aluminum Alloy Studies, Thesis, Iowa State University, 1962.
67. A. I. Schindler and D. J. Gillespie, Hall Coefficient of Superconducting and Normal Niobium–25% Zirconium, Report NRL-5874, Naval Research Laboratory, Nov. 9, 1962.
68. Southern Research Institute, The Thermal Properties of Twenty-Six Solid Materials to 5000°F or Their Destruction Temperatures, USAEC Report ASD-TDR-62-765, August 1962.
69. N. V. Dokukina and F. I. Shamrai, Phase Equilibrium and Properties of the Alloys of the W-Nb-Si System, *Poroshkovaya Met., Akad. Nauk Ukr. SSR*, 2(6): 32-41 (1962).
70. N. V. Ageev and M. S. Model, Decomposition of the Solid Solution of Niobium and Titanium in Chromium, *Dokl. Akad. Nauk SSSR*, 148: 84-85 (January-February 1963).
71. D. J. Cometto, Characteristics of the Omega Transformation in Zirconium-Niobium Alloys, Thesis, Case Institute of Technology, 1963.
72. W. Showak, The Solid Solubility of Zirconium in Copper, *Trans. AIME*, 224: 1297-1298 (December 1962).
73. V. N. Svechnikov and A. Ts. Spektor, Constitution Diagram of $ZrCr_2$-$ZrFe_2$ System, *Sb. Nauchn. Tr. Inst. Metallofiz., Akad. Nauk Ukr. SSR*, No. 16: 145-152 (1962).
74. V. N. Svechnikov and A. Ts. Spektor, Phase Diagram of Iron-Zirconium Alloys, *Sb. Nauchn. Tr.*

*Inst. Metallofiz., Akad. Nauk Ukr. SSR*, No. 16: 136-144 (1962).

75. W. D. Wood, H. W. Deem, and C. F. Lucks, Thermal Radiative Properties of Selected Materials, Report DMIC-177(Vol. 2), Battelle Memorial Institute, Defense Metals Information Center, Nov. 15, 1962.
76. J. T. Waber, K. Gschneidner, Jr., A. C. Larson, and M. Y. Prince, Prediction of Solid Solubility in Metallic Alloys, USAEC Report LADC-5380, Los Alamos Scientific Laboratory, 1962.
77. R. L. Andelin, Self-Diffusion in Single-Crystal Tungsten and Diffusion of Rhenium Tracer in Single-Crystal Tungsten, USAEC Report LA-2880, Los Alamos Scientific Laboratory, Apr. 22, 1963.
78. I. S. Lundy and J. I. Federer, A Method for Separating Grain-Boundary and Lattice Diffusion Effects in Polycrystalline Materials, *Trans. AIME*, 224: 1285 (December 1962).
79. W. D. Kingery, R. L. Coble, A. R. Cooper, Jr., and T. R. Clevenger, Jr., Basic Research in Ceramics and Noncrystalline Systems, USAEC Report TID-18434, Massachusetts Institute of Technology, Mar. 30, 1963.
80. H. J. Borchardt, Yttrium-Tungsten Oxides, *Inorg. Chem.*, 2: 170-173 (February 1963).
81. L. C. F. Blackman, Lattice Defects and the Sintering of Oxides, *Ind. Chemist*, 39: 23-26 (January 1963).
82. M. E. Bell, W. R. Buessem, R. Roy, and C. C. Crowe, Fundamental Studies in High Temperature Materials Phenomena, Scope I. High Temperature–Pressure Physical Property Measurements, USAEC Report TID-18412, Mar. 12, 1963.

Section V

Reactor Materials

# Special Fabrication Techniques

## Melting, Hot and Cold Working

Nuclear Metals[1] has reported preliminary observations made during studies concerned with the secondary working of refractory-metal alloys. Results indicate that the niobium–2 wt.% rhenium and niobium–5 wt.% rhenium alloys can be rolled at 1000°C but that higher temperatures will be required for the tantalum–5 wt.% rhenium alloy. It has also been noted that after extensive cold working tantalum can be fully recrystallized by heating 1 hr at 1300°C.

Electron-beam heating techniques are being employed at the Bureau of Mines[2] for purification studies on yttrium and zirconium. The yttrium metal is being doped with additions of various elements stoichiometrically equal to 25 and 100% of the oxygen content. Additions of carbon, hafnium, lanthanum, molybdenum, niobium, tantalum, thorium, and zirconium have been investigated. The failure of these elements to lower the oxygen content of the yttrium is attributed to the high free energy of formation and low vapor pressure of $Y_2O_3$. Other additions are contemplated. The hardness of zirconium buttons decreased as the carbon additions were increased from 50 to 200% of the oxygen equivalent.

Oak Ridge[3] has prepared single crystals of iodide zirconium, up to $\frac{3}{4}$ in. wide by 3 in. long, and of Zircaloy-2, $\frac{1}{4}$ in. wide by 2 in. long. Localized electron-beam heating was used to produce a steep temperature gradient which moved the beta-to-alpha transformation front along the specimen at a rate of $\frac{1}{2}$ to 1 in./min. The maximum length of crystals grown by this technique appears to be limited only by the length of the strip that can be moved past the electron-beam gun.

Despite the emphasis now placed upon refractory metals and compounds, there remains interest in improving the quality of reactor fuels for low-temperature operation and in the techniques used in their manufacture. Representative of the research in these areas are the studies conducted at Hanford, Battelle, Los Alamos, and Nuclear Metals.

Battelle Memorial Institute[4] has reported the results of a recent study concerned with the coefficient of friction between uranium and steel in the high alpha ranges of 1050 to 1200°F. The results indicate that the coefficient of friction in this temperature range is relatively independent of temperature and that it increases with die surface roughness.

Los Alamos Scientific Laboratory[5] is using a dashpot stirrer to increase yield and outgassing when melting plutonium. It is stated that a 5.5-kg ingot of plutonium–2.5 wt.% iron was prepared with a 97% yield from a charge containing 45% lathe turnings. The stirrer eliminated outgassing during pouring. A plutonium-cerium-cobalt alloy with 8 g of plutonium per cubic centimeter was heated to 800°C, stirred, and poured to produce a homogeneous ingot.

(N. E. Daniel)

## Cladding

### Cladding by Rolling and Swaging

In the field of densification of $UO_2$ by swage cladding, a European[6] firm working under Euratom auspices has made significant developments. Hot swaging with a two-jaw machine resulted in a total cross-section reduction of 30%, accomplished in two cold-swaging steps and one hot-swaging step at 750°C. The density obtained thereby was 92.25 ± 0.5% of theoretical.

Investigators at Hanford[7] developed a process for swage compaction of loose physically mixed

$PuO_2$ and $UO_2$ powders clad with Zircaloy. Coarse $UO_2$ powder is blended with $UO_2$-$PuO_2$ fine powder by an incremental loading technique. This technique has an advantage in that the $PuO_2$ enrichment can be varied along the length of the fuel rod for power flattening. A 19-rod cluster was fabricated and cold swaged to 90% of theoretical density. The single-piece fuel rods were 88 in. long and were spirally wrapped with spacing wires.

At Vallecitos Atomic Laboratory,[8] concepts for $UO_2$ fuel-element fabrication have been investigated. The concepts include swaging over pellets, powder compaction by swaging, and powder compaction by hot swaging, all employing a stainless-steel cladding with a wall thickness of 10 mils. Collapsible end plugs were used in the fuel rods as an economy measure to eliminate machining operations after swaging. Hot swaging of the fuel rods with 10-mil-thick stainless-steel cladding resulted in fuel densities as high as 95.2% of theoretical. Ten fuel rods clad with 16-mil-thick type 304 ELC stainless-steel tubing are being irradiated in the Vallecitos Boiling-Water Reactor.

One paper presented at the Research Reactor Fuel Element Conference[9] described fabrication of the fuel-element plates utilized in the first critical test elements for the 100-Mw High-Flux Isotope Reactor. This reactor will use type 6061 aluminum-clad involute-shaped fuel plates containing a radial fuel element. Since the inner annulus plate contained a burnable poison, a dispersion type fuel consisting of 26 wt.% $U_3O_8$ and 0.07 wt.% $B_4C$ in aluminum was selected for the fuel-bearing portion of the plate. A 24 wt.% uranium–aluminum alloy was utilized in the outer plate. The authors evaluated various methods for forming the involute-plate contour to the close tolerances dictated by element design. (R. J. Diersing)

## Pressure Bonding

Several production-size Pressurized-Water-Reactor core 2 plate type fuel elements were fabricated by the gas-pressure-bonding technique.[10] Optimum bonding parameters of 1550 to 1625°F and 10,000 psi for 4 hr were established for self-bonding of the Zircaloy-4 cladding material. Evaluation of the bond interfaces showed that usually 95% of the contact area was metallurgically bonded, which indicates complete grain growth across the original interface. Results of evaluations on fuel-cladding reaction, corrosion resistance, dimensional stability, effect of postheat-treatment, etc., indicate that acceptable fuel elements can be successfully fabricated when the variables are held within reasonable limits.

In studies[11,12] dealing with the evaluation of uranium dioxide powders in terms of their initial compacting and pressure-bonding characteristics, major emphasis has been placed on optimizing particle sizes in the compacts, evaluating mixtures containing micronized $UO_2$, and minimizing cladding thickness. Methods are being studied for agglomerating micronized $UO_2$ and for vibration packing and pressure bonding the product. In recent tests a series of fuel rods clad with Inconel X was gas-pressure bonded for 3 hr at 2100°F. The rods were subjected to a simultaneous increase in pressure and temperature to achieve bonding conditions. Examinations for density and stoichiometry are now under way.

In conjunction with this work, 31 fuel rods clad with 10- or 15-mil-thick Inconel X tubing were pressure bonded. The deformation that occurred during bonding caused many leaks in the cladding, which suggests that the Inconel X is more brittle than stainless steel.

Gas-pressure bonding is also being used at Battelle[11,12] to densify premixed dispersions of oxide-coated $UO_2$ particles. A desired void volume in the final structure is sought in order to accommodate volume changes that occur during oxidation of $UO_2$. Particles coated with $Al_2O_3$ have been densified in a BeO matrix with a retention of 26% void volume when bonding at 1150°C and 10,000 psi. Various combinations of temperature and pressure have been evaluated according to the quantity of void volume retained. The following tabulation lists the results obtained to date on this system.

| Bonding conditions | | |
|---|---|---|
| Temp., °C | Pressure, psi | Porosity in $UO_2$ phase, % |
| 1550 | 2,500 | 56 |
| | 5,000 | 56 |
| | 10,000 | 26 |
| 1230 | 2,500 | 44 |
| | 5,000 | 12.1 |
| | 10,000 | 9.7 |
| 1290 | 5,000 | 9.4 |

Bonded specimens were given an oxidation test at 980°C for 1 hr. No detectable weight change was observed. Metallographic inspection showed that no cracking had occurred and that a trace of oxidation had occurred at exposed surfaces. (G. R. Goetsch)

## Diffusion Bonding

Solid-state diffusion bonding of tungsten to tungsten was investigated at Los Alamos[13] using various interface coatings to promote diffusion. Good bonds were obtained at 2350°C using a ram pressure of 1400 psi and holding for 2 hr in a hydrogen atmosphere. Surface coatings of tungsten oxide or molybdenum-tungsten deposits from carbonyl decompositions were reported to give the best results. Inclusions were present in some areas of the bonds although grain growth had occurred across most of the original interface. (D. C. Carmichael)

## Extrusion Cladding

An important consideration in any cladding process is the integrity of the bond between the core and the cladding. Chalk River[14] has studied the effect of argon purity in the heating chamber on the bond strength between uranium test flats and aluminum claddings.

It was found that, with a pure argon atmosphere and an aluminum temperature of 800 to 900°F, a brittle intermetallic compound, $UAl_3$, was formed at the interface between the uranium and aluminum. Low and inconsistent bond strengths were attributed to the presence of the $UAl_3$.

With an atmosphere of 90 to 92% argon (balance dry air) and an aluminum temperature of 800°F, consistently good bonds with strengths of 14,000 to greater than 24,000 psi were obtained. The oxidation of the uranium flat during preheating prevented the formation of $UAl_3$.

With a 75 vol.% argon–25 vol.% dry-air mixture and an aluminum temperature of about 910°F, good bond strengths (greater than 18,000 psi) were obtained on two of three clad flats tested. The third clad flat had a low bond strength because it oxidized excessively during a heating time twice as long as that of the others.

With 40 to 47 vol.% argon in dry air and an aluminum temperature of 800°F, good bonds were obtained less frequently. The oxidizing effect of the argon-air mixture was considered to be excessive.

The effect of thermal exposure on the bond strength of clad flat plates was also studied. The bond strengths of plates with good initial bonds were not affected when heated at 350°F for times up to 168 hr. The bond strength of plates with no barrier between the aluminum and uranium was reduced significantly when exposed at 525°F for 80 hr, due to the formation of $UAl_3$.

Varying the aluminum-to-uranium cladding pressures between 6,000 and 25,000 psi had little or no effect on the bond strength.

(D. C. Drennen)

## Canning

Recent developments[15] in the packing characteristics of oxide fuels by vibratory-compaction techniques have been reported for both fused and high-fired uranium dioxide powder. The fused powder was compacted in a cylindrical glass tube, and both single- and multiple-particle-size components were used. All the single-particle-size specimens, except the −325-mesh specimen, packed to their highest density within 2 min, whereas the −325-mesh specimen required in excess of 30 min. The larger particle sizes (−8 +20 mesh) required lower frequency vibration (60 cps with an amplitude of 2 mm) than did the finer (−325 mesh) powder (200 to 480 cps with an amplitude of 2 mm). The multiple-particle-size-component specimens had an optimum size distribution that corresponded to the following compositions: 66 wt.%, −6 +8 mesh; 16 wt.%, −36 +48 mesh; and 18 wt.%, −200 mesh. This combination of particle sizes was packed to a relative density of 85% using frequencies from 60 to 480 cps and frequency amplitudes from 0.03 to 2 mm. Relative densities of 83% were achieved when a binary mixture of −3 +10 mesh fused particles and −50-mesh high-fired particles of uranium dioxide were vibratorily packed.

The jacketing operation for the Argonne Fast Source Reactor fuel core is described in a recent report.[16] The core consists of 4.5-in.-diameter uranium disks enriched to 93 wt.% $U^{235}$. These disks are sealed in 0.005-in.-thick nickel cans to prevent oxidation of the core and contamination of the coolant system with released fission products. The nickel cans were evacuated and sealed by brazing.

Two new vibratory-compaction processes are described in a recent Hanford report.[17] In one

process, transverse excitation of thin-wall cladding suspended vertically from a horizontal bar was used to produce 8-ft-long $UO_2$ rods in SAP and stainless-steel tubing. Transverse accelerations greater than 50 g were used at frequencies ranging from 180 to 2500 cps. Compaction efficiencies of 91% were achieved using this technique. A second vibratory-compaction method was described in which the cladding tubes were heated to 800 to 900°C during the loading and compacting operations. Some distortion of the cladding tubes was noted during cooling. It is believed that hot vibrational compaction of fuels clad in aluminum and stainless steel may increase bulk fuel densities and reduce fabrication time. (E. G. Smith, Jr.)

## Electroplating

Adhesion failures at Hanford for nickel-clad, extruded uranium fuel material were attributed to delays in transferring the material from the anodic, 10% nitric acid etching solution to the nickel plating bath.[18] Electroplating techniques for improving adhesion have been reported by several sites from time to time,[19–21] and it appears that the Hanford difficulties might be resolved by adopting one of these.

A neutral or slightly alkaline solution containing ammonium nitrate is recommended[22] to anodize zirconium and hafnium with no uncontrolled attack.

Uranium oxide layers deposited on aluminum anodes in dilute, uranyl nitrate solutions were evaluated for uniformity by checking alpha count rates. The authors described the films as being uniformly thick and solidly adherent.[23]

High-density, high-purity plutonium metal is electrorefined at Los Alamos in a fused-salt mixture of sodium chloride, potassium chloride, and plutonium chloride or plutonium fluoride in a magnesia-yttria cell. The fused-salt electrolyte and the liquid-metal anode are mechanically stirred to prevent polarization. Refined metal was collected as a liquid on tungsten cathode. Yields on a 3.5-kg scale exceeded[24] 95%. (W. H. Safranek)

## Nonelectrolytic Chemical-Plating Techniques

Methods of preparing materials in bulk form and as thin films, as overlay coatings, and as diffusion coatings are discussed in this review section.

Increased attention is being given to chemical vapor deposition as a useful production tool to technology in many areas.[25–27] Examples are summarized briefly below. Additional investigation of methods of preparing niobium and tantalum has been carried out.[28] Magnesium or sodium reduction of the respective chlorides by the Kroll process yielded useful products. A process for chemical vapor deposition of tungsten by hydrogen reduction of $WF_6$ was patented.[29] A novel technique was employed in the preparation of zirconium by reduction of the chloride with alkali metals.[30] Foils of 34 elements for use as nuclear targets were prepared on metallic and nonmetallic substrates by chemical vapor deposition.[31] A comprehensive table listing the halides used as source materials in this work was presented.

Pyrolytic carbon, deposited at temperatures above 2000°C on heated carbon rods by pyrolysis of propane, possessed a two-layered structure, the inner layer (next to the deposition surface) being more highly oriented and graphitized than the outer layer.[32] Chemical vapor deposition is being studied as a means of suppressing the vaporization loss from carbide cathodes in a thermionic cell, operating at 2100 to 2500°K, by the chemical addition of hydrogen and halogens in the cell.[33] A new, dry process for the production of $UO_2$ powder from $UF_6$ by fluidization and particle-coating techniques was developed.[34] The process involves a two-step procedure wherein $UF_6$ is converted to solid uranyl fluoride in the first step by reaction with steam, and uranium dioxide is produced in the second step by reduction of the uranyl fluoride with a mixture of steam and hydrogen. A nuclear fuel consisting of uranium carbides dispersed in a carbon medium was made by contacting finely divided carbon with $UF_6$ to form $UF_4$, which then reacts with the surrounding carbon to form uranium carbides.[35]

In the field of overlay coatings, chromium was deposited at 375°C by thermal decomposition of chromium dicumene in the presence of hydrogen or argon as a carrier gas.[36] The hot hardness of electroless nickel coatings containing 6.8 to 10.5% phosphorus was evaluated[37] after heating in the temperature range 75 to 1000°F. Coatings retain useful hardness provided a temperature of 700°F is not exceeded. Alumina and ceramic fuel wafers were coated by the pyrolysis of methane at 2075°F in a rotating

quartz reactor.[38] Graphite bodies can be coated with a multiple coating of zirconium carbide, zirconium nitride, and mixed niobium-zirconium carbides to form a coating resistant to corrosion and erosion and generally impervious to the passage of fission-product gases.[39]

Techniques similar to those used in coating nuclear fuel particles are being employed to form diffusion type silicide coatings on refractory-metal parts.[40] Many organizations are intensively investigating the utility of improved diffusion type silicide and related coatings as a means of protecting refractory-metal structures against oxidation at high temperatures.[41a–41d] However, no completely satisfactory coating scheme has been devised. The results of coating studies of molybdenum,[42] niobium,[43–46] tantalum,[47] and vanadium[48,49] were described.

(E. M. Sherwood)

### Ceramic Coatings

A patent[50] has recently been granted on a method for making thin-walled silicon carbide articles or graphite articles coated with silicon carbide. A mixture of carbon, silicon carbide, and a polymeric binder is formed into sheets. These sheets are then shaped as desired or applied as a coating. The article is then heated to 3000 to 4000°F in the presence of excess silicon.

Niobium alloys are potentially useful at high temperatures, but they must be protected if used in an oxidizing environment. The Bureau of Naval Weapons recently has investigated the comparative merits of available coatings on D-14 alloy, and TAPCO Division of Thompson Ramo Wooldridge, Inc.,[51] has evaluated three of the coatings selected on Fansteel 85 (Nb–28 Ta–10 W–1 Zr) as a preliminary step in a design study. All three coatings gave equivalent or better protection at 2000°F on FS-85 than on D-14 in a test in which the coated pieces were bent and then subjected to cyclic oxidation. At 2600°F, the TAPCO coating was more protective, the Pfaudler coating somewhat less, and the Vought coating gave virtually no protection.

(B. W. King)

## Welding and Brazing

Much of the welding work reported recently is concerned with niobium and niobium alloys with minor emphasis on other refractory metals. Other studies are concerned mainly with the refinement of techniques for welding end closures on reactor fuel elements.

Table V-1 COMPARISON OF BEND TRANSITION TEMPERATURES OF NIOBIUM ALLOYS MADE BY TUNGSTEN-ARC AND BY ELECTRON-BEAM WELDING*[52]

| Alloy | Transition temp., °F | |
|---|---|---|
| | Tungsten-arc welds | Electron-beam welds |
| FS-82 | −100 | −280 |
| FS-82HS | 150 | −80 |
| D-31 | 550 | 250 |
| F-48 | 350 | 250 |

*Welds made with best parameters found for each alloy.

Gerken and Faulkner[52] have published the results of a study of welding the FS-82, FS-82HS, D-31, and F-48 niobium-base alloys. Inert-gas tungsten-arc welds in 0.060-in. sheets of FS-82 and FS-82HS gave bend transition temperatures of −100 and 150°F, respectively. The welding conditions were 15 in./min, 150 to 160 amp, 14 to 16 volts, and a helium atmosphere. The high transition temperature of FS-82HS is attributed to its high oxygen content, 0.13 vs. 0.08% in the FS-8L alloy. FS-82 can be welded outside a weld chamber with careful helium shielding. The D-31 alloy can be welded satisfactorily using the same parameters and a postweld heat-treatment

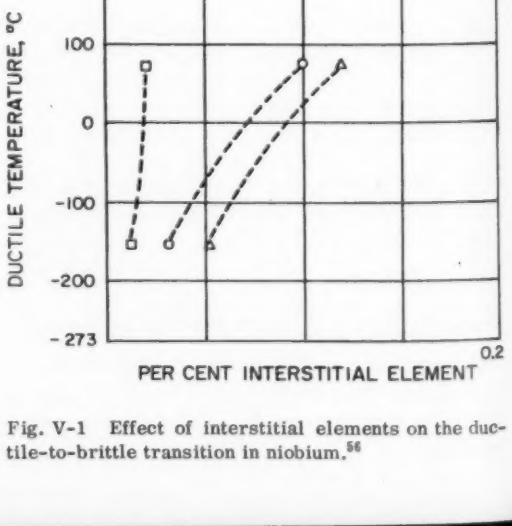


Fig. V-1 Effect of interstitial elements on the ductile-to-brittle transition in niobium.[56]

of 2100°F for 24 hr. The bend transition temperature for such welds will be about 100°F. If the postweld heat-treatment is omitted, the tansition temperature will be above 500°F. Nonchamber welding of D-31 is not recommended. Thick sheet welds in D-31 are subject to weld cracking. The best weld ductility in the F-48 alloy was obtained with the same welding parameters but with a 500°F preheat added.

appears to be a good adjunct to the work of Gerken and Faulkner. A classical aging and overaging reaction occurring in the range 1500 to 1800°F results in embrittlement of the alloy.

Bell Aerosystems Company[55] also is investigating the weldability of commercial niobium alloys. The alloys are C-129 and SCb-291. Bend transition temperatures for tungsten-arc inert-gas welds, as welded, for SCb-291 were −275°F

Table V-2 BRAZING ALLOYS FOR TANTALUM*[60]

| | Composition (balance niobium), wt.% | Best brazing temp., °C | Fillet size | | Comments |
|---|---|---|---|---|---|
| | | | Alloy side | Back side† | |
| CB-4F | 5 V | 2400 | Large | Medium | Less than 0.005-in. erosion |
| CB-4E | 10 V | 2275 | Medium | Medium | Less than 0.005-in. erosion |
| CB-4H | 15 V | 2250 | Large | Large | |
| CB-4D | 20 V | 2150 | Medium | Medium | |
| CB-4I | 25 V | 2125 | Large | Large | Less than 0.003-in. erosion |
| CB-4C | 30 V | 2100 | Large | Large | Nonmetallics in joint |
| CB-4J | 40 V | 2000 | Medium | Medium | Less than 0.001-in. erosion |
| CB-4K | 50 V | 1950 | Medium | Medium | Less than 0.001-in. erosion |
| CB-46J | 10 Ta−30 V | 2100 | Medium | Medium | |
| CB-46H | 10 Ta−40 V | 2100 | Small | Small | |
| CB-46B | 20 Ta−20 V | 2400 | Small | Small | |
| CB-46G | 20 Ta−30 V | 2150 | Small | Small | |
| CB-46I | 20 Ta−40 V | 2000 | Small | Small | |
| CB-46C | 30 Ta−20 V | 2425 | Medium | Small | Fillet surface rough |
| CB-46F | 30 Ta−30 V | 2275 | Medium | Medium | |
| CB-46D | 40 Ta−25 V | 2400 | Small | Small | Less than 0.003-in. erosion |
| CB-46E | 50 Ta−25 V | 2425 | Medium | Small | Fillet surface rough |

*All specimens were hydrogen-brazed T-sections (with vacuum or inert-atmosphere cooling).
†Side opposite location of preplaced brazing alloy on T-section.

The bend transition temperature will be about 350°F, but it can be lowered to 100°F by a 2500°F, 4-hr postweld heat-treatment.

Electron-beam welds made by Gerken and Faulkner in the four alloys studied were all much more ductile than the tungsten-arc welds. A comparison of the bend transition temperatures is shown in Table V-1.

In a continuation of the work of Gerken and Faulkner, the D-36, FS-85, Cb-752, B-66, and X-110 alloys are under study.[53] Data available to date are preliminary. These data indicate that the transition temperature for electron-beam welds in D-36 and Cb-752 is near that of the base metal but it is raised significantly for the FS-85 and B-66 alloys. Tungsten-arc welding raises the transition temperature of all these alloys.

A study of the aging characteristics of a niobium−1 wt.% zirconium alloy at Oak Ridge[54]

transverse and −225°F longitudinal. The base metal had a transition temperature of −320°F. Welding seriously impairs the transition temperature of C-129, raising it from less than −320 to about 80°F.

Platte,[56] in studying the weldability of many, mostly noncommercial, niobium alloys, has determined the effects of several elements on the bend transition temperature. Figure V-1 shows the effect of the interstitial elements. It can be seen why the FS-82HS alloy welded by Gerken and Faulkner showed poor ductility. Other added elements (titanium, molybdenum, vanadium, hafnium, and zirconium) except titanium and hafnium raised the ductile-to-brittle transition temperature. Titanium is detrimental up to 1 wt.% and then becomes less so. Alloys with 10 wt.% titanium were ductile at liquid-nitrogen temperatures. A 1 wt.% hafnium alloy was also ductile at these temperatures. A weld in a 10

wt.% tungsten–niobium alloy was 90 to 95% as strong as the base metal at 2000°F.

The technique of utilizing the advantages of both welding and brazing in a single joint was demonstrated recently. The technique of first welding and then "back-brazing" to increase the integrity of the joint was used to fabricate a heat exchanger for the Molten-Salt Reactor.[57] Hastelloy N (INOR-8) tubes were welded flush with the header and then brazed from the back side at 1850°F. Inspection by the Lamb-wave nondestructive-testing technique[58] showed that all 326 joints were complete. Cross sections taken from a full-size mockup of the heat exchanger verified the usefulness of the technique. The back-brazing technique was patented recently.[59]

Hanford[17] has developed a technique for making end closures in Zircaloy-2-clad fuel elements containing thorium fuels. Complete bonding of the cap to the fuel has been the main problem. The fuel must be oxide free to get a complete bond. The zirconium–2.5 wt.% beryllium brazing alloy is now chemically etched and then melted into the closure area with an electron beam. Etching and brazing are accomplished in the vacuum chamber without opening it to air. The bond is complete and free of voids and oxides.

The brazing of refractory metals for use at temperatures near the useful maximum of the base metals is of considerable interest at present. Consequently many agencies, including AEC facilities, the Air Force, and NASA, are involved in brazing-alloy-development programs.

General Electric[60] has completed a preliminary study of brazing alloys for tantalum. The work was related to the niobium-tantalum-vanadium ternary system and the niobium-vanadium system. These systems present a choice of alloys that melt between 3540 and 4350°F. The alloys are all readily workable and can be fabricated into sheet or wire. During brazing, they show reasonable flow, form moderate fillets, and do not seriously erode the tantalum-base metal. Table V-2 summarizes the results obtained. In another report by General Electric,[61] an evaluation of the following systems for brazing tantalum is covered: tantalum-vanadium, tantalum-hafnium, tantalum-chromium, tantalum-titanium, tantalum-silicon, and niobium-vanadium.

Four brazing alloys with good metallurgical compatibility and high-temperature strength when used on niobium-base materials are reported by General Electric.[62] The work was done on F-48. The alloys are:

Table V-3 TENSILE-SHEAR PROPERTIES FOR BRAZED LAP JOINTS*[62]

(Braze Alloys on Niobium Alloy F-48)

| Braze† alloy | Overlap, in. | Test temp., °F | Braze shear‡ strength, 1000 psi | Parent alloy‡ tensile strength, 1000 psi | Location of failure |
|---|---|---|---|---|---|
| AS-540 | 0.1020 | 500 | 27.3 | 61.3 | P.M. |
| AS-540 | 0.116 | 2500 | 7.9 | 18.6 | Braze |
| AS-540 | 0.109 | 2500 | 8.9 | 19.8 | Braze |
| AS-541 | 0.101 | 500 | 27.3 | 78.0 | P.M. |
| AS-541 | 0.096 | 2500 | 9.9 | 19.7 | Braze |
| AS-546 | 0.102 | 500 | 24.5 | 56.8 | P.M. |
| AS-546 | 0.100 | 500 | 18.1 | 39.3 | Braze |
| AS-546 | 0.118 | 2500 | 7.8 | 19.9 | Braze |
| AS-546 | 0.112 | 2500 | 7.9 | 20.2 | Braze |
| AS-547 | 0.089 | 500 | 21.4 | 48.3 | P.M. |
| AS-547 | 0.096 | 500 | 16.9 | 36.9 | P.M. |
| AS-547 | 0.103 | 2500 | 9.5 | 20.3 | Braze |
| AS-547 | 0.106 | 2500 | 8.3 | 19.6 | Braze |

*Test conditions: elevated-temperature test conducted in vacuum of 4 to $6 \times 10^{-4}$ torr. Head rate: 0.01 in./min.

†All brazements tested in as-brazed condition.

‡Values underlined represent the shear or tensile strength in the failure area.

| Designation* | Composition, wt.% | Brazing temp., °F | Service temp., °F |
|---|---|---|---|
| AS-540 | 60 V–30 Nb–10 Ti | 3300 | 2500 |
| AS-541 | 60 V–30 Nb–10 Ti–2 C | 3300 | 2500 |
| AS-546 | 60 V–30 Nb–10 Zr | 3200 | 2500 |
| AS-547 | 59 V–29 Nb–10 Zr–2 Si | 3100 | 2500 |

*Lap-joint properties for these alloys in F-48 are given in Table V-3.

The General Electric study included some work on the brazing of unalloyed tungsten and on the diffusion bonding of refractory alloys. A brazing alloy, AS-517 (Nb–2.2 B), produced joints with excellent strength at 3000°F with no significant effect on the low-temperature ductility. The diffusion studies demonstrated that useful strengths at high temperatures can be obtained even though unfavorable physical properties of the joint components promote the formation of brittle interface constituents. The joint combinations studied were: niobium–1 wt.% zirconium to molybdenum–0.5 wt.% titanium; niobium–1 wt.% zirconium to 316 stainless steel; niobium–1 wt.% zirconium to L-605; F-48 to molybdenum–0.5 wt.% titanium; F-48 to 316 stainless steel; F-48 to L-605; molybdenum–0.5 wt.% titanium to 316 stainless steel; molybdenum–0.5 wt.% titanium to L-605; molybdenum–0.5 wt.% titanium to R-41; niobium–1 wt.% zirconium to copper; copper to 316 stainless steel; and beryllium to 316 stainless steel.

(R. M. Evans)

## References


1. Nuclear Metals, Inc., Fundamental and Applied Research and Development in Metallurgy, USAEC Report NMI-2114, Apr. 12, 1963.
2. Bureau of Mines, Quarterly Metallurgical Progress Report No. 18, for the Period January 1 to March 31, 1963, USAEC Report USBM-U-1031.
3. Oak Ridge National Laboratory, Apr. 8, 1963. (Unpublished)
4. E. S. Hodge, R. J. Carlson, E. G. Bodine, and E. G. Smith, Jr., Measurement of the Coefficient of Friction Between Uranium and Steel at High Alpha-Uranium Temperatures, USAEC Report BMI-X-226, Battelle Memorial Institute, Apr. 9, 1963.
5. Los Alamos Scientific Laboratory, Quarterly Status Report on LAMPRE Program for Period Ending February 20, 1963, USAEC Report LAMS-2875, Mar. 22, 1963.
6. P. Himmelstein, W. Hoppe, H. Kroll, B. Liebmann, and C. Neumann, Production of Swaged Fuel Elements. Quarterly Report No. 10, October 1–December 31, 1962, USAEC Report EURAEC-535, Nuklear-Chemie und -Metallurgie G.m.b.H.
7. R. E. Bardsley and R. E. Sharp, Fabrication of $UO_2$-$PuO_2$ Swage Compacted Fuel Elements, USAEC Report HW-SA-2683, Hanford Atomic Products Operation, November 1962.
8. E. A. Lees, Fabrication of Fuel Elements by Swaging, USAEC Report GEAP-3918, General Electric Company, Vallecitos Atomic Laboratory, May 21, 1962.
9. Oak Ridge National Laboratory, Research Reactor Fuel Element Conference, September 17–19, 1962, Gatlinburg, Tennessee, USAEC Report TID-7642.
10. F. O. Bingman and C. R. Woods, Gas Pressure Bonding of Production Size PWR Core 2 Plate Type Fuel Elements Containing Ceramic Fuel, USAEC Report WAPD-245, Westinghouse Electric Corp., Bettis Atomic Power Laboratory, May 1963.
11. R. W. Dayton and R. F. Dickerson, Progress Relating to Civilian Applications During April 1963, USAEC Report BMI-1630, Battelle Memorial Institute, May 1, 1963. (Classified)
12. R. W. Dayton and R. F. Dickerson, Progress Relating to Civilian Applications During March 1963, USAEC Report BMI-1624, Battelle Memorial Institute, Apr. 1, 1963. (Classified)
13. R. I. Batista, G. S. Hanks, and D. J. Murphy, Elevated Temperature Diffusion Bonding of Tungsten to Tungsten Under Pressure, USAEC Report LA-2751, Los Alamos Scientific Laboratory, Mar. 22, 1963.
14. Atomic Energy of Canada, Ltd., British Patent No. 927159, Method of Producing a Diffusion-Resistant Bond Between Uranium and Aluminum, Published 29 May 1963.
15. Oxide and Carbide Fuels, Japan-U. S. Newsletter No. 1, February 1963.
16. W. R. Burt, Jr., Fabrication of the Fuel and Blanket for the Argonne Fast Source Reactor (AFSR), USAEC Report ANL-6107, Argonne National Laboratory, January 1963.
17. Hanford Atomic Products Operation, Research and Development Programs Executed for the Division of Reactor Development, Quarterly Progress Report, October–December 1962, USAEC Report HW-76559, January 1963.
18. F. W. Albaugh, Reactor and Fuels Laboratory Monthly Report, March 1963, USAEC Report HW-77046A, Hanford Atomic Products Operation, Apr. 15, 1963. (Classified)

19. J. G. Beach, W. C. Schickner, C. R. Konecny, and C. L. Faust, Electroplated Metals on Uranium, USAEC Report BMI-912 (Del.), Battelle Memorial Institute, May 7, 1954.
20. M. H. Binstock, Fuel Element Development for Piqua OMR, USAEC Report NAA-SR-5119, Atomics International, June 30, 1960.
21. F. Brossa and M. Airola, Improvements in the Procedure of Electroplating Metals, Particularly Uranium Bars for Nuclear Reactor Fuel Elements, Belgian Patent 600,262, Feb. 16, 1961.
22. A Process for the Anodic Surface Treatment of Zirconium, Hafnium, and Their Alloys, British Patent 916,190, Jan. 23, 1963.
23. H. O. Denschlag and G. H. Herrmann, Electrolytic Deposition of Uniform and Solid Uranium Oxide Layers on Aluminum (in German), *Nukleonik*, 4: 277-279 (October 1962).
24. L. J. Mullins and J. A. Leary, Multikilogram Electrorefining of Plutonium Metal, USAEC Report LADC-5471, Los Alamos Scientific Laboratory, Oct. 17, 1962.
25. A. Brenner, Deposition of Metals from the Vapor Phase and Similarity of the Process to Electrodeposition, *Trans. Inst. Metal Finishing*, 83: 123-130 (1961).
26. J. M. Blocher, Jr., Chemical Vapor Deposition—A Rediscovered Tool for Molecular Engineering, *Battelle Technical Rev.*, 12(3): 2-7 (March 1963).
27. R. Bakish, Vapor-Phase Metallurgy, *Intern Sci. Technol.*, No. 18: 54-60 (June 1963).
28. T. T. Campbell, F. E. Block, G. B. Robidart, and J. L. Schaller, Preparation of Tantalum and Columbium by Metallic Reduction of Their Chlorides, *U. S. Bur. Mines, Rept. Invest.*, No. 6080 (1962).
29. A. Brenner and W. E. Reid, Jr., Vapor Deposition of Tungsten, U. S. Patent 3,072,983, Jan. 15, 1963.
30. J. Valecek, Low-Temperature Thermal Reduction of Zirconium Tetrachloride with Alkali Metals, USAEC Translation AEC-tr-5363 [translated from *Jaderna Energie*, 8(1): 21 (1962)].
31. L. D. F. Allen, Preparation of Foils for Nuclear Particle Targets, USAEC Report LA-2769, Los Alamos Scientific Laboratory, Dec. 20, 1962.
32. T. Noda, M. Inagaki, and H. Kato, Relations Between the Degree of Orientation and the Conditions of Deposition of Pyrolytic Graphite, *Bull. Chem. Soc. Japan*, 35: 1471-1474 (September 1962).
33. L. Yang, A. F. Weinberg, S. Langer, and R. G. Hudson, Carbide Cathode Studies. Physical and Chemical Redeposition, USAEC Report GA-3642, General Atomic Division, General Dynamics Corp., Jan. 30, 1963.
34. I. E. Knudsen, H. E. Hootman, and N. M. Levitz, A Fluid-Bed Process for the Direct Conversion of Uranium Hexafluoride to Uranium Dioxide, USAEC Report ANL-6606, Argonne National Laboratory, February 1963.
35. J. G. Lewis and H. A. Ohlgren, Process of Manufacturing Nuclear Fuel, U. S. Patent 3,089,785, May 14, 1963.
36. W. H. Metzger, Jr., Chromium Plating by Thermal Decomposition of Chromium Dicumene, *Plating*, 49(11): 1176 (November 1962).
37. K. T. Ziehlke, Hot Hardness of Electroless Nickel Coatings, USAEC Report K-1460, Oak Ridge Gaseous Diffusion Plant, Oct. 10, 1962.
38. L. J. Goetz and W. H. Britton, The Pyrolytic Carbon Coating of Ceramic Fuel for the Second Shippingport Reactor Core, USAEC Report WAPD-272, Westinghouse Electric Corp., Bettis Atomic Power Laboratory, November 1962.
39. R. J. Pyle and G. L. Allen, Coated Carbon Element for Use in Nuclear Reactors and the Process of Making the Element, U. S. Patent 3,073,717 (to USAEC), Jan. 15, 1963.
40. R. E. Reel, Investigation of an Inert Fluidized Bed Coating Reactor, Report MDR-2-24958, The Boeing Company, Aug. 31, 1962.
41. Papers presented at Seventh Meeting, Refractory Composites Working Group, Palo Alto, California, March 12–14, 1963.
    *a.* L. Sama and C. D. Dickinson, High-Temperature Protective Coating for Refractory Metals, Parts I and II.
    *b.* P. J. Chao, G. J. Dormer, B. S. Payne, Jr., J. B. Whitney, and J. Zupan, Research in Protective Coatings for Refractory Metals.
    *c.* J. C. Withers, High Temperature Oxidation Resistant Coatings.
    *d.* R. L. Halise, S. C. Colburn, and R. E. Mihalco, Development and Evaluation of Refractory Metal Coatings.
42. G. J. Dormer and P. J. Chao, Manufacturing Methods for High Temperature Coating of Large Molybdenum Parts, Interim Engineering Report, July 1–October 1, 1962, The Pfaudler Company, Oct. 31, 1962.
43. J. Zupan, P. J. Chao, and J. B. Whitney, Development of Practical Techniques for Applying Protective Coatings to Columbium Alloys, Quarterly Progress Report No. 2, September 1–November 30, 1962, The Pfaudler Company, Dec. 15, 1962.
44. J. Zupan, P. J. Chao, and J. B. Whitney, Development of Practical Techniques for Applying Protective Coatings to Columbium Alloys, Quarterly Progress Report No. 3, December 1, 1962–February 28, 1963, The Pfaudler Company, Mar. 15, 1963.
45. J. D. Gadd, Design Data Study for Coated Columbium Alloys, Bimonthly Technical Progress Report No. 5, August 21–October 21, 1962, Report AD-289857, TAPCO Division of Thompson Ramo Wooldridge, Inc., Nov. 21, 1962.
46. J. D. Gadd and R. A. Jefferys, Advancement of High Temperature Protective Coatings for Colum-

bium Alloys, Report ASD-TDR-62-934, Thompson Ramo Wooldridge, Inc., November 1962.

47. L. Sama, High-Temperature Oxidation-Resistant Coatings for Tantalum Base Alloys, Report ASD-TDR-63-160, General Telephone and Electronic Laboratories, Inc., February 1963.
48. J. J. Rausch and F. C. Holtz, High-Temperature Oxidation Protective Coatings for Vanadium-Base Alloys, Bimonthly Report No. 2, November 13, 1962–January 12, 1963, Report ARF-B6001-2, Illinois Institute of Technology, Armour Research Foundation, Feb. 9, 1963.
49. J. J. Rausch and F. C. Holtz, High-Temperature Oxidation Protective Coatings for Vanadium-Base Alloys, Bimonthly Report No. 3, January 13, 1963–March 12, 1963, Report ARF-B6001-3, Illinois Institute of Technology, Armour Research Foundation, Apr. 8, 1963.
50. J. R. Johnson, Thermally Resistant Articles and Methods for Thin Fabrication, U. S. Patent No. 3,079,316 (to Minnesota Mining & Manufacturing Co.), Feb. 26, 1963.
51. J. D. Gadd, Design Data Study for Coated Columbium Alloys. Bimonthly Report No. 3, April 21–June 21, 1962, Report AD-278727, TAPCO Division of Thompson Ramo Wooldridge, Inc., July 21, 1962.
52. J. M. Gerken and J. M. Faulkner, Welding Characteristics of Commercial Columbium Alloys, *Welding J. (N. Y.)*, 42(2): 84s-96s (February 1963).
53. Thompson Ramo Wooldridge, Inc., Cleveland, Ohio, preliminary information under Air Force Contract AF 33(657)-9446.
54. E. A. Franco-Ferreira and G. M. Slaughter, Welding of Columbium–1% Zirconium, *Welding J. (N. Y.)*, 42(1): 18s-24s (January 1963).
55. Bell Aerosystems Company, Buffalo, New York, preliminary information under Air Force Contract AF 33(657)-8555.
56. W. N. Platte, Welding Columbium and Columbium Alloys, *Welding J. (N. Y.)*, 42(2): 69s-84s (February 1963).
57. Oak Ridge National Laboratory, Molten-Salt Reactor Program, Semiannual Progress Report for Period Ending January 31, 1963, USAEC Report ORNL-3419, June 3, 1963.
58. K. V. Cook and R. W. McClung, Development of Ultrasonic Techniques for the Evaluation of Brazed Joints, *Welding J. (N. Y.)*, 41(9): 404s-408s (September 1962).
59. P. Patriarca, C. E. Shubert, and G. M. Slaughter, Method of Making Plate Connection, U. S. Patent 3,078,551 (to USAEC), Feb. 26, 1963.
60. General Electric Company, Flight Propulsion Laboratory Department, High-Temperature Materials Program Progress Report No. 23, Part A, USAEC Report GEMP-23A, May 31, 1963.
61. General Electric Company, Flight Propulsion Laboratory Department, High-Temperature Materials and Reactor Components Development Programs. Volume I. Materials, Second Annual Report, USAEC Report GEMP-177A, Feb. 28, 1963.
62. W. R. Young and E. S. Jones, Joining of Refractory Metals by Brazing and Diffusion Bonding, Report ASD-TDR-63-88, General Electric Company, January 1963.

# *NUCLEAR SCIENCE ABSTRACTS*

The U. S. Atomic Energy Commission, Division of Technical Information, publishes *Nuclear Science Abstracts (NSA)*, a semimonthly journal containing abstracts of the literature of nuclear science and engineering.

*NSA* covers (1) research reports of the U. S. Atomic Energy Commission and its contractors; (2) research reports of government agencies, universities, and industrial research organizations on a world-wide basis; and (3) translations, patents, books, and articles appearing in technical and scientific journals.

Complete indexes covering subject, author, source, and report number are included in each issue. These are cumulated quarterly, semiannually, and annually providing a detailed and convenient key to the literature.

## Availability of *NSA*

**SALE** *NSA* is available on subscription from the Superintendent of Documents, U. S. Government Printing Office, Washington 25, D. C., at $22.00 per year for the semimonthly abstract issues and $15.00 per year for the four cumulated-index issues. Subscriptions are postpaid within the United States, Canada, Mexico, and all Central and South American countries, except Argentina, Brazil, British and French Guiana, Surinam, and British Honduras. Subscribers in these Central and South American countries, and in all other countries throughout the world, should remit $27.50 per year for subscriptions to semimonthly abstract issues and $17.50 per year for the four cumulated-index issues.

**EXCHANGE** *NSA* is also available on an exchange basis to universities, research institutions, industrial firms, and publishers of scientific information. Inquiries should be directed to the Division of Technical Information Extension, U. S. Atomic Energy Commission, P. O. Box 62, Oak Ridge, Tennessee.

TECHNICAL PROGRESS REVIEWS may be purchased from Superintendent of Documents, U. S. Government Printing Office, Washington 25, D. C. for $2.00 per year for each subscription or for $0.55 per issue. The use of the coupon below will facilitate the handling of your order.

POSTAGE AND REMITTANCE: Postpaid within the United States, Canada, Mexico, and all Central and South American countries except as hereinafter noted. Add $0.50 per year, or $0.15 per single issue, for postage to all other countries, including Argentina, Brazil, British and French Guiana, Surinam, and British Honduras. Payment should be by check, money order, or document coupons, and MUST accompany order. Remittances from foreign countries should be made by international money order, or draft on an American bank, payable to the Superintendent of Documents, or by UNESCO book coupons.

*order form*

SUPERINTENDENT OF DOCUMENTS
U. S. GOVERNMENT PRINTING OFFICE
WASHINGTON 25, D. C.

Enclosed:
document coupons ☐ check ☐ money order ☐

Charge to Superintendent of Documents No. _____

Please send a one-year subscription to

- ☐ ISOTOPES AND RADIATION TECHNOLOGY
- ☐ NUCLEAR SAFETY
- ☐ POWER REACTOR TECHNOLOGY
- ☐ REACTOR FUEL PROCESSING
- ☐ REACTOR MATERIALS

(Each subscription $2.00 a year; $0.55 per issue.)

4485

SUPERINTENDENT OF DOCUMENTS
U. S. GOVERNMENT PRINTING OFFICE
WASHINGTON 25, D. C.

(Print clearly)

Name _____

Street _____
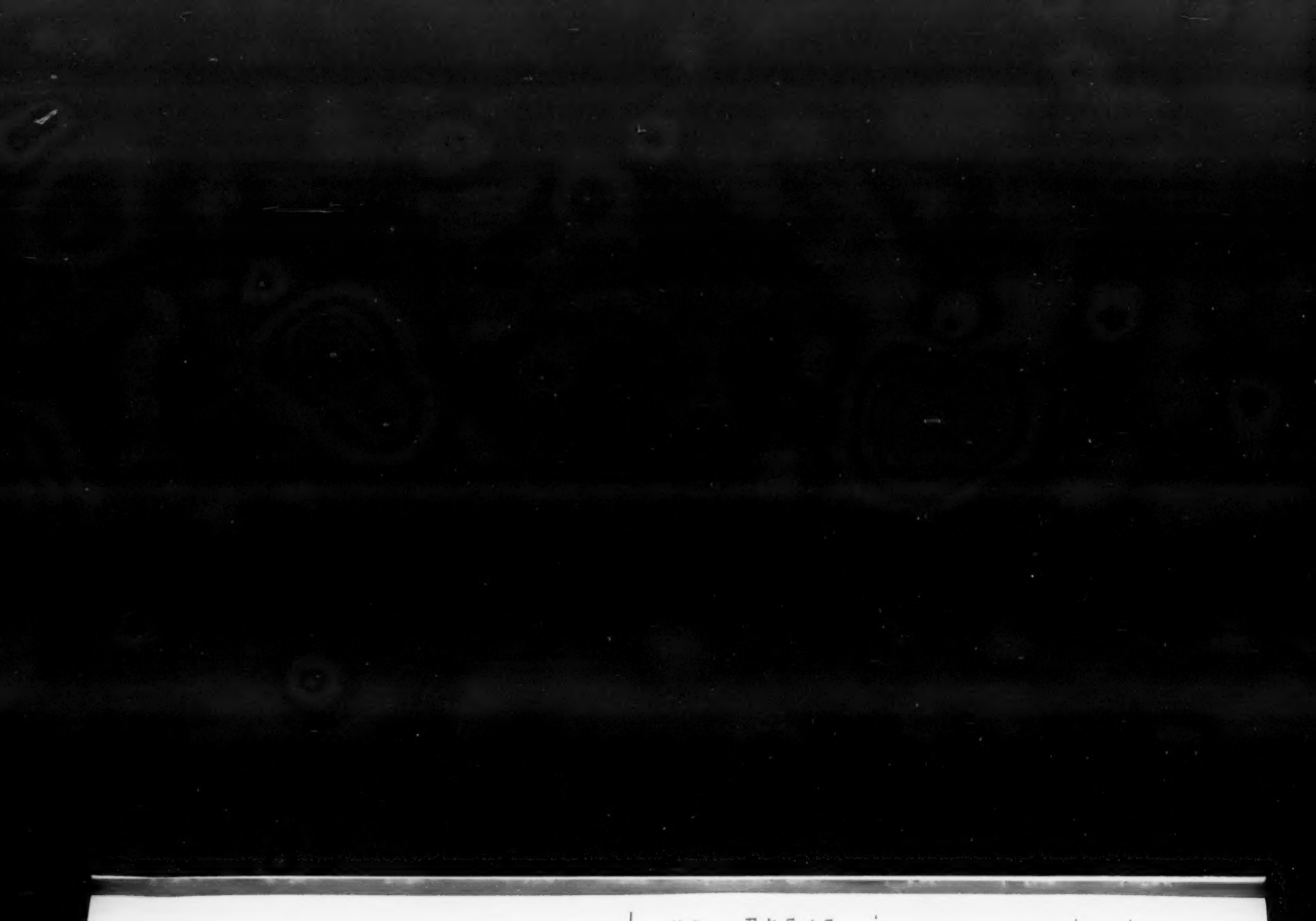
City _____ Zone ____ State _____